Ministry for Primary Industries
Manatū Ahu Matua

Scenarios of Storminess and Regional Wind Extremes under Climate Change

March 2011

MPI Technical Paper No: 2018/50

Prepared for Ministry for Primary Industries
by Brett Mullan, Trevor Carey-Smith, Georgina Griffiths, Abha Sood

ISBN No: 978-1-77665-961-6 (online)
ISSN No: 2253-3923 (online)

August 2018

Disclaimer

While every effort has been made to ensure the information in this publication is accurate, the Ministry for Primary Industries does not accept any responsibility or liability for error of fact, omission, interpretation or opinion that may be present, nor for the consequences of any decisions based on this information.

Requests for further copies should be directed to:

Publications Logistics Officer
Ministry for Primary Industries
PO Box 2526
WELLINGTON 6140

Email: brand@mpi.govt.nz
Telephone: 0800 00 83 33
Facsimile: 04-894 0300

This publication is also available on the Ministry for Primary Industries website at
http://www.mpi.govt.nz/news-and-resources/publications/

Scenarios of Storminess and Regional Wind Extremes under Climate Change

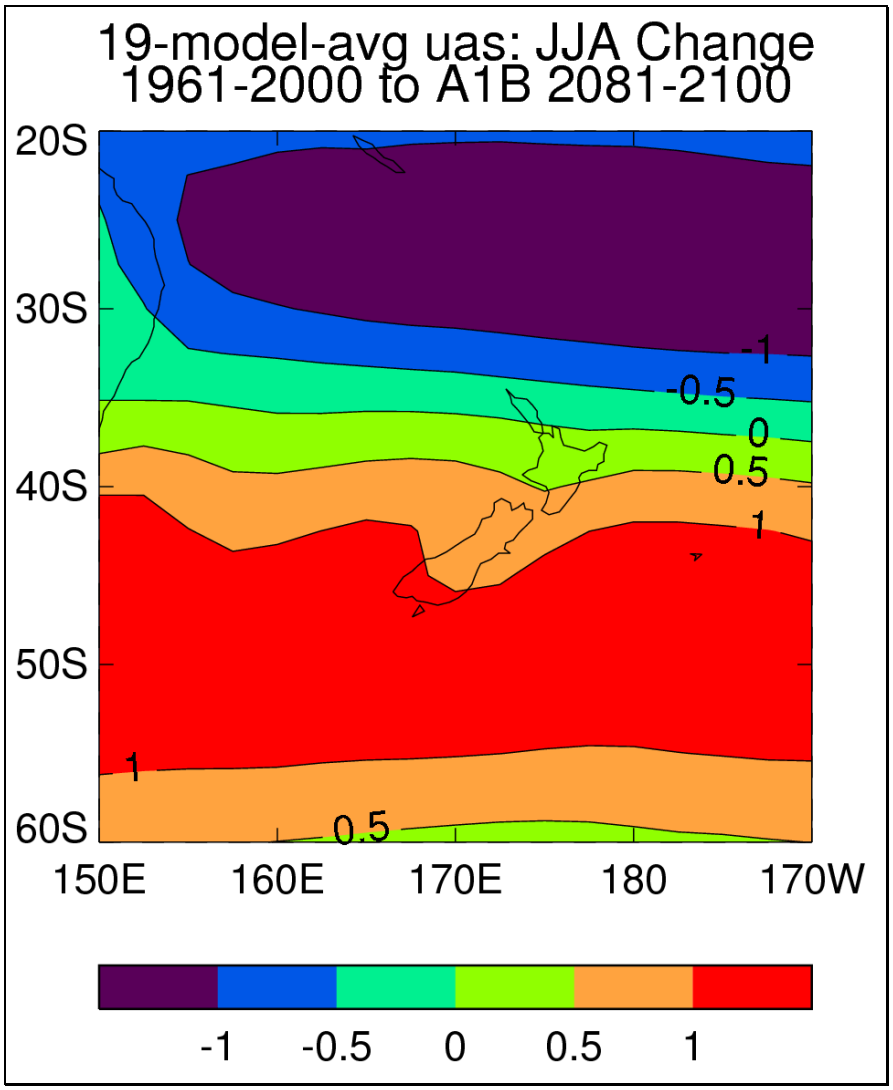

NIWA Client Report: WLG2010-31
March 2011
NIWA Project: SLEW093

Scenarios of Storminess and Regional Wind Extremes under Climate Change

Brett Mullan
Trevor Carey-Smith
Georgina Griffiths
Abha Sood

NIWA contact/Corresponding author

Brett Mullan

Prepared for

Ministry of Agriculture and Forestry

NIWA Client Report: WLG2010-31
March 2011

NIWA Project: SLEW093
FRST Contract: C01X0817

National Institute of Water & Atmospheric Research Ltd
301 Evans Bay Parade, Greta Point, Wellington
Private Bag 14901, Kilbirnie, Wellington, New Zealand
Phone +64-4-386 0300, Fax +64-4-386 0574
www.niwa.co.nz

Contents

Reviewed by:

Dr James Renwick

Principal Scientist

Approved for release by:

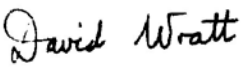

Dr David Wratt

Chief Scientist, Climate

Formatting checked

ABT

Executive Summary

Wind is a difficult climatological variable to work with, and to model, because wind can vary so much over short distances and short time periods. However, surface winds are driven mainly by the large-scale circulation which global climate models (GCMs) are generally able to capture adequately.

Several parallel and complementary approaches are taken in this report, involving low resolution global model pressure and wind fields, and high resolution three-dimensional dynamical output from the NIWA regional climate model (RCM). This allows us to build up a picture of projected changes in: prevailing winds and weather patterns, storm frequency and intensity, extreme winds, and severe convective weather.

The principal findings of this study are that, based on multiple lines of investigation, the frequency of extreme winds over this century is likely to increase in almost all regions of New Zealand in winter, and decrease in summer especially for the Wellington region and the South Island. However, the magnitude of the increase in extreme wind speed is not large – only a few per cent by the end of the century under the middle-of-the-range A1B emission scenario.

In addition, it is likely that there will also be an increase in cyclone activity over the Tasman Sea in summer and a decrease in activity south of New Zealand. (In this report, 'cyclone' refers to a sub-tropical or mid-latitude low pressure centre and not to a tropical cyclone.)

The following sections summarise the main results from the parallel analyses performed in this study.

Chapter 2 – Historical wind extremes

In this chapter, Kidson weather types are used as a framework to understand the causes and variations of extreme winds. Kidson types are grouped into three basic regimes defined as "Trough" (occurring approximately 38% of the time, averaged over the year), 'Zonal" (25% of the time), and 'Blocking" (37% of the time).

Using spatially interpolated wind speed data from 1997-2008, strong winds are shown to affect large parts of New Zealand primarily through four weather types (T, SW, W, and HNW); that is, two of the trough types and two of the zonal types (See Figure 1 and Table 2 for the Kidson classification).

The above result agreed well with a separate analysis of extreme wind gust data and reports of wind damage. Here, it was additionally found that strong winds from Kidson types NE and HSE are confined mainly to Northland, Auckland, and Waikato (which includes the Coromandel), while Kidson type W affects mainly Southland and parts of Otago and Canterbury.

Chapter 3 – Future changes in circulation patterns and wind distributions

The Kidson weather typing scheme was applied to daily mean sea level pressure fields from 23 GCMs used in the Intergovernmental Panel on Climate Change (IPCC) 4th Assessment Report (AR4, see Table 1 for model details) for 40 years of their 20th century runs. The frequency of Kidson types from these GCM runs was matched with the distribution of observed Kidson types, as a means of testing the performance of the GCMs.

The top six performing GCMs are *iap, giss-er, hadcm3, miroc-hires, miroc-medres,* and *mri* (See Table 1 for model details).

Daily mean sea level pressure (MSLP) data from the future (2081-2100) scenario runs SRES A1B and SRES A2 (medium to high emission scenarios) were then analysed, and the simulated future frequencies of the Kidson types evaluated.

The projected change in the trough types over the winter season are almost the reverse of those in summer, with trough types T and SW in winter projected to become more frequent (less frequent in summer). This may lead to an increase in the frequency of extreme winds (related to trough types) in almost all regions in winter (decreased frequency in summer), but especially Wellington and the South Island regions.

All three zonal types (W, HNW, and H) are projected to decrease in frequency in summer but increase in frequency in winter. The weather types (especially W and HNW) have their biggest influence on the occurrence of extreme winds in Canterbury, Otago and Southland. Thus, the projections suggest fewer extreme winds in summer, but more extremes in winter, for the south and east of the South Island. As an example of the magnitude of the frequency changes: type SW (associated with extreme winds through the west and central parts of the North Island, and coastal Otago) decreases in summer from about 9% of the time to 7% of the time, whereas the frequency increases in winter from about 11% of the time to 13% of the time, under the A2 scenario by 2100.

Further, an increase in the frequency of summer extreme winds, associated with increased blocking weather types, could occur in Northland, Coromandel, Bay of Plenty, Gisborne and Taranaki. In winter, the reverse case is projected.

Chapter 4 – Cyclone strengths and frequencies in the NZ region

The focus of this chapter is on validating GCM representation of cyclone density (or frequency) and intensity in the New Zealand region against ERA40 reanalysis and consequently examining the differences between the current and future climate for a selection of scenarios.

Based on three fields (cyclone density, radius and central pressure) combined, the top ten performing GCMs for the New Zealand region are *ingv_echam5, csiro_mk3.5, gfdl_cm2.1, mpi_echam5,*

miroc3_hires, ncar_ccsm3.0, iap_fgoals1.0, gfdl_cm2.0, mri_cgcm_232, and *ncar_pcm1* (See Table 1 for model details).

The future scenarios are presented for two time periods, 2046–2065 and 2081–2100, and for three SRES emission scenarios B1 (low emissions), A1B and A2 (medium to high emissions).

The analysis confirmed results from previous studies showing that there is likely to be a poleward shift in the cyclone track in a future, warmer climate. In the New Zealand context, this equates to a reduction in the number of cyclones over the North Island and to the east of the country in winter, with the chance of slightly increased cyclone frequency to the south of the country. In summer, however, it is likely that there will be increased cyclone activity over the Tasman Sea and a decrease in activity south of New Zealand.

Cyclone intensity is likely to decrease over New Zealand in both summer and winter. However, a significant intensification is possible south of the country during winter. This could produce a stronger pressure gradient over the South Island, and a possible increase in extreme winds in that part of New Zealand.

These seasonal changes in cyclone density are consistent with the Chapter 3 findings of the likely changes in the Kidson circulation types. Only three Kidson types have low pressure centres near New Zealand and north of 45°S: types TSW, NE and R. Chapter 3 concluded that the frequency of all three types is projected to decrease in winter and increase in summer.

Chapter 5 – Extreme wind pattern analysis

This chapter describes observed trends in extreme winds from gridded ERA40 reanalysis data, and then determines whether the climate models also identify similar trend patterns for the 20th century period. Trends out to 2100 are then analysed for 14 GCMs under the AR4 SRES A1B emission scenario (a medium emission scenario), and agreement between models is assessed.

The trend in extreme (99th percentile) winds over New Zealand, diagnosed from 1961-2000 ERA40 reanalysis data, suggests a weak increase in extreme winds over the southern and western South Island and no change or weak decrease over the northern North Island. Two of the global models, *miroc32_hires* and *cnrm_cm3,* stand out as having extreme wind trend patterns that closely match ERA40 over 1961-2000 for both winter and summer separately.

The trend patterns increase in intensity for the 14 models and the ensemble mean over the "Past & future period" (1961–2100). Most of the trend patterns show increases in extreme winds in the Tasman Sea, and over and south of the South Island. The related change in MSLP pattern is consistent with a more frequent zonal Kidson regime. However, the magnitude of the wind change is small, at most a few per cent of the 99 percentile wind speed in the current climate. Four GCMs (*cnrm_cm3,*

csiro_mk35, *gfdl_cm21*, *mpi_echam5*) have trend patterns that are well separated from the background noise, and these four have the strongest linear trends that are significant at the 1% level.

This analysis focuses on coherent spatial patterns of change in extreme winds. However, even at the individual GCM grid-point scale, the magnitude of extreme changes is small. The 99th percentile extreme daily wind for 1961-2000, averaged over the New Zealand domain, lies between 10 and 15 m/s across the 14 GCMs. Over the period to 2100, this 99th percentile is either almost unchanged or increases by only a few tenths of a m/s. Those patterns that show statistically significant trends (at the 1% level) have increases in their extreme winds over New Zealand of only a few tenths of a m/s by 2100, and do not occur very often.

Chapter 6 – Severe weather indices from the New Zealand regional climate model

This section examines how three indices of severe weather – the K-index, Convective available potential energy (CAPE), and vertical wind shear – vary between current and future regional climate model (RCM) simulations over New Zealand. Substantial increases are detected in the first two of these indices, suggesting an increase in vigorous small-scale convective events and, by inference, in the occurrence of local extreme winds such as downdrafts or gust fronts.

The 99th percentile in the modified K-index increases by between 3 and 6% over most of New Zealand between the control and the A2 (future emission scenario) simulation, with the largest increases over the South Island.

The frequency of extreme CAPE events also increases in the future A2 simulation. For summer, the largest increase in CAPE occurs in the Tasman Sea and over the South Island and central North Island. For autumn, the increase is fairly uniform over the domain, with the smallest increases over the land. For spring, the pattern is also quite uniform (although smaller in magnitude than for autumn), but the smallest increases are now over the ocean. For winter, the largest increases are in the south of the domain, but as this is the region with the lowest CAPE values, this increase is not so important for possible extreme wind events.

While we might expect vigorous small-scale convection to be more common and more intense in a future warmer climate, further work would be required to relate these severe weather indices to quantitative changes in extreme surface winds.

1. Introduction

1.1 Philosophy for assessing future changes to storms and extreme winds

The key research questions we want to address in this report are: "What changes are likely in the incidence of damaging strong winds", and "Will storminess increase for New Zealand under global warming"? We are interested in improving our understanding of wind and storm changes not only at the broader Tasman Sea scale, but also the implications at the finer Regional Council district scale. In the process of addressing extremes, we will increase our knowledge of the full distribution of daily winds and weather patterns, a major advance over what was available in MfE (2008) which was based almost solely on analysis of monthly mean data.

Wind is a difficult climatological variable to work with, and to model, because wind can vary so much over short distances and short time periods. Surface winds are driven mainly by the large-scale circulation which global climate models are generally able to capture adequately. However, surface roughness and topography can substantially modify the large-scale flow, and the detailed spatial and temporal pattern of wind fluctuations. Global models, with at best a resolution of about 1° latitude – longitude (>100km) in general, cannot hope to resolve these details. A resolution of the order of 30km, typical of many regional climate models, is also too coarse. Webster *et al.* (2008) showed that a resolution of 12km or finer was necessary to successfully simulate features of severe weather in New Zealand's mountainous environment.

The data sets we are working with here – an ensemble of global climate models (GCMs), and the New Zealand Regional Climate Model (RCM) – therefore cannot provide a realistic intensity of wind extremes that might be experienced at a point (Pryor *et al.*, 2006). A further limitation is that the GCM data are only available as daily-average values.

Thus, much of the information about changes in strong winds is necessarily qualitative, although we provide quantitative results where feasible. Several parallel and complementary approaches are taken, involving low resolution global model pressure and wind fields, and high resolution three-dimensional dynamical output from the NIWA RCM. This allows us to build up a picture of projected changes in: prevailing winds and weather patterns, storm frequency and intensity, extreme winds, and severe convective weather.

1.2 Previous work

In New Zealand, winds in mountainous areas, including down slopes and along valley floors, are frequently strong when vigorous mid-latitude weather systems move over the country (Sturman and Tapper, 1996). Downslope windstorms in particular are significant because the winds are potentially very damaging, and some parts of New Zealand are notorious for their history of extreme downslope (lee) winds. For example, Hill (1979) records a downslope windstorm in 1975 where gusts over 160 km/hr caused considerable wind-throw damage at Eyrewell Forest on the Canterbury Plains. Wendelken (1966) also catalogued damage to this same forest from downslope storms that occurred in 1945 and 1964. In the 1975 storm a gust of 194 km/hr was recorded at Kaikoura. In January 2004, an active cold front moving up the country produced very high wind speeds over the northern South Island region that blew down power pylons built to withstand winds of 200 km/hr (Webster *et al*., 2008). High winds can also result in costly damage to horticultural crops such as kiwifruit vines in areas such as the Bay of Plenty (e.g. in April and November 2001).

In its Fourth Assessment Report, the Intergovernmental Panel on Climate Change (IPCC, 2007) gives very limited information of expected changes in storms and winds. The most confident statements relate to tropical cyclones: "it is likely that future tropical cyclones will become more intense, with larger peak wind speeds and more heavy precipitation associated with ongoing increases in sea surface temperatures". Tropical cyclones do not directly affect New Zealand, but after transition to an extra-tropical thermal and circulation structure they can pass over the country and bring heavy rainfall and strong winds (eg., cyclone Giselle (better known as the "Wahine storm") in April 1968, and cyclone Bola in March 1988).

The only other statement in the Summary for Policymakers of IPCC (2007) relating to storms and winds as they could affect New Zealand states: "extra-tropical storm tracks are projected to move poleward, with consequent changes in wind, precipitation and temperature patterns, continuing the broad pattern of observed trends over the last half-century".

This dearth of information on winds and storms reflects the lack of research studies in international journals on this topic prior to 2007. However, this is starting to change as analyses are made of the IPCC multi-model archive of global climate model data and independent regional climate model studies (Beniston *et al.*, 2007; Ray, 2008; Rockel and Woth, 2007). NIWA has recently developed new climate change scenarios for New Zealand derived from a selection of IPCC Fourth Assessment global models, supplemented by NIWA's regional model (RCM). These scenarios, as documented in MfE (2008), focus primarily on temperature and rainfall changes, but also suggest that

changes in wind are likely. Preliminary analysis of RCM data suggests a future increase in strong winds over at least part of New Zealand is possible.

There is a growing literature on historical and current trends in strong winds and storms. Salinger *et al.* (2005) examined trends in extreme pressure gradients and extreme daily wind gusts across New Zealand since the 1960s. They found an increase in the number and strength of extreme westerly wind episodes to the south of the country, but only a slight increase over New Zealand itself. An overall increase in Southern Hemisphere mid-latitude westerly winds over recent decades is widely recognised, and has been attributed to a combination of both the ozone hole and increasing greenhouse gases (Thompson and Solomon, 2002). These observed trends are also reproduced in the climate models. The picture for Southern Hemisphere extra-tropical cyclones is more complicated. Studies have found increases in the number of rapidly intensifying cyclones (Lim and Simmonds, 2002), but also regional varying trends in the average intensity and the average number of cyclones (Simmonds and Keay, 2000a and b).

1.3 Key Data Sources: Historical Observations and Model Output

1.3.1 Observed data

The National Climate Database (http://cliflo.niwa.co.nz/) maintained by NIWA is the principal repository of New Zealand climate data, and contains statistical summaries (such as monthly averages or 30-year normals) as well as raw data (such as hourly or daily frequencies). Measurements of extreme gust wind speeds were extracted from the database tables and used in Chapter 2 of this report.

Daily average wind speed observations have been used to develop a gridded wind speed data set, following the thin-plate smoothing spline approach described in Tait *et al*. (2006). The interpolated data cover New Zealand on a 0.05° latitude by 0.05° longitude grid, and the data set is known as the Virtual Climate Station Network (VCSN). Wind speed values are available every day from 1-Jan-1997. Chapter 2 uses the VCSN wind speeds to identify circulation patterns that lead to extreme winds.

The other historical data sets used in this project are global re-analysis fields, specifically for near-surface wind (at 10-metre altitude) and for mean sea-level pressure (MSLP). These "re-analysis" data sets use historical observations incorporated into a state-of-the-art weather prediction model that serves to produce dynamically balanced and physically consistent meteorological fields, removes or smoothes outliers, and results in a globally complete gridded data set. Throughout the

report, use is made of either the European Centre Re-Analysis (ERA40, Uppala *et al.*, 2005), or the NCAR/NCEP[1] Re-analysis (NCEP, Kalnay *et al.*, 1996).

1.3.2 Climate Model output

Simulated data are taken from an ensemble of global climate models from the World Climate Research Programme's (WCRP's) Coupled Model Intercomparison Project phase 3 (CMIP3). The simulations from these models were analysed for the IPCC Fourth Assessment (AR4), and have been archived for use internationally in impact studies. These data are described in Meehl *et al.* (2007), and in this report will be referred to as either AR4 or CMIP3 data.

The CMIP3 data cover the historical or '20th century' climate period, approximately 1880 to 2000, and the 'future' climate period 2001 to 2100 or beyond. The 20th century simulations ("20c3m") are not constrained by observed data, except very generally through time series of greenhouse gas concentrations, solar radiation, volcanic aerosols, and (in some cases) stratospheric ozone concentrations. The future simulations followed the IPCC SRES scenarios B1 (low), A1B ('middle-of-the-road') and A2 (high). Some data for the 20th century, and for one or more of the future scenarios, are available for up to 23 models (Table 1). Whereas the monthly data cover the full period of the simulation (e.g., 1880-2000 and 2001-2100), the daily data are archived (with a couple of exceptions) for specified windows: 1961-2000 for the 20th century, and 2046-2065 and 2081-2100 for the 21st century.

The MfE (2008) guidance manual described statistically downscaled projections derived from monthly mean data for 12 of these CMIP3 models. (A total of 17 models were considered initially, but 5 were rejected for poor performance in simulating the historical climate). In this report, we make use of daily data, either 10-metre winds or MSLP. One of the MfE (2008) models, *ukmo_hadgem1*, has no archived data on the daily time-scale. Table 1 shows what models are available for the different scenarios. The finest resolution GCM of 1.1° latitude grid spacing corresponds to a distance of about 120km at New Zealand's latitude range.

NIWA uses a version of *ukmo_hadcm3* for its global climate experiments (Bhaskaran *et al.*, 1999), along with the UKMO regional climate model configured for New Zealand conditions (Bhaskaran *et al.*, 2002). The GCM and RCM have been run at NIWA for the periods 1970-2000 ("20c3m" forcing) and 2070-2100 (SRES B2 and A2 forcing) (Dean et al., 2006). RCM output from the 20th century and future A2 run is used in Chapter 6 of this report.

[1] National Center for Atmospheric research/National Centers for Environmental Prediction

Table 1: Information on IPCC Fourth Assessment GCMs, along with a record of what daily mean sea-level pressure (MSLP) and near-surface zonal wind (U10m) data are available in the 20th century period (20c3m) and the future scenarios SRES A1B and A2. 'Y' indicates model data are available. The column headed MfE shows what models were used (tick) or discarded (cross) in the Guidance Manual, where only monthly means were considered.

Model Name	Country	Resolution	MfE (2008)	20c3m		A1B		A2	
		Lat x Lon		Mslp	U10m	Mslp	U10m	Mslp	U10m
bccr_bcm20	Norway	1.9° x 1.9°		Y	Y	Y	Y	Y	Y
cccma_cgcm31_t47	Canada	3.75° x 3.75°		Y	Y	Y	Y	Y	Y
cccma_cgcm31_t63	Canada	1.9° x 1.9°	✓	Y	Y	Y	Y		
cnrm_cm3	France	1.9° x 1.9°	✓	Y	Y	Y	Y	Y	Y
csiro_mk30	Australia	1.9° x 1.9°	✓	Y	Y	Y	Y	Y	Y
csiro_mk35	Australia	1.9° x 1.9°		Y	Y	Y	Y	Y	Y
gfdl_cm20	USA	2.0° x 2.5°	✓	Y	Y	Y	Y	Y	Y
gfdl_cm21	USA	2.0° x 2.5°	✓	Y	Y	Y	Y	Y	Y
giss_aom	USA	3.0° x 4.0°	×	Y	Y	Y	Y		
giss_model_eh	USA	4.0° x 5.0°	×	Y					
giss_model_er	USA	4.0° x 5.0°		Y	Y	Y	Y	Y	Y
iap_fgoals_10g	China	2.8° x 2.8°		Y	Y	Y	Y		
ingv_echam4	Italy	1.1° x 1.1°		Y	Y	Y	Y	Y	Y
inm_cm30	Russia	4.0° x 5.0°	×	Y	Y	Y	Y	Y	Y
ipsl_cm4	France	2.5° x 3.75°	×	Y	Y	Y	Y	Y	Y
miroc32_hires	Japan	1.1° x 1.1°	✓	Y	Y	Y	Y		
miroc32_medres	Japan	2.8° x 2.8°		Y	Y	Y	Y	Y	Y
miub_echog	Korea/ Germany	3.75° x 3.75°	✓	Y	Y	Y	Y	Y	Y
mpi_echam5	Germany	1.9° x 1.9°	✓	Y	Y	Y	Y	Y	Y
mri_cgcm232a	Japan	2.8° x 2.8°	✓	Y	Y	Y	Y	Y	Y
ncar_ccsm30	USA	1.4° x 1.4°	✓	Y		Y		Y	
ncar_pcm1	USA	2.8° x 2.8°	×	Y				Y	
ukmo_hadcm3	UK	2.5° x 3.75°	✓	Y				Y	
ukmo_hadgem1	UK	1.25°x1.875°	✓						
Total # Models			12	23	19	20	19	18	15

1.4 Analysis Methodology and Report Layout

Material from the various analysis strands are synthesized to give an overall picture of likely changes to New Zealand's wind climate over the 21st century, with particular emphasis on strong winds. As with other scenario guidance, a range of changes are indicated by the suite of models examined.

1.4.1 Chapter 2: Historical Wind Extremes

The pattern of prevailing winds, and their variation through the seasons, not only has a major influence on rainfall distribution over New Zealand, but also on the occurrence of strong winds (Sturman and Tapper, 1996).

Chapter 2 starts by reviewing the synoptic weather type classification of Kidson (2000). The daily occurrence of Kidson's 12 weather types is matched against extreme winds from both the gridded (VCSN) wind speed data and from station observations (National Climate Database). This historical setting provides a framework for interpreting how future projected wind and pressure changes – and thus future projected Kidson weather types – may influence extreme wind occurrence. McInnes *et al.* (2005) provide an Australian example of how various synoptic types can successfully be related to the frequency of strong wind occurrence.

1.4.2 Chapter 3: Projected changes in circulation and wind

Chapter 3 starts with a brief overview of projected changes in the daily wind distribution in the Tasman-New Zealand region. Particular attention is paid to the west-east (zonal) wind, and whether the daily wind is westerly or easterly. The emphasis here is on the distribution rather than the extreme winds, but is a necessary introduction because wind changes on the daily time-scale for New Zealand have not been discussed previously elsewhere. The occurrence of westerly *versus* easterly winds has important implications for regional rainfall.

The Kidson synoptic types are then diagnosed for selected CMIP3 models and scenarios. Changes between 20th and 21st century climate in the frequency of various weather types, when combined with the results of Chapter 2, give an excellent indication of changing wind risk. As an additional benefit of the Kidson typing, the CMIP3 models can be validated on their simulations of historical weather patterns.

1.4.3 Chapter 4: Projected changes in cyclonic storms

Software from the University of Melbourne (Simmonds and Keay, 2000a) is applied to analysing the position of low pressure centres in gridded model data from the CMIP3 multi-model ensemble archive. The CMIP3 data are only available once per day, and this makes it difficult to 'track' storm centres from one day to the next (there are too many ambiguities if a centre fills or a new low develops in the 24 hours since the previous day's map). However, the frequency and intensity of storms can readily be calculated. The same software package is applied to the reanalysis (ERA40) data set.

Chapter 4 validates the CMIP3 models in terms of their 20th century storm frequencies and intensities near New Zealand, and then goes on to describe any systematic changes in projected future climate. This chapter does not explicitly consider extreme winds, but knowledge of any changes in storm position, frequency and intensity will provide qualitative information on changes in extreme wind risk. Such analyses have been successfully performed in other parts of the world (Leckebusch et al., 2006; Semmler et al., 2008).

1.4.4 Chapter 5: Pattern analysis to identify extreme wind changes

In this chapter, a new analysis technique is described that identifies trend patterns in noisy data – trend empirical orthogonal function (TEOF) analysis. TEOFs are first calculated for the historical 1961-2000 period, from both reanalysis (ERA40) and CMIP3 wind speed data. This first step provides yet another validation measure for the CMIP3 models. The method does not require a continuous time series, and is applied to just the top 1-percentile of daily winds in the New Zealand region. The trend EOFs are then calculated over the past (1961-2000) period combined with the two future periods (2046-2065 and 2081-2100) for a number of the CMIP3 models of Table 1.

1.4.5 Chapter 6: Regional Model changes in indices of severe weather

Past research at the New Zealand Meteorological Service, and ongoing research by NIWA, has documented many examples and case studies where severe weather (e.g. thunderstorms, severe gales, and hail) can be related to broader synoptic weather patterns. For example, Steiner (1989) examined 14 severe hailstorms identified from crop insurance claims and found they all occurred in the rear of the leading cold front of a cyclone system.

Thunderstorms often produce severe turbulence that can result in destructive surface winds, hail and tornadoes. The global climate models, and even the much higher resolution regional climate model, are unable to directly reproduce these weather phenomena which have scales of just tens of kilometers and last only a few hours. However, there are various ways for identifying larger-scale or "environmental" conditions that foster such severe weather (Brooks *et al.*, 2003). These severe weather "indices" can be adequately characterized by the 3-dimensional dynamical fields generated by the regional climate model, although the global models are still not well-suited to this type of analysis.

Thus, Chapter 6 calculates two different indices associated with the occurrence of severe weather, using output from the NIWA RCM. Changes in these indices between

the 20th century (1971-2000) and the end of the 21st century (2071-2100) are described. The indices selected are:

- Convective Available Potential Energy (CAPE): This is a parameterised measure of the vertically integrated buoyant energy available to a storm. Given some simplifying assumptions, CAPE can be shown to have a direct mathematical relation to the maximum updraft speed in a storm. The strongest updrafts that can grow in environments of large CAPE are able to support the growth of large hailstones and intense rainfall rates, which can lead to intense downdrafts and strong horizontal outflow winds.

- Vertical shear of the horizontal wind vector: Large vertical shear promotes storm-scale rotation and helps sustain deep updrafts, which together enhance storm organization and promote the intensity and longevity of thunderstorms.

Another stability index sometimes used is the Showalter Index (Showalter, 1953), which is essentially a simpler version of CAPE.

Such work on relating changes in severe weather to a changing climate caused by greenhouse gas increases is still very new, but some studies are now being done overseas (e.g. Trapp et al., 2007).

2. Historical Wind Extremes

This chapter sets the historical context for subsequent sections that discuss future projections of wind in the New Zealand region. Extreme winds are associated, of course, with weather systems (usually intense low pressure centres), and it is therefore important to develop climatologies of such synoptic events. Some weather patterns will impact on one part of New Zealand but not another. The frequency of the various weather patterns changes with the seasons, and also from year to year with natural variability such as the El Niño-Southern Oscillation.

Kidson (2000) developed a synoptic classification of weather types as they affected New Zealand. Here, we use the Kidson weather types as a unifying framework within which to understand the causes and variations of extreme winds. The occurrence of extreme winds associated with the Kidson circulation types are analysed from two separate sources:

- Daily wind speeds interpolated from station observations onto the 0.05 degree Virtual Climate Station grid

- Daily and sub-daily observations of winds from NIWA's National Climate Database, and reports of wind damage

2.1 Kidson circulation types

Kidson (2000) analysed 40 years of daily weather maps from the NCEP reanalysis dataset, and diagnosed 12 weather types that affect New Zealand. NIWA has maintained and updated the time series, so that the weather types are available every 12 hours (at 00 GMT and 12 GMT) from 01-Jan-1958 to the present.

Figure 1 shows the 12 Kidson weather types, which were grouped into three basic regimes that Kidson (2000) defined as "Trough" (occurring approximately 38% of the time averaged over the year), 'Zonal" (25% of the time), and 'Blocking" (37% of the time). There is some seasonal variation in the frequency of each weather type and regime: the main change is in the summer season where there is a reduced frequency of the three zonal types, which is compensated for by an increased frequency of four of the five blocking types (excluding type HE).

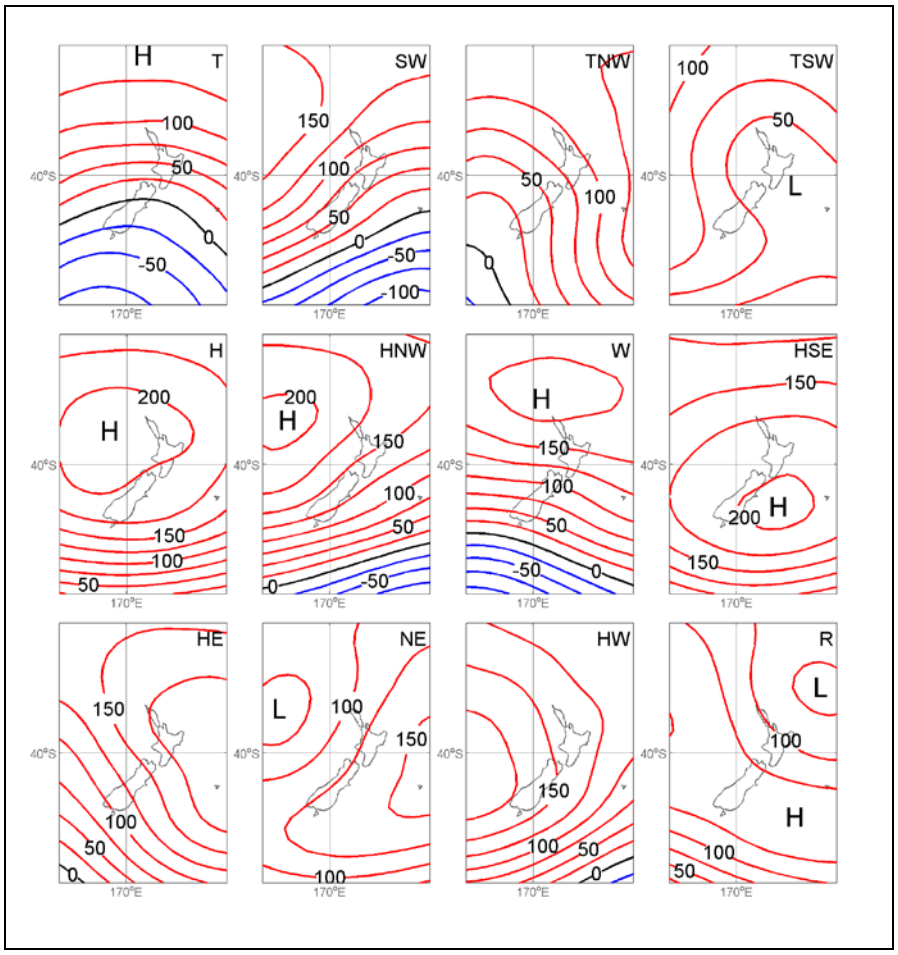

Figure 1: Kidson circulation types (Kidson, 2000), in terms of 1000hPa geopotential heights (m). The circulation type is given by the acronym in the top right-hand corner of each panel, defined in Table 2 below.

Table 2: The 12 Kidson weather types, grouped into three regimes

Regimes	**Weather Types**
"Trough" weather types	T = Trough SW = South-Westerly flow TNW = Trough in North-Westerly flow TSW = Trough in South-Westerly flow
"Zonal" weather types	H = High pressure over the country HNW = High to North-West of NZ W = high to north with Westerly flow over NZ
"Blocking" weather types	HSE = High pressure to South-East of NZ HE = High pressure to East of NZ NE = North-Easterly flow HW = High pressure to West of NZ R = Ridge lying across central and southern NZ

The computer code used to diagnose the Kidson weather types on the NCEP reanalysis data has been adapted so that it can be applied to other data sets, both historical and model projections. The algorithm was initially applied to a different re-analysis historical data set, known as ERA40 (Uppala, 2006), which covers the period September 1957 to August 2002. For the period in common between the NCEP and ERA40 data sets (January 1958 to August 2002), the exact match between 12-hourly weather maps is only 82% across the 12 Kidson types, increasing to 92% across the three regimes. This may seem rather low, but highlights the basic uncertainty in assigning an instantaneous weather map to a cluster type. No undefined types are permitted. The clustering calculates a metric defining how close a particular weather map is to each of the 12 clusters (Kidson types), and selects the closest match. Table 3 provides an example for the first five days of 1958, where six (out of 10) weather types agree exactly; in a further three cases, the second closest match in the ERA40 analysis agrees with that type selected for the NCEP analysis.

Table 3: Comparison of Kidson weather types selected in the first five days of 1958: NCEP closest Kidson type (2nd column), ERA40 closest Kidson type (3rd column), ERA40 second and third closest weather type (columns 4 and 5). For the ERA40 analysis, the metric is also shown; a smaller value means a closer match.

Day/Hour	NCEP	ERA40 (metric)	ERA40 2nd closest (metric)	ERA 3rd closest (metric)
1958 01 01 00	TSW	TSW (0.57)	T (0.67)	SW (1.17)
1958 01 01 12	T	TNW (0.52)	T (0.55)	TSW (0.62)
1958 01 02 00	SW	T (0.66)	TSW (0.77)	SW (0.83)
1958 01 02 12	SW	SW (0.49)	T (0.85)	TSW (0.96)
1958 01 03 00	SW	SW 0.93)	HW (1.00)	TSW (1.03)
1958 01 0312	SW	T (0.90)	SW (1.00)	TSW (1.06)
1958 01 04 00	TSW	TSW (0.73)	SW (0.83)	T (0.85)
1958 01 0412	TSW	SW (0.47)	TSW (0.65)	T (0.65)
1958 01 05 00	TSW	TSW (0.53)	SW (0.55)	T (0.57)
1958 01 05 12	T	T (0.45)	SW (0.54)	TSW (0.58)

2.2 Wind Extremes from gridded VCS dataset

In this section, we describe how the observed wind speed over New Zealand varies according to the Kidson weather type. The observations used represent the daily average wind speeds, and so are lower than the highest hourly mean winds or the gust wind speeds. Thus, they are not the true extremes, but we would expect the patterns of the highest daily averages to be closely related to the true wind extremes.

Climate station observations of daily mean wind speed have been interpolated onto a 0.05° latitude by 0.05° longitude regular grid of 11,491 points over New Zealand (See Tait et al., 2006, for a general description of the approach, applied there to rainfall observations). Surface wind speed information is a difficult weather element to work with, since small changes in the site environment (buildings, growth/cutting of trees, aging instruments) can have a major influence on the measured wind speed. Although NIWA has calculated the interpolated wind speeds for the period starting from 1972, the analysis is not considered very reliable until 1997 (Tait, pers. comm.). Thus, the following analysis uses the gridded data (also known as the Virtual Climate Station, or VCS, data) only for the 12-year period 1997-2008.

At each of the VCS grid-points, the daily wind speeds were sorted to identify the threshold for the top 1 per cent of observations. Figure 2 shows the spatial and temporal variation in the top 1% of winds. The spatial variation is no surprise; the highest 1-percentile winds exceed 15 m/s, and occur around the south coast of Wellington and Wairarapa, and also over Stewart Island and the southern edge of the South Island. At the other end of the scale, any winds above about 7 m/s lie in the top 1-percentile for much of the Waikato and inland Nelson. The lower panel of Figure 2 shows the very large variability from day to day in wind speeds, again as expected. With a total of 11,491 grid-points, we would expect on average that 115 points, if they are independent, will exceed their 1 percentile each day. The temporal distribution is very uneven though; through the 11-year period there are a number of occasions when more than one-quarter of the country (~3000 grid-points) lies in the top 1 percent.

Having identified the value of the top 1% wind speed at each grid-point, we now sort these highest wind speed days according to the Kidson weather type. Figure 3 shows the results. Note the maps give conditional probabilities: that is, given the wind is in the top 1%, what is the probability that the weather pattern corresponds to a particular Kidson type. The yellow through red areas on each map show which parts of the country are most likely to be affected by strong winds as a function of the weather type. Only four weather types (T, SW, W, and HNW) affect large parts of New Zealand; that is, two of the trough types and two of the zonal types (Table 2). Weather types TSW, R, HW, TNW, and H only occasionally result in extreme (top 1 percentile) winds. The remaining types (NE, HE, and HSE) have a restricted regional impact. For example, type NE affects mainly the Coromandel peninsula and Northland.

Thus, we can make use of these probability maps, along with projected changes in each Kidson type (chapter 4), to identify which parts of New Zealand are likely to experience an increase or decrease in extreme winds.

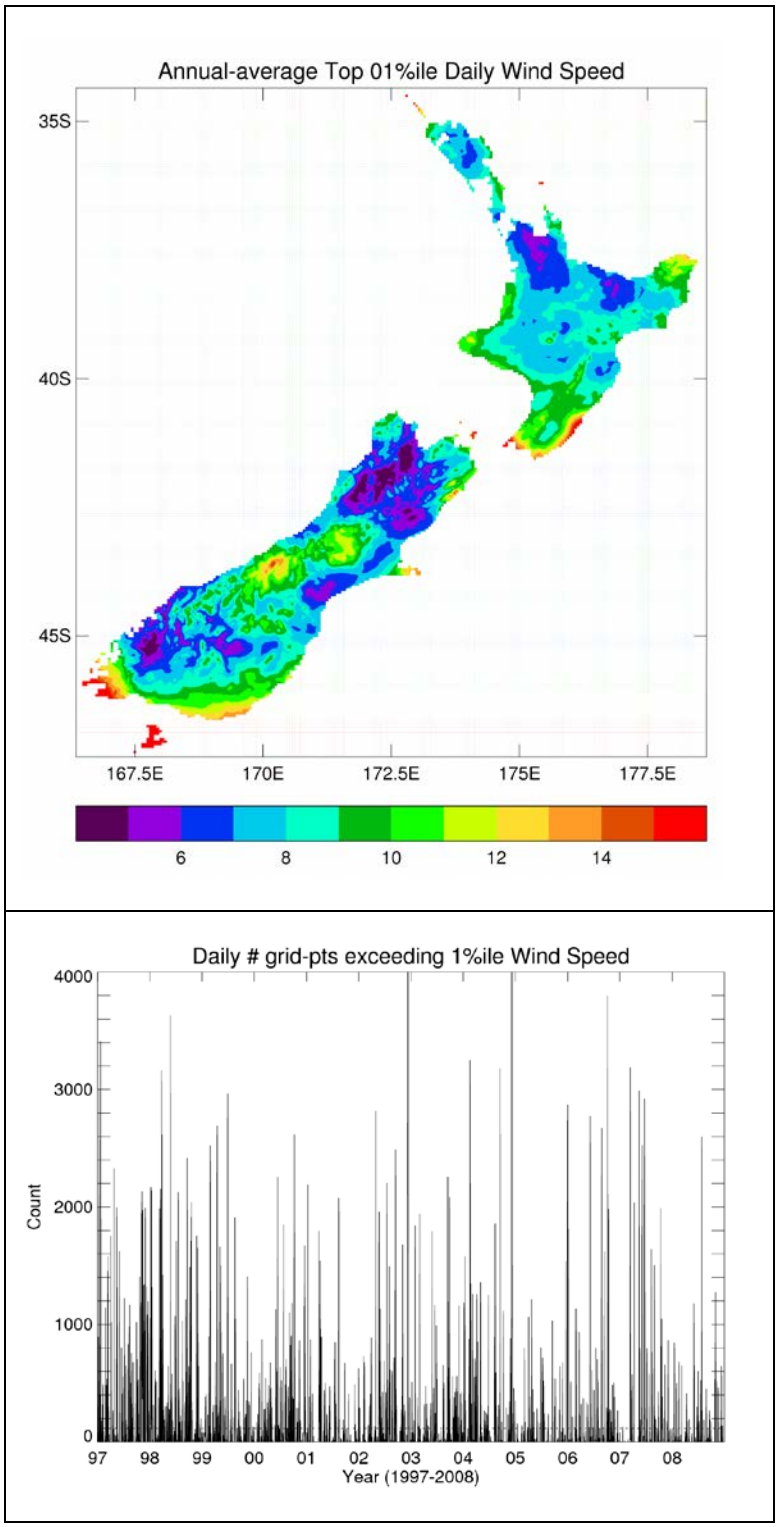

Figure 2: Spatial distribution (top panel) and temporal variation (bottom panel) of the top 1% of daily wind speeds (in m/s) over the 11,491 grid-points in NIWA's VCS wind data set. The horizontal dashed line in the lower panel marks a count of 115, the average daily expectation of the number of grid-points exceeding the 1 percentile.

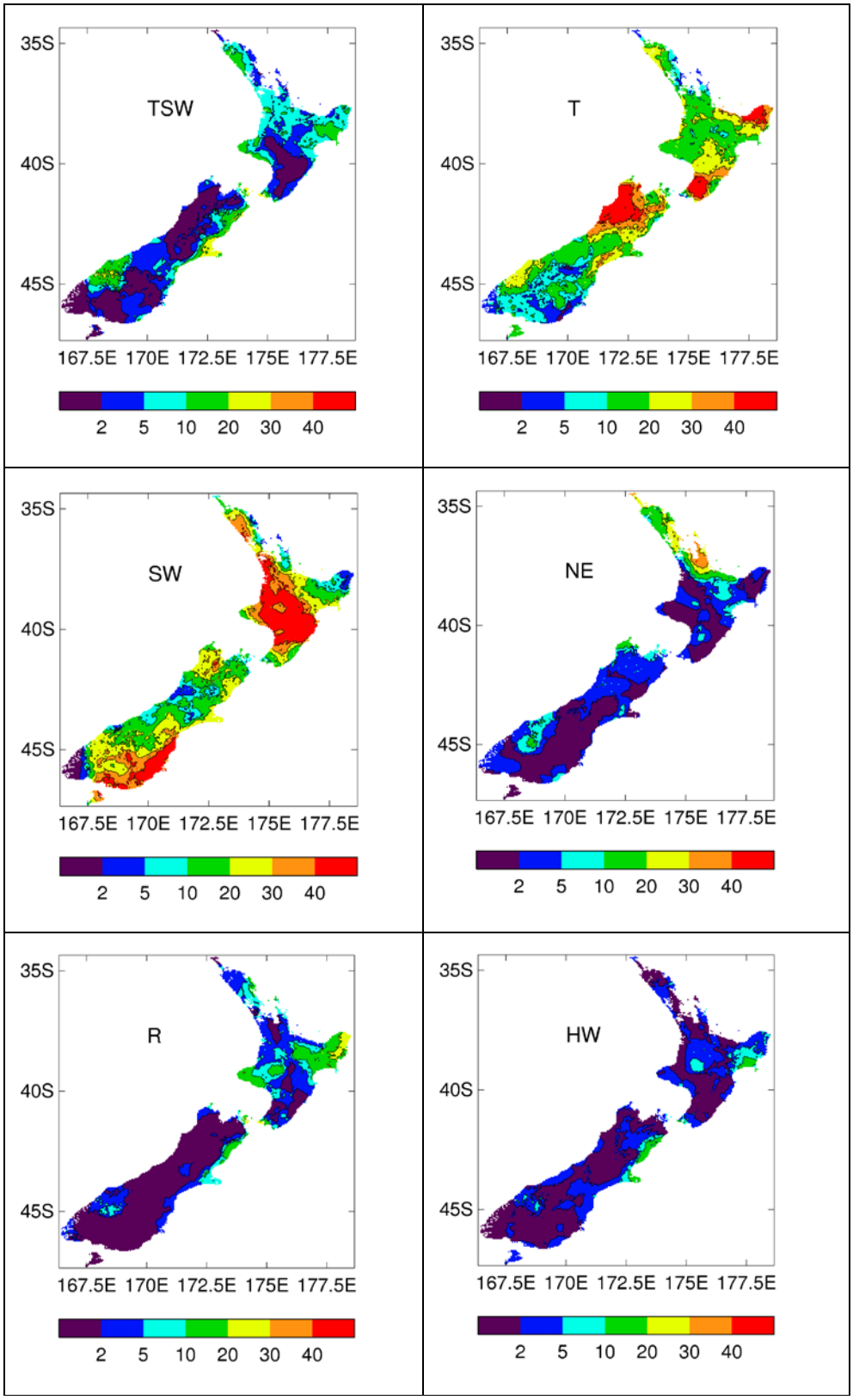

Figure 3a: Observed spatial variation of extreme winds for six of the 12 Kidson weather types. Maps show the percent frequency of occurrence of each Kidson type, given that the daily wind speed is in the top 1% at each 0.05°x0.05° grid point over New Zealand.

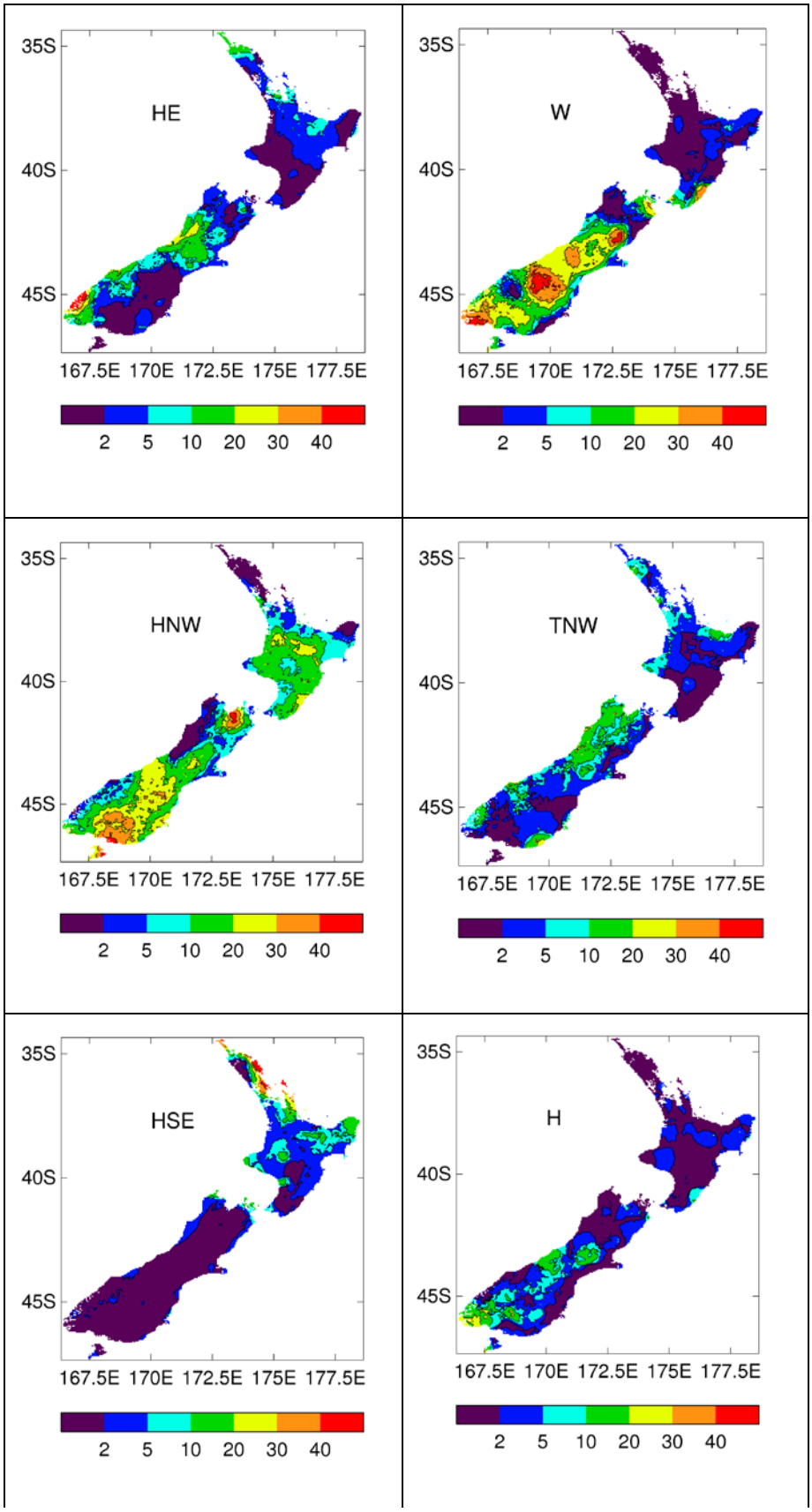

Figure 3b: As Figure 3a, but for the other six Kidson types.

2.3 Regional wind extremes from historical archives

The VCS analysis covered just 12 years of the recent record in terms of wind speed information. In order to make the results more robust, an extensive search of historical archives and reports was carried out (Table 4), to identify the occurrence and impact of string winds over a much longer period.

Table 4: Historical data sources used in compiling information on New Zealand wind extremes (see References list for full citation)

1. NIWA Hazards database (compiled by Julia Oh)
2. Burgess, 2004
3. Burgess et al, 2006
4. Burgess et al, 2007
5. Baldi et al, 2008
6. NIWA monthly climate summaries (http://www.niwa.co.nz/our-science/climate/publications/all/cs)
7. Vector reports (Griffiths et al, 2004, Turner et al, 2006, and Turner et al, 2007)
8. Somerville et al, 1989
9. NIWA National Climate Database (http://cliflo.niwa.co.nz/)
10. ERA40 99th percentile winds
11. Daily weather maps from NCEP or ERA40 re-analyses

2.3.1 Identification of historical extreme wind events

The aim here is to identify historical dates associated with extreme wind occurrence, or damage, in New Zealand, and classify the associated dates with a Kidson weather type, based on ERA40 data.

The search for extreme wind occurrence was undertaken regionally, based on 14 regions (Northland, Auckland, Waikato, Bay of Plenty, Gisborne, Hawkes Bay, Taranaki, Manawatu-Wanganui, Wellington, Nelson-Marlborough, West Coast, Canterbury, Otago, and Southland). These regions are the same as the Regional Council boundaries in all instances, except for the Nelson-Marlborough region, which merges the Territorial Authority (TA) areas Tasman, Nelson, and Marlborough.

Extreme wind occurrences were sought for the period September 1957 - August 2002 inclusive, this being the period over which ERA40 daily Kidson weather type

classifications exist, and between September 2002 and December 2008 inclusive (when NCEP Kidson weather type classifications were used).

Two approaches were used to identify dates of extreme wind occurrence. The first was to search the NIWA National Climate Database for *observations* of extreme winds; that is, when anemometer records showed a daily maximum wind speed above a threshold of 90 km/hr (which corresponds to 49 knots, or 25 m/s, or "storm force" on the Beaufort scale[2]), or above 103 km/hr (56 knots, 29 m/s, "violent storm force") in the case of Wellington and Southland, both of which have a high wind speed climatology.

A second approach was to determine dates of widespread, or severe, extreme winds via damage reports, media, or various NIWA reports containing damage or wind information. This approach was taken because of a lack of longer-term anemometer records (sites with wind data before 1970 and which are still active today, are quite rare), as well as known problems with anemometer data (i.e. homogeneity problems because of instrumentation changes and/or exposure change such as growth of trees).

Overall, media reports were "data sparse" in the 1950s, 1960s, 1970s and 1980s, relative to the 1990s and 2000s. This is probably because of the electronic dissemination of information has increased dramatically with the advent of the Internet. Also, the number of regular wind observing stations in the National Climate Database has increased since the 1990s, with the change to AWS (automatic weather stations). The consequence is that there are more "damage" dates, or observed extreme wind dates, in the latter part of the record, but this does not necessarily reflect a "more extreme" wind climate.

Overall, 14 regional files were produced, which contained dates of observed extreme winds, or reported wind-damage events, as well as the associated Kidson weather types, the data source, and any pertinent damage/impact information (these excel files are available from NIWA but not included as part of this report). When daily peak mean wind speed, daily average mean wind speed, and daily maximum gust data were available, these were included in the file. Several regions, such as Wellington, had numerous extreme wind events, and so culling was performed to ensure only about the top 1% of events were included in each file. It was notable that in regions of lower population, such as the West Coast of the South Island, media reporting on extreme wind events was quite low. In each file, only the top 1% of events (or less) was selected for analysis and weather typing (equating to no more than three days per year, on average, being typed).

[2] Beaufort scale, http://en.wikipedia.org/wiki/Beaufort_scale

In the Hazards database, the decision on whether to include an event was, occasionally, quite subjective:

- Localised tornado events were not included.
- Flooding/heavy rain events with gusts < 110 km/hr were not included.

When damage was 'maritime' in nature, it was not always included. For example, storm force winds blowing a ship into a wharf causing damage was included; loss of life at sea was not included, as many other factors (tides, sea state, boat handling) could influence this.

All of the reports and climate summaries (listed as 2-8 in the source list, Table 4) were read, and dates manually extracted into the files, when the event was extreme in an annual sense. In the Forestry reports (source 8, Table 4) there was an issue with some dates missing, but usually other sources could narrow down the likely date range.

A daily maximum gust file was produced from NIWA's National Climate Database (source 9, Table 4), based on long-term wind sites for all 14 regions, for all gusts > 90 km/hr (103 km/hr for Southland and Wellington). It was reassuring to see that the top gusts often replicated dates already found through the Hazards database, or other reports.

Finally, a count of weather types, and a plot of these, was produced for each of the 14 New Zealand regions (Figure 4). The results generally agree very well with the VCS maps (Figure 3). For example, strong winds from Kidson types NE and HSE are confined mainly to Northland, Auckland, and Waikato (which includes the Coromandel). Kidson type W affects mainly Southland and parts of Otago and Canterbury. Kidson type HNW gives consistent results (comparing Figure 3 and Figure 4) for Otago, Southland and Canterbury, but not for Nelson-Marlborough. The two results also agree for weather types R (Gisborne, Taranaki, Bay of Plenty), T (Bay of Plenty, Wellington, Nelson, West Coast), and SW (many areas, particularly Otago/Southland, Hawkes Bay, Manuwatu-Wanganui, Taranaki, Waikato, Auckland).

This general agreement on the association of extreme winds with daily weather types gives us confidence that the Kidson synoptic typing is an appropriate and robust framework within which to assess future changes in extreme winds over New Zealand.

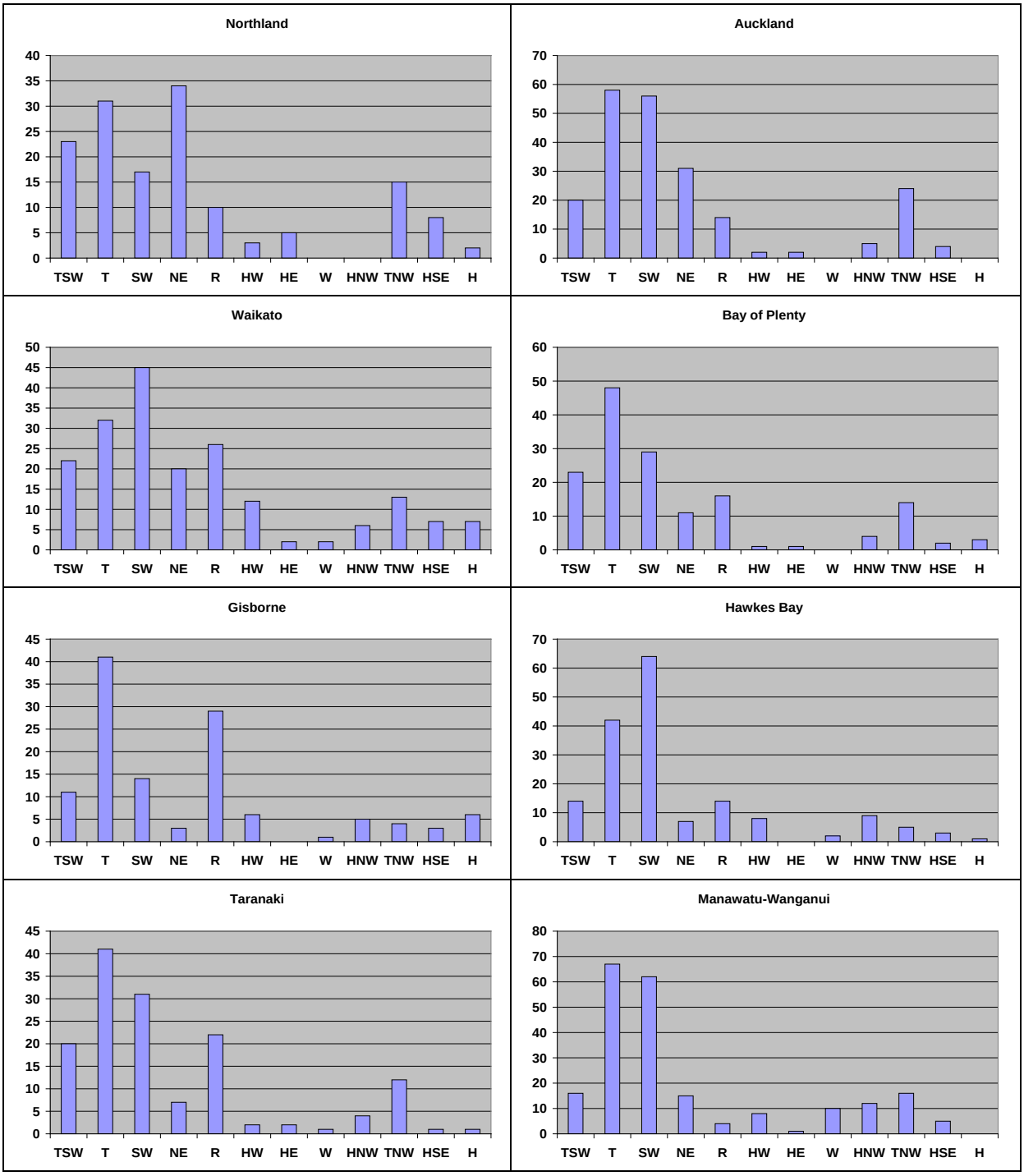

Figure 4a: Occurrence (in days) of extreme winds (approximately top 1 percent), subdivided by Kidson weather type, over the period 1957-2008, for eight North Island regions, as determined from historical archives.

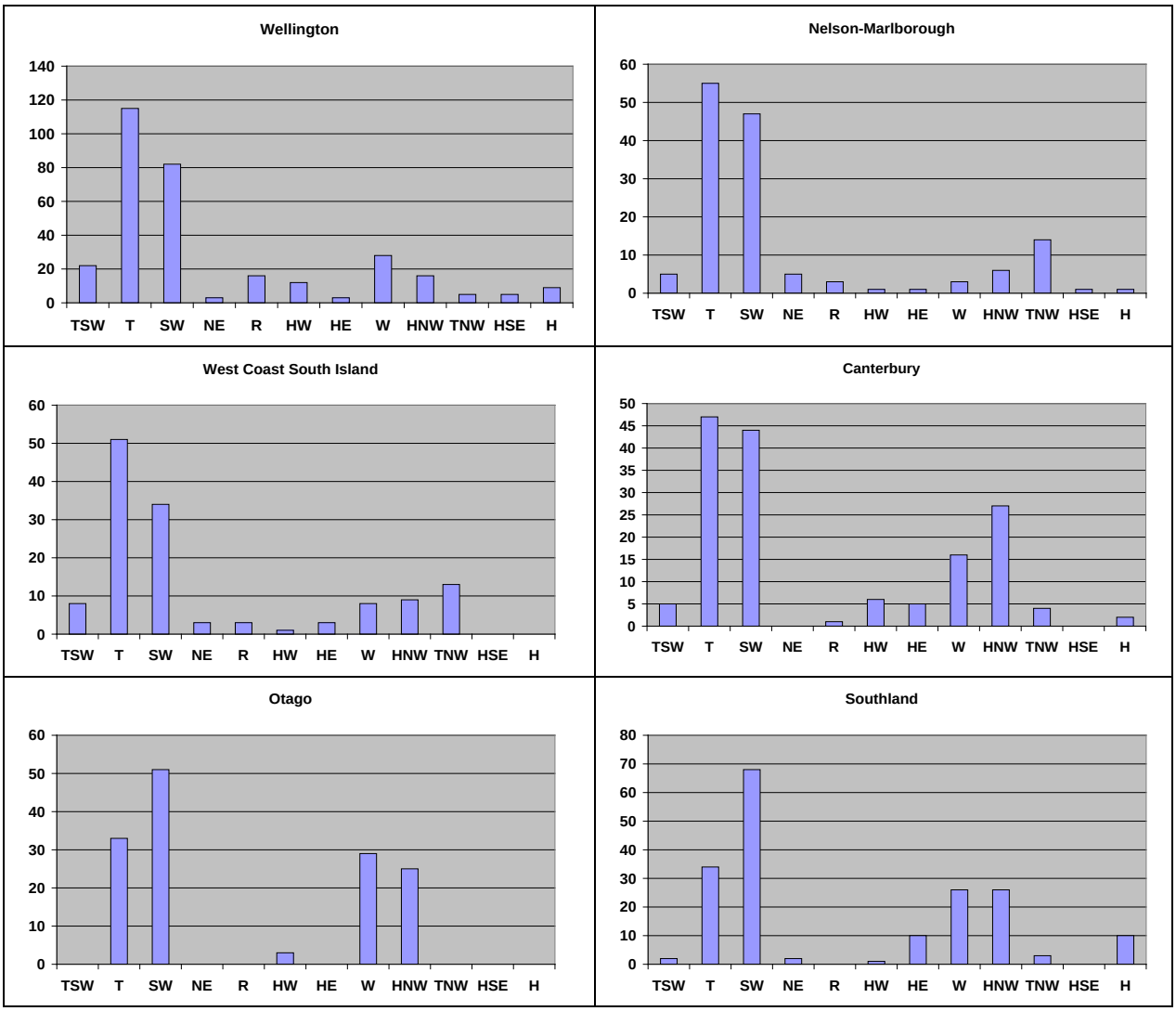

Figure 4b: As Figure 4a, but for the remaining six regions of New Zealand.

2.3.2 Low centre positions associated with extreme winds

Whenever the occurrence of extreme winds was noted, the location of the low pressure centre primarily responsible was also identified. The 'positions' of the low centres were classified into sectors, as denoted in Figure 5. The sectors fan out from New Zealand into the Tasman Sea and Pacific Ocean. Two additional 'sectors' were added, denoted by NI (North Island) and SI (South Island), when a low centre was very close to or crossing the New Zealand land area.

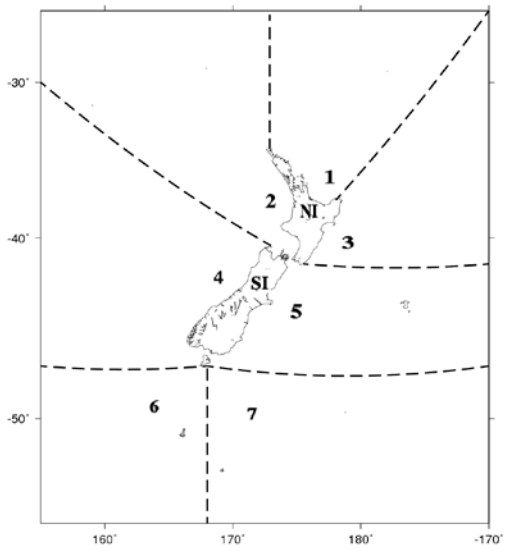

Figure 5: Classification of "low pressure centre" sectors associated with historical extreme winds

Figure 6 shows histograms of the low centre counts associated with extreme winds in each of the 14 Regional Council regions. For some regions, just one or two sectors stand out as contributing to most of the extreme wind situations. For example, for Northland 72 out of the 170 identified extremes (42%) were associated with lows approaching the North Island from the northwest (sector 2 in Figure 5).

The Auckland and Bay of Plenty regions were most affected by low centres in sector 2 (northerly flow) or sector 5 (southwesterly flow). Lows approaching the North Island from the north (sector 1) and northeast (sector 3) were the major contributors to extreme winds in the Gisborne region. The lows needed to be further south (sectors 3, 5, 7) to affect Hawkes Bay.

For Wellington, more than half the extreme wind situations (55%) were associated with lows in sectors 5 and 7; that is, south of Wellington and east of the South Island. Lows in these sectors were also the most important for extreme winds in Manawatu-Wanganui, Nelson-Marlborough, West Coast and Canterbury. For Southland, nearly half (47%) of the extreme wind cases had lows in sector 7, with sector 6 being the next most common location.

The global climate models do not have sufficient resolution to readily identify local wind extremes. However, they are quite able to resolve the major weather systems and predict changes in preferred storm tracks. Thus, classifying the positions of low centres can help us understand how the regional frequency of extreme winds might be influenced under changing climatic conditions.

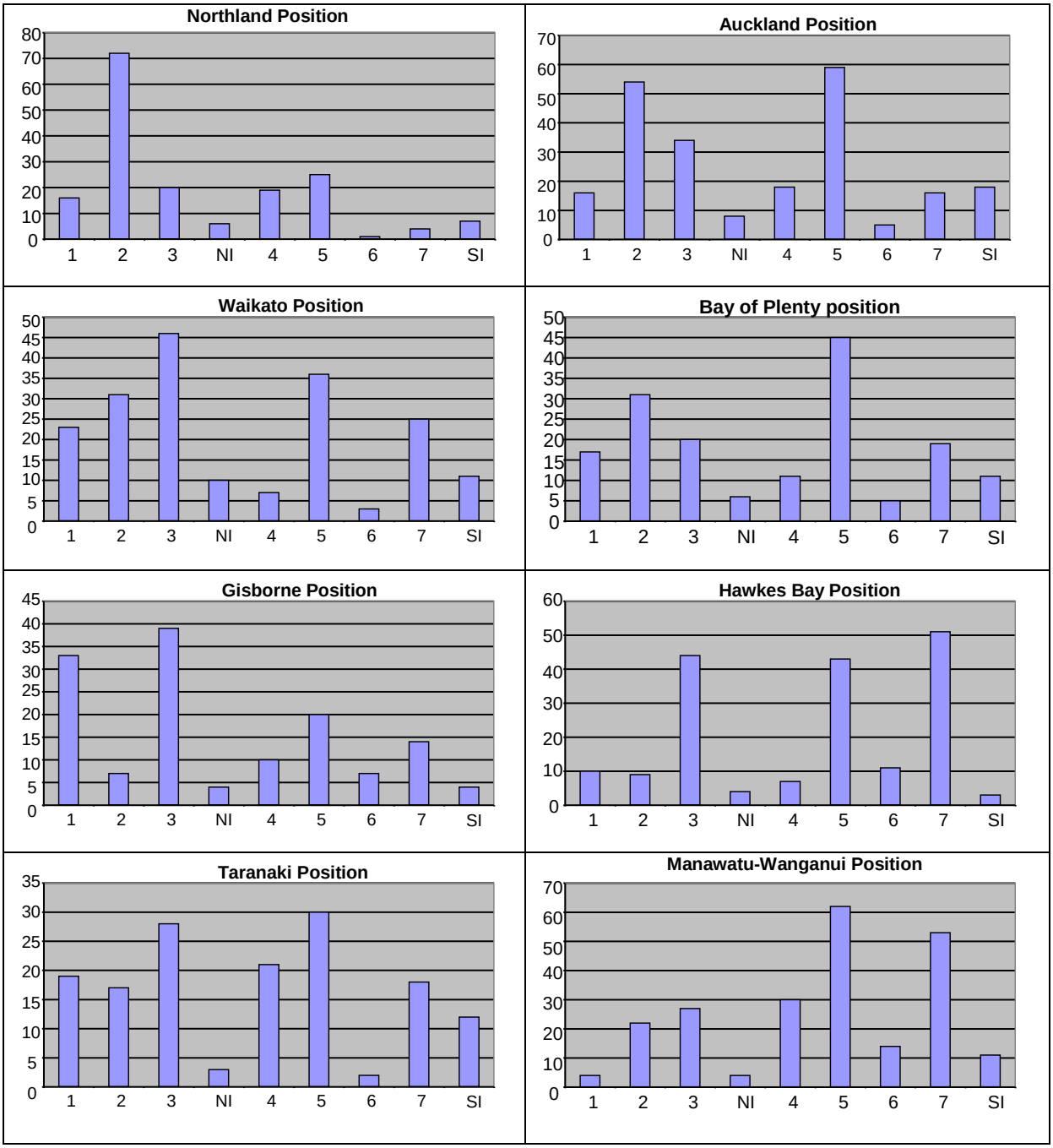

Figure 6a: Numbers of low centres in each sector (see Figure 5), associated with the top 1% of extreme winds in eight Regional Council regions, covering the period September 1957 to December 2008.

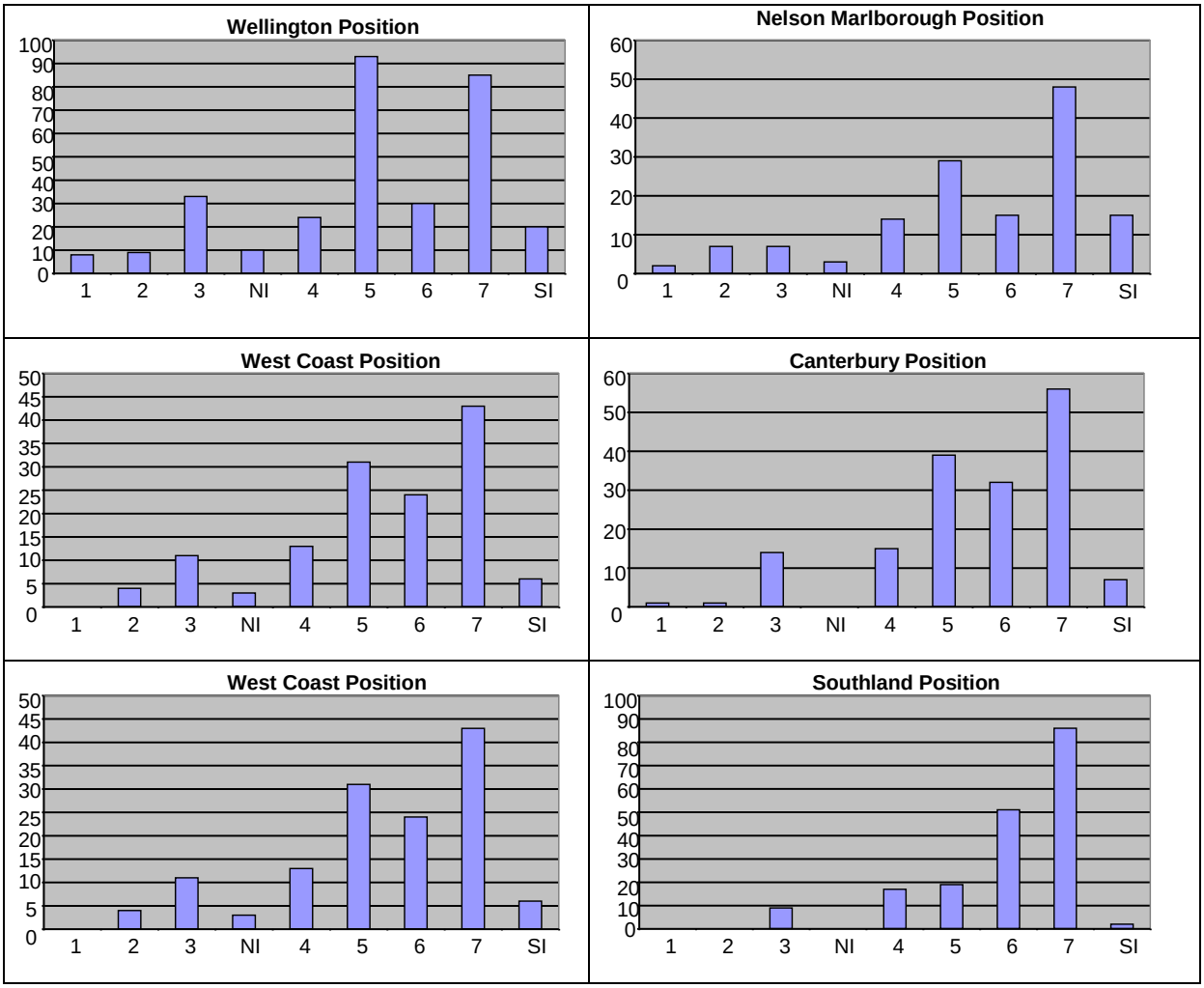

Figure 6b: As Figure 6a, for the remaining six Regional Council regions.

3. Future changes in circulation patterns and wind distributions

This chapter describes changes to circulation patterns and wind distributions in the New Zealand region, as diagnosed from the global climate models (GCMs) of the IPCC Fourth Assessment (AR4). The focus is on the daily data which has not previously been analysed for New Zealand (for example, MfE (2008) just examined monthly averages from which only weak inferences could be drawn about wind patterns). Table 1 shows the numbers of models available which provided daily pressure and wind data to the IPCC data archive. For example, there are 23 GCMs with daily pressure data for the 20th century simulation (20c3m).

3.1 GCM trends in Kidson circulation types

The Kidson weather typing algorithm was applied to daily mean sea level pressure data from 23 AR4 GCMs (as in Table 1) for 40 years of the 20c3m run. Some of the models are known to have deficiencies in their monthly pressure and wind fields, so we first validate the models in terms of how their 20th century climate matches with the distribution of observed Kidson types. Note that we can only look at the overall climatological distributions and cannot match up the actual daily Kidson types and sequences, since the GCMs are free-running models unconstrained by any observations over 1961-2000 except for greenhouse gas concentrations and volcanic eruptions. Hence, while the GCMs are expected to reproduce well the *statistics* of the daily weather, they will not reproduce the observed daily *sequence* of weather events.

A metric was designed to validate key features of the daily Kidson types, where each model was compared against the climatology from the ERA40 re-analysis over the same period 1961-2000. As a minimum, we would like the climate models to have a similar frequency of each weather type to that observed in ERA40, and to show a similar seasonal variation. Calculations were made of the following:

- The frequency of each Kidson weather type (KT) by calendar month over 1961-2000, for the 23 GCMs and for the ERA40 observations;
- The root-mean-square difference between the KT frequencies (model versus ERA40) over the whole year (the “Annual” metric);
- The root-mean-square differences between the KT frequencies (model versus ERA40) aggregated over the four seasons (the “Seasonal” metric);
- The root-mean-square difference between the KT frequencies (model versus ERA40) for summer minus those for winter (the “Summer-Winter” metric).

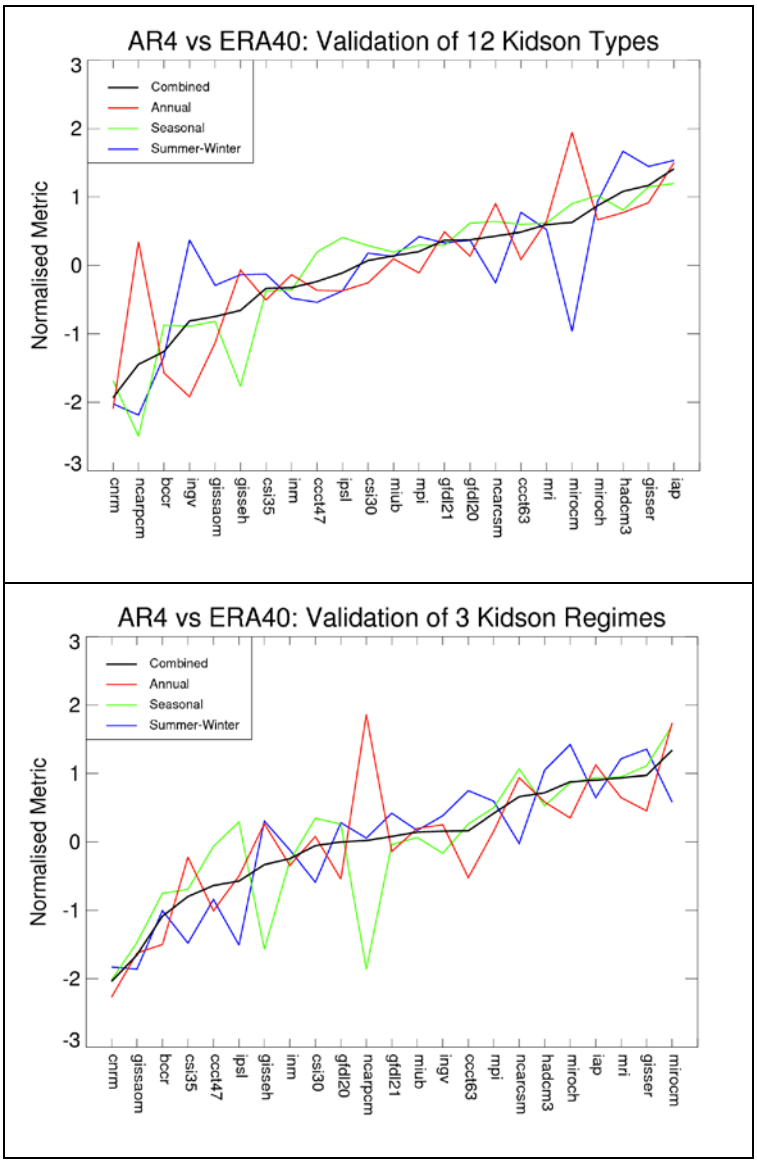

Figure 7: Normalised metric showing the ranking of each AR4 GCM in terms of its fidelity in reproducing the climatological distribution of the 12 Kidson types (top panel) and the 3 Kidson regimes (bottom panel). Higher values represent better model performance. Coloured lines apply to the 3 separate metrics as defined in the text, and the black line is the average over all three.

The three RMS differences were then transformed into a normalized metric, which increases with skill, given by

$$m = -\left[\frac{R - \mu_R}{\sigma_R}\right]$$

where R is the RMS difference (Annual, Seasonal or Summer-Winter), and μ_R and σ_R are the mean and standard deviation of R, respectively. The minus sign is needed because *R* is smallest for the best model, and we want *m* to increase with skill. The metrics for the individual features are shown with coloured lines, with the black line the average of the three metrics.

Figure 7 shows the rankings in terms of performance on the Kidson types (top panel), and also when the individual types are aggregated into the three regimes (bottom panel). Where the individual weather types do not match well with observation (ERA40), there is the possibility of compensation across a regime, so the ordering of the models is not quite the same in the two panels. However, the top six models are common to both validation checks: *iap, giss-er, hadcm3, miroc-hires, miroc-medres,* and *mri* (in descending order for the 12 weather types). The top model over the Kidson types is the Chinese GCM *iap,* which has a normalized metric aggregate score of +1.41. (For comparison, the NCEP re-analysis over the same period has a normalized metric score of +3.20, relative to the ERA40 re-analysis). The poorest performing models are (from worst): *cnrm, bccr, giss-aom,* and somewhat surprisingly, *csiro_mk3.5*.

Daily pressure data from the future scenario runs SRESA1B and SRESA2 were then analysed, and the simulated future frequencies of the Kidson types evaluated. Results are summarized in Figure 8 for the summer and winter seasons, and in Table 5 for the four seasons and the annual case. Changes in the frequency of each Kidson type were calculated over all models available for each scenario (see Table 1), and also for the top 10 available models (as determined from the validation assessment, Figure 7). Figure 8 gives the frequency changes averaged over the "top 10" models; however, where this differs significantly from zero, the change has the same sign when averaged over all 20 (A1B) or 18 (A2) models. Note too that the changes are larger under the stronger greenhouse-gas forcing (ie, A2, red lines).

The graphs are shown for the summer and winter seasons because it was found that the changes over the full calendar year were very small. The current climatology of the Kidson types is also plotted on Figure 8 to place the changes in context.

For the trough types, the trough in southwesterly flow (TSW) is projected to increase in frequency by about 4% by late this century on average, which would promote it to the third most frequent summer weather pattern (about 13% of the time). However, trough types T and SW are projected to become less frequent in future summers. While there is little change overall in the summer frequency of trough-type weather patterns, the changing mix (increased TSW type, decreased T and SW types) would be

likely to affect the occurrence of strong winds. For all New Zealand regions with the exception of Northland (Figure 4), trough types T and SW are more important than type TSW in the generation of extreme winds. We might therefore expect that the frequency of extreme winds in summer, as they relate to trough weather types, would decrease over New Zealand, especially for Wellington region and all of the South Island[3].

The projected change in the trough types over the winter season are almost the reverse of those in summer. Thus, the opposite comments apply, viz: an increase in the frequency of extreme winds (related to trough types) in almost all regions, but especially Wellington and the South Island regions.

The zonal weather types show the clearest pattern of seasonal change; all three zonal types (W, HNW, H) are projected to decrease in frequency in summer but increase in frequency in winter. The weather types (especially W and HNW) have their biggest influence on the occurrence of extreme winds in Canterbury, Otago and Southland. Thus, the projections suggest fewer extreme winds, associated with zonal weather types, in summer but more extremes in winter for the south and east of the South Island. Zonal type H is the most frequent of all weather types in winter (Figure 8, 16.3% occurrence over 1961-2000 according to the ERA40 re-analysis), and the projections suggest it will become even more dominant.

For the five blocking types (NE, R, HW, HE, HSE), the main changes projected by the models are for types NE and R to become more common in summer but less common in winter, so again there is compensation over the year. Type NE affects mainly Northland, Coromandel and Bay of Plenty, whereas type R affects mainly Gisborne and Taranaki (Figures 3 and 4). Thus, an increase in the frequency of summer extreme winds, associated with increased blocking weather types NE and R, could occur in the regions identified above. Types NE are most common in the summer season anyway (10.2% for NE, 7.4% for R), and type NE with northeasterly flow into the Bay of Plenty is projected to become the second most common summer weather pattern (after HSE). These blocking types are only rarely associated with extreme winds in Wellington and the South Island.

[3] Note that there is a caveat to this statement. We are examining the changing frequency of each weather type but not the intensity of the low pressure centre. So the comment relates to frequency of extreme winds, not the actual intensity of the events.

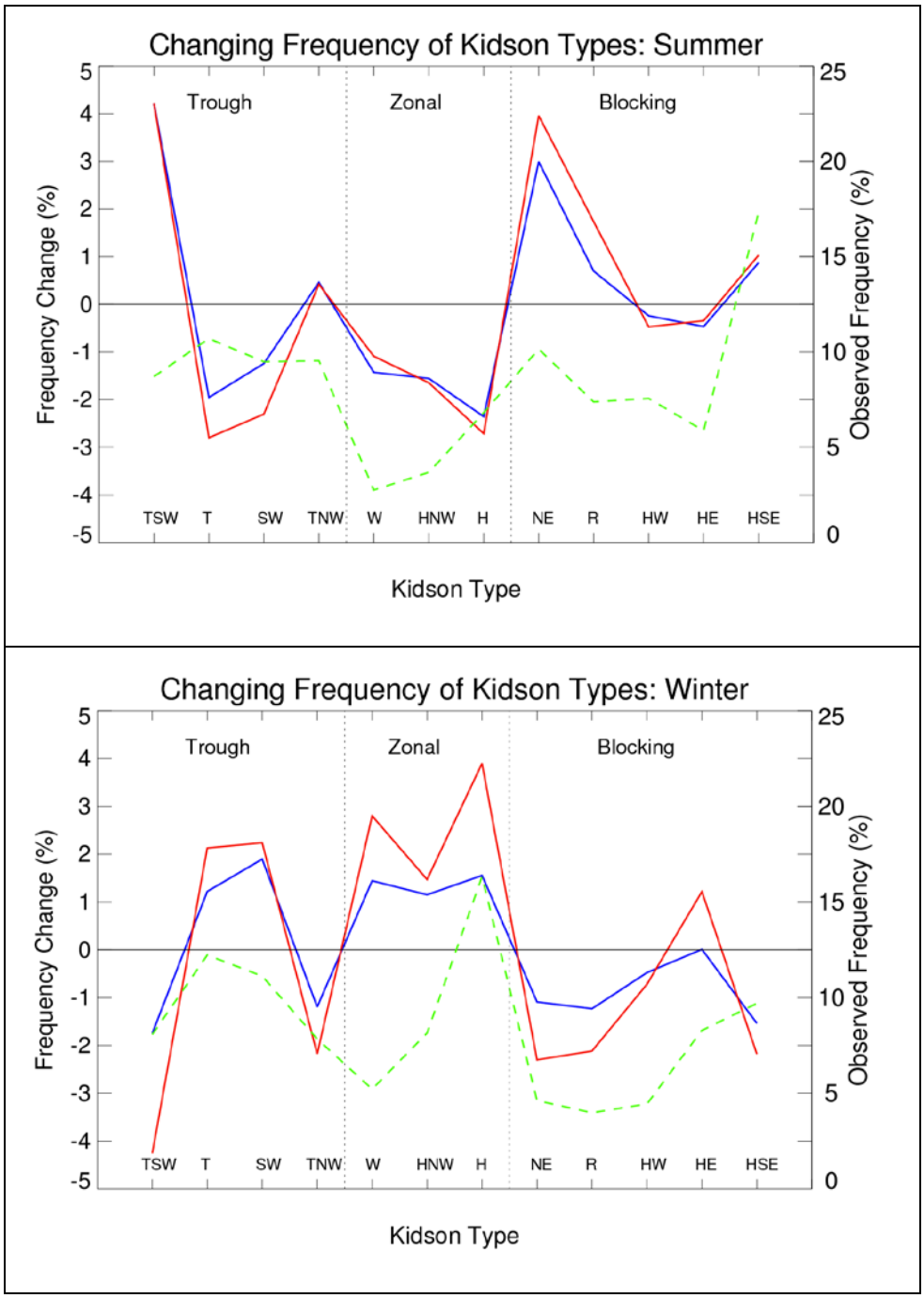

Figure 8: Observed frequency 1961-2000 (dotted green line, right-hand ordinate scale), and projected frequency change 1961-2000 to 2081-2100 (blue, SRESA1B scenario; red, SRESA2 scenario, left-hand ordinate scale) of the 12 Kidson weather types for summer (top) and winter (bottom) seasons. The types are identified along the bottom of each graph, and are grouped by regime, as labelled. The changes are averaged over the 10 best-validating models, as identified in the top panel of Figure 7.

Tables 5 and 6 provide similar information to Figure 8, but all four seasons are shown, and there is also a breakdown by regime as well as by the individual weather type. It can be seen that the autumn changes follow those of summer, whereas spring has similar frequency changes to winter. For the overall regimes, the most notable projected changes are for a decrease in the zonal weather patterns in summer and autumn, and an increase in winter and spring; and an increase in blocking in autumn and a decrease in winter. There is virtually no signal in the annual statistics.

Table 5: Significant changes in Kidson type frequencies, between 1961-2000 and 2081-2100, by season and SRES scenario. A "+" or "–" sign indicates that the frequency increases or decreases, respectively. Cells are only populated where the average change exceeds the standard deviation, based on the top 10 validating models (Figure 7). A bold "+" or "–" indicates <u>all 10 models</u> (or all that have data for that scenario) have the <u>same sign</u> in the frequency change. A "*" next to the sign indicates the average frequency change is at least twice the standard deviation across the 10 models.

	Trough Types				Zonal Types			Blocking Types				
Season / **Scenario**	**TSW**	**T**	**SW**	**TNW**	**W**	**HNW**	**H**	**NE**	**R**	**HW**	**HE**	**HSE**
Ann: A1B			+					+				
A2												
Sum: A1B					–	–*	–*	+				
A2	+	–	–*		–*	–*	–*	+				
Aut: A1B					–*	–*	–	+	+			
A2					–	–*	–	+	+*			
Win: A1B			+*	–				–	–			–
A2	–*	+	+*	–	+*	+	+*	–*	–	–		–
Spr: A1B			+									
A2			+	–	+	+		–	–		–	

Table 6: As Table 5, but for the 3 regimes instead of the 12 individual weather types.

	Trough	Zonal	Block
Annual: A1B			
A2			
Summer: A1B		–	
A2		–*	
Autumn: A1B		–	+
A2		–	+
Winter: A1B			–
A2	–	+*	–*
Spring: A1B			
A2		+	

3.2 GCM projections of daily wind distributions

Whereas the previous section examined the daily pressure data, this section considers daily near-surface winds[4], and focuses on the zonal west-east component identified by the model variable labelled "uas".

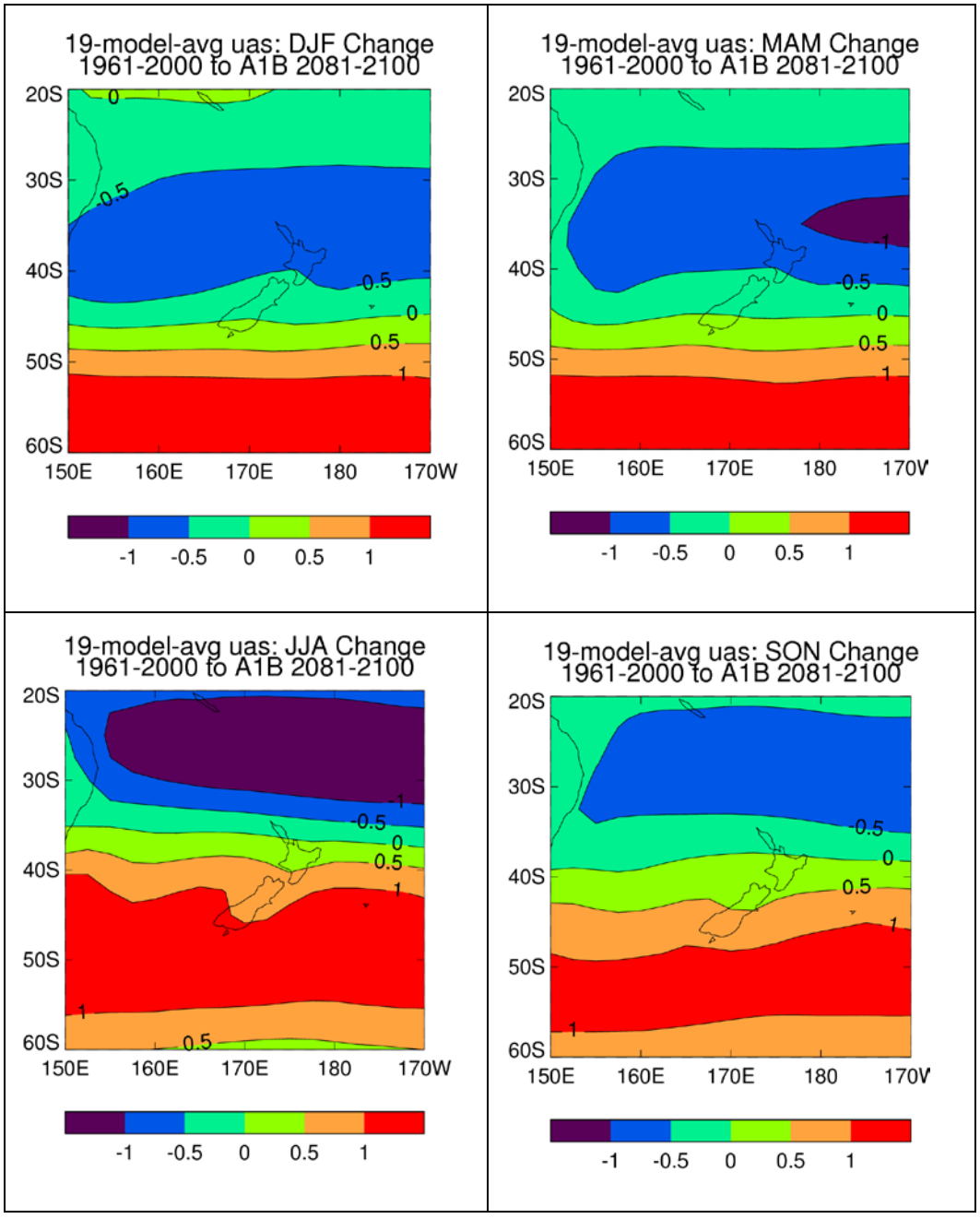

Figure 9: Projected change (in m/s) in the west-east component of the 10-m wind between 1961-2000 and 2081-2100, averaged over 19 GCMs run under the SRESA1B scenario: each season is shown separately.

[4] In the climate models, "near-surface" is interpreted as the 10-metre wind.

Figure 9 shows the 19-model average change in the seasonal mean west-east wind, as calculated from the daily wind data, between the 20th century simulation over 1961-2000 and the SRESA1B simulation at the end of this century, 2081-2100. In all seasons there is an increasing easterly tendency over or north of the North Island. In the summer and autumn seasons, there is an increase in easterly (in practice, this will more commonly be a decrease in westerly) over the entire country with the exception of Otago and Southland. In winter and spring, the easterly tendency is confined to the north of the North Island from about Coromandel Peninsula northwards, with the remainder of New Zealand experiencing an increasing westerly tendency.

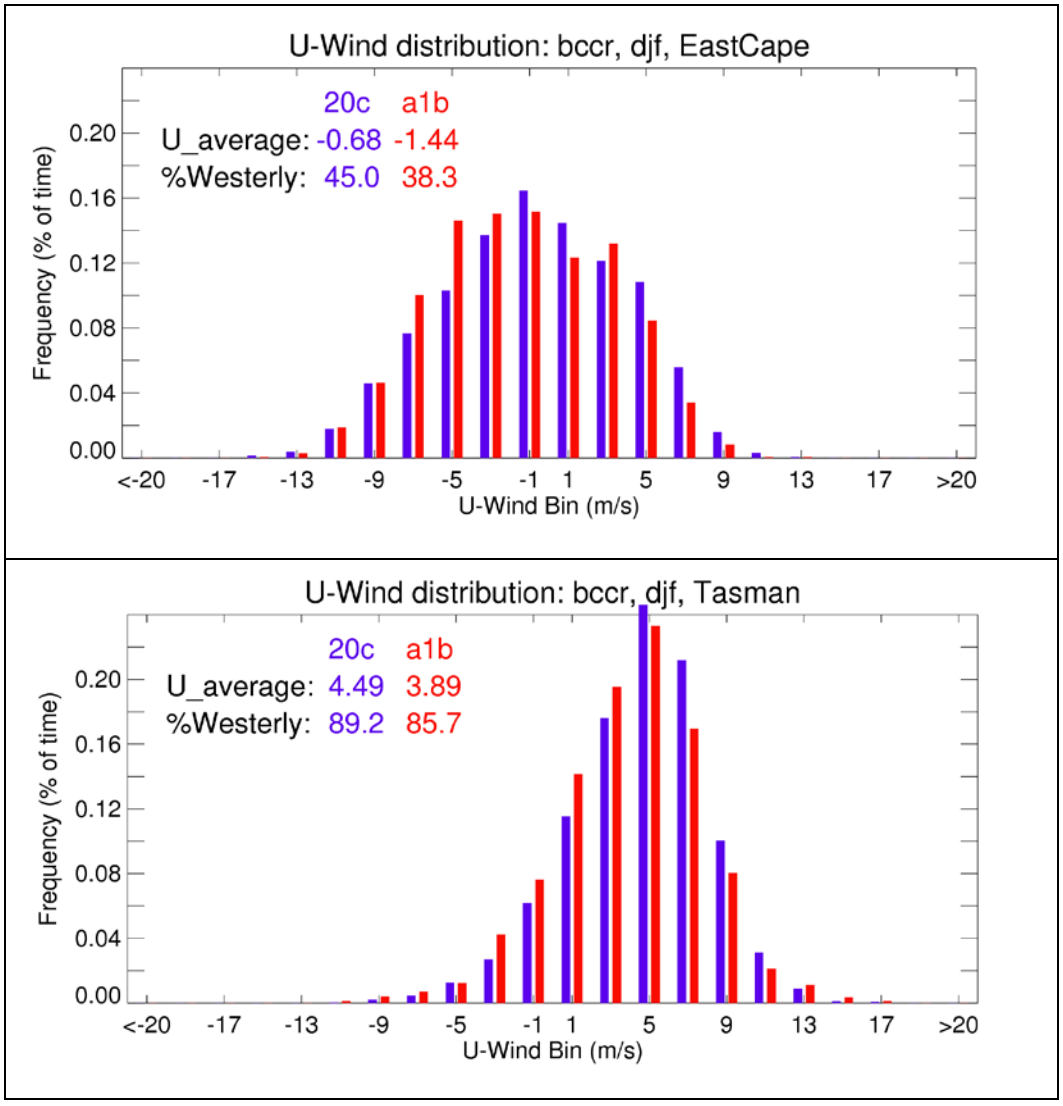

Figure 10: Example histogram of daily west-east wind distribution in summer from the bccr GCM (see Table 1). Daily wind speeds are grouped into 4 m/s bins, and show as blue bars for the 20th century (1961-2000) and red bars for SRESA1B in 2081-2100. The inset numbers show the average westerly (negative if easterly), and the percentage of westerly days. Results are shown for two grid-points, to the east of the North Island ("East Cape", and to the west of the South Island ("Tasman").

Figure 9 only shows the seasonal means, but with access to daily wind data we can examine the full distribution. Figure 10 shows an example for the *bccr* global climate model in the summer season. The histogram plots show the daily wind distributions at two grid-points: the "Tasman" grid-point at 45S, 165E is selected as representing wind flow onto the west of the South Island, and the "East Cape" grid-point at 35S, 180 as representing air flow onto the east of the North Island. Both points are sufficiently far from the country that the different GCM representations of New Zealand topography should not adversely affect the wind flow results.

For this particular model, the "Tasman" west-east wind in summer decreases from 4.5 to 3.9 m/s between 1961-2000 and 2081-2100, along with a drop in the percentage of westerly days from 89.2% to 85.7%. At the "East Cape" grid-point in the same season, the mean wind is an easterly (negative sign convention) and is projected to increase from 0.7 to 1.4 m/s as a seasonal average. The frequency of individual days with easterly flow increases from about 55% to 62%.

Similar calculations were made for all 19 GCMs (Table 1) with daily wind data for the A1B scenario. The result is summarised for each season in Figure 11, where the "probability" of an increase in the number of westerly days is mapped over the Tasman-New Zealand region. What we are calling the probability here is actually the percentage of the 19 models that show an increase. At this stage, there is uncertainty about how well the AR4 climate models span the full range of possible responses of the global climate system to greenhouse-gas warming.

On this basis of the AR4 model sample available, the simulated wind changes suggest there is at least an 80% chance of an increasing number of easterly days in the summer (DJF) and autumn (MAM) seasons over the North Island from about Hamilton to East Cape northwards. The tendency for more easterly versus more westerly days is about 50:50 at Christchurch in these seasons; south of Christchurch the tendency is for more increases in westerly days in summer and autumn.

The situation in winter (JJA) and spring (SON) is quite different. There is a 50:50 chance of more easterly versus westerly days over Northland, but for the remainder of the country the likelihood of more westerly days increases as one moves south. By Christchurch, there is a 90% chance of an increase in westerly days in winter and spring.

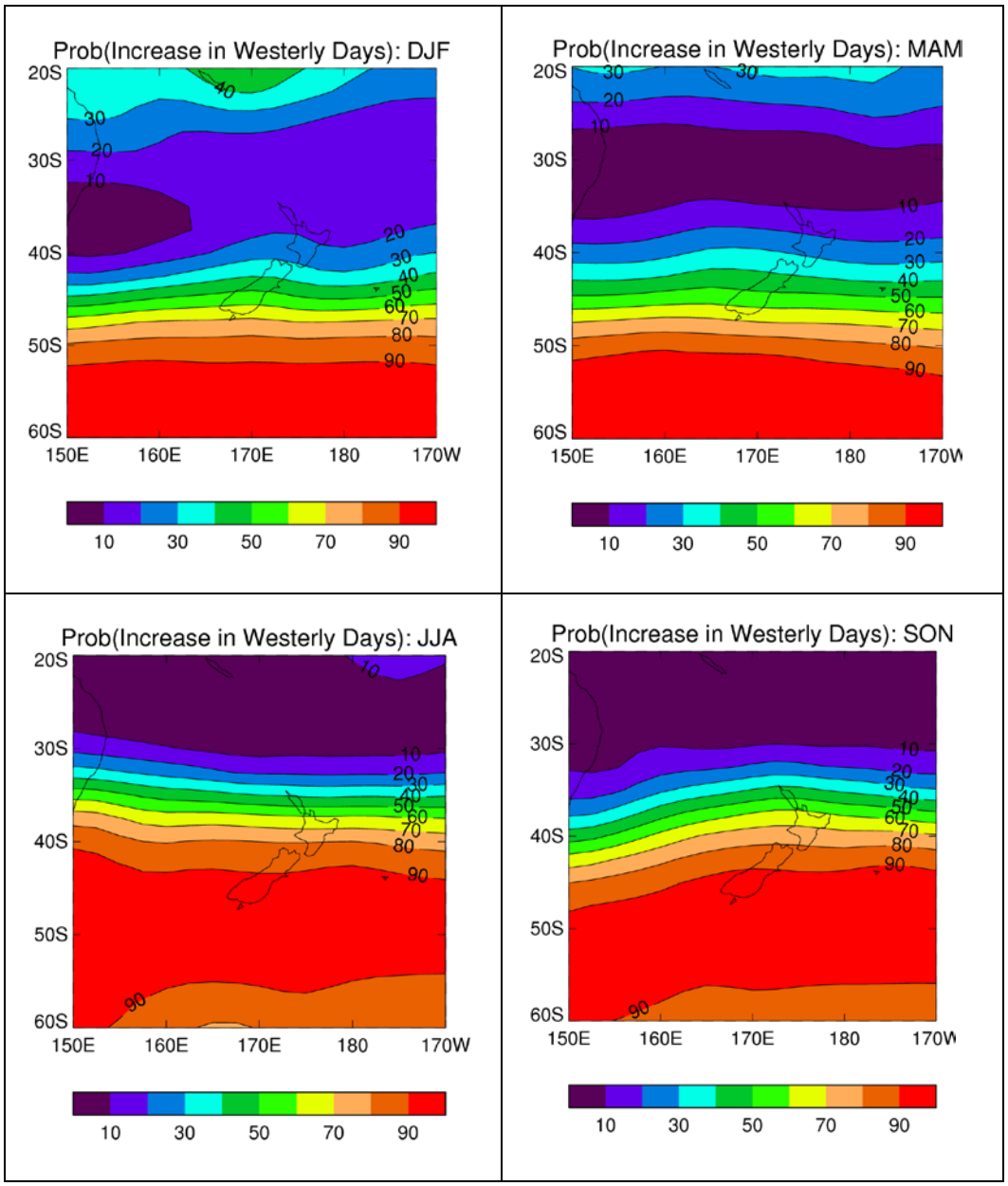

Figure 11: Probability that the number of westerly days will increase, separately for each of the four seasons, between the current climate (1961-2000) and 2081-2100 under an SRESA1B emission scenario.

4. Cyclone Strengths and Frequencies in the New Zealand Region

Extra-tropical cyclones play a dominant role in determining the local weather and in particular are often the underlying cause of extreme wind events. Understanding how the intensity and frequency of cyclones[5] may change in a future, warmer climate can therefore give insight into how extreme wind events may change.

Investigations of cyclone activity are generally done with the aid of cyclone detection software, which can either operate on gridded reanalysis data or output from global or regional climate models. For a recent review of studies into the present and future characteristics of extra-tropical cyclones see Ulbrich *et al.* (2009).

Using NCEP reanalysis data, it has been shown that in the Southern Hemisphere (SH) mid-latitudes (40–60° S), the frequency of cyclones (depicted as the cyclone density) has decreased over the last 4 decades of the 20th century (Fyfe, 2003; Simmonds and Keay, 2000a and b). However cyclone intensity in this latitude band has, in general, increased during this time.

Climate model predictions of changes between present and future climate scenarios show similar patterns. Using the ECHAM5 coupled climate model, Bengtsson *et al.* (2006) found that in the SH there is a poleward shift of the storm track, resulting in a reduced cyclone density from 35–60° S in summer and 30–45° S in winter in the New Zealand region. They attribute this shift to a poleward movement of the maximum zonal Sea Surface Temperature (SST) gradient.

Over the whole hemisphere, Bengtsson *et al.* (2006) found a decrease in cyclone density, except for the strongest storms for which there was a slight increase in density. These results echo those found by Lambert and Fyfe (2006) using an ensemble of IPCC AR4 global climate models. They found that in the SH the models simulated a reduction in the total number of events and an increase in the number of intense events.

Lim and Simmonds (2009) demonstrated that the reduction of SH extra-tropical cyclone frequency and depth (a proxy for intensity) in the mid-latitudes but a slight increase in the high latitudes is a result of tropical upper-tropospheric warming. This increases the meridional temperature gradient at high latitudes and contributes to the increase in cyclone activity from 50–60° S.

[5] Note that 'cyclone' as used here does not include tropical cyclones.

The study presented here applied storm identification software to daily mean sea level pressure output from an ensemble of climate models from the World Climate Research Programme's (WCRP's) Coupled Model Intercomparison Project phase 3 (CMIP3). The simulations from these models were analysed for the IPCC Fourth Assessment (see Table 1). The particular focus was on validating the CMIP3 models' representation of cyclone density (a proxy for frequency) and intensity in the New Zealand region against ERA40 reanalysis and consequently examining the differences between the current and future climate for a selection of scenarios.

4.1 Storm Identification

The low-identification component of the storm tracking software system developed at the University of Melbourne was used in this study (Simmonds and Keay, 2000a; Simmonds *et al.*, 1999).

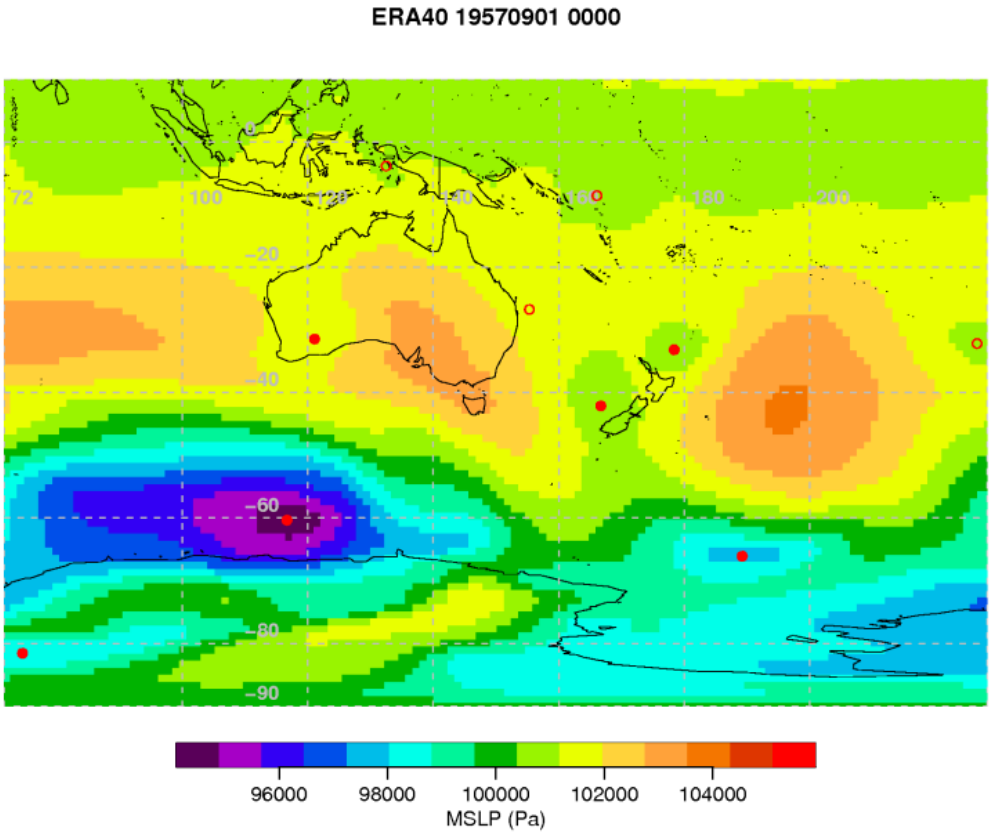

Figure 12: The MSLP field valid at 1957-09-01 00 UT (Universal Time) from ERA40 reanalyses. Cyclone identification is depicted using red filled circles for closed lows and open circles for open lows. As part of the identification process, the depth, radius and minimum central pressure of the low is also estimated.

The low-finding routine begins by searching for a maximum in the Laplacian of the mean sea-level pressure (MSLP) field. The position of the associated pressure

minimum is then located by iterative approximation to the centre of the ellipsoid of best fit to the pressure surface. If a closed centre cannot be found or does not lie within a very small distance, the routine also searches for an "open depression". The Laplacian of the pressure in the vicinity of the centre can be taken to be a measure of the strength of the system and systems that fail to reach a specified minimum strength can then be excluded.

For the purpose of validating the 20th century CMIP3 simulations, the storm identification process was first applied to the ERA40 reanalysis data set. An example of storm identification using ERA40 reanalysis data is shown in Figure 12.

4.2 Validation of CMIP3 models

4.2.1 Cyclone Density

Mean cyclone density (a proxy for cyclone frequency) has been calculated for ERA40 data and CMIP3 AR4 models (where data was available). A comparison of cyclone density in the NZ region for 1961-2000 is shown in Figure 13.

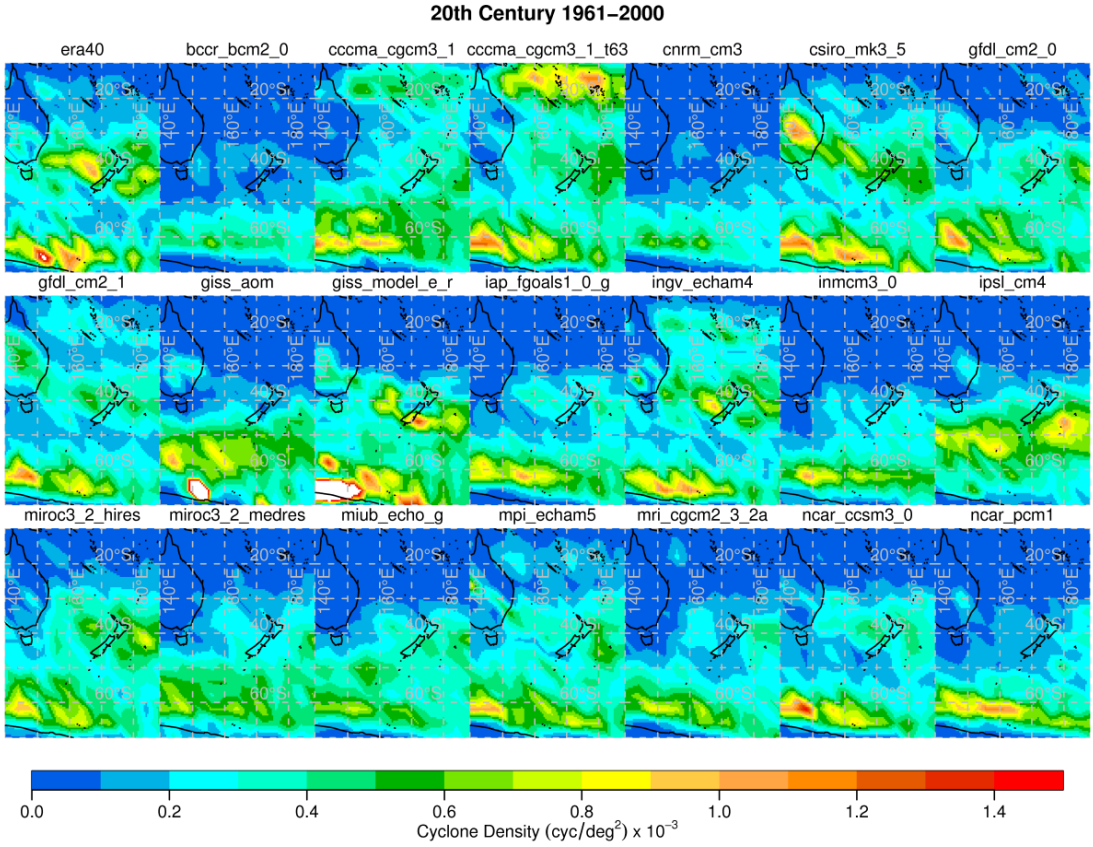

Figure 13: Cyclone density in the New Zealand region for the ERA40 reanalysis data set (top left) and 20 CMIP3 global climate models. Each map covers the region 10–70°S and 140°E —170°W.

The ERA40 reanalysis data set shows two main regions of cyclone activity, one around latitude 40°S and the other south of 60°S (top left map in Figure 13). There is also a weak region of activity north of 20°S.

It is evident that some of the CMIP3 models reproduce the ERA40 climatology more accurately than others. Most simulate the band of strong cyclone activity south of New Zealand well, although *ipsl* and *giss_aom* place it closer to New Zealand between 50 and 55°S. The increased cyclone density at 40°S is only reproduced well by a subset of models, namely: *csiro_mk3.5, gfdl_cm2.1, giss_er,_ingv, miroc3_hires, mpi,* and *ncar_ccsm3*. However, most of the models have some hint of increased activity around New Zealand. A small number of models have the 40°S maximum either much too weak or missing entirely: *bccr, cnrm, giss_aom*, and *ncar_pcm1*.

The weak region north of 20°S noted above is overestimated in two of the models (the Canadian *cccma* models at t47 and t63 resolution), completely missing in most models, and only represented well in four models (*csiro_mk3.5, gfdl_cm2.1, ingv*, and *mpi*). Note, also, that the *csiro_mk3.5* model has a local maximum in cyclone density over eastern Australia. This feature is present in the observations (ERA40), and in a number of the other models, but is much more pronounced in *csiro_mk3.5*.

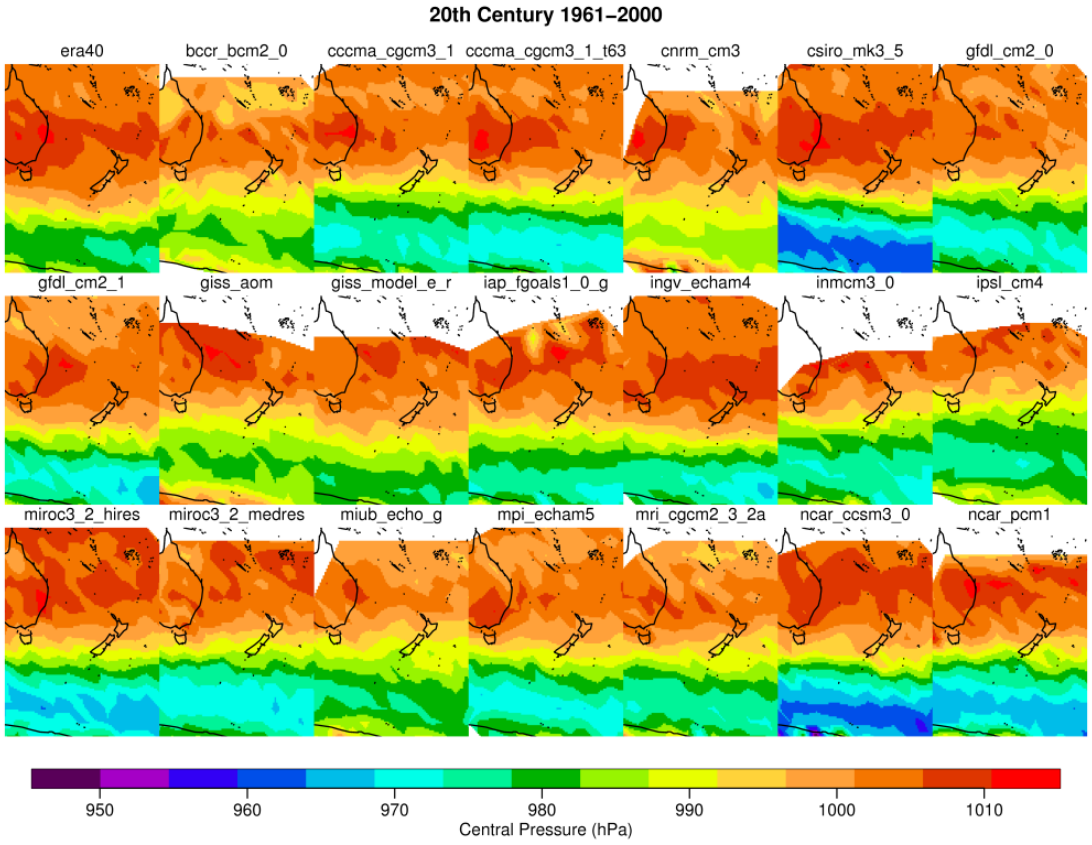

Figure 14: As in Figure 13, but for cyclone central pressure. Blank spaces on the maps indicate where almost no low centres were found for that model.

4.2.2 Cyclone Central Pressure and Cyclone "Radius"

A comparison between ERA40 reanalysis and each of the CMIP3 climate models for the mean annual central pressure of identified cyclones is shown in Figure 14. This figure shows much more consistency between ERA40 and the ensemble members. The majority of CMIP3 models show a spatial pattern very similar to ERA40, although a number have significant differences in the magnitude of the central pressure; in particular *csiro_mk3.5* and *ncar_ccsm3* have much deeper systems for latitudes south of 50° S.

The cyclone identification process also calculates a "radius" attribute for each low centre that is detected. This is calculated using a method which finds the area of the region around the low centre where the Laplacian is positive (for details see Simmonds and Keay, 2000a). Comparisons between the ERA40 reanalysis and each of the CMIP3 climate models for cyclone "radius" (not shown), displayed less spatial variability than cyclone density and pressure. However, four models (*bccr_bcm2.0, cnrm_cm3, inm_cm3.0* and *miub_echog)* had a significantly larger average "radius" than ERA40.

4.2.3 Selection of CMIP3 Models

By calculating the spatial correlation and RMS difference of the cyclone density, central pressure and radius, it is possible to select the AR4 models which best reproduce the actual cyclone climatology.

Figures 15 and 16 rank the AR4 models using three fields (cyclone density, radius and central pressure) combined. Figure 15 uses just spatial correlation where the correlation coefficient has been transformed into a normalised metric, m_R, which increases with skill, given by

$$m_R = \frac{R - \mu_R}{\sigma_R}$$

where R is the spatial (or 'pattern') correlation coefficient between the cyclone statistic for a given model and the same statistic for ERA40, and μ_R and σ_R are the mean and standard deviation of R, respectively, across all 20 models. The correlations of the individual fields are shown with thin lines; the combined correlation with thick black line.

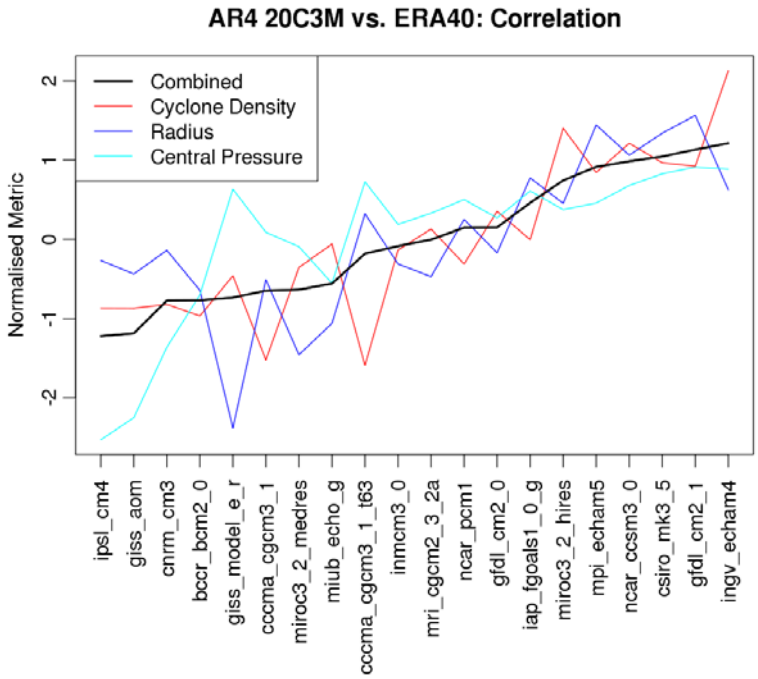

Figure 15: Spatial correlation between ERA40 and each CMIP3 ensemble member for cyclone density (red), radius (blue) and central pressure (cyan) plotted as a normalised metric. Higher values represent better model performance. The mean of these three correlation metrics is shown by the black line.

Figure 16 shows both spatial correlation and RMS difference, where the RMS difference metric is calculated using the equation above, except in this case $R = -$ RMS. The coloured lines show either the correlation or RMS difference metric after combining the three fields (the spread of the three fields is shown by the shading). The green line and shading are therefore a repeat of Figure 15, although the models are ordered differently. The solid black line combines the correlation and RMS difference.

In both Figures 15 and 16, the CMIP3 models are sorted so that the black line is increasing.

When examining just spatial correlation, there is a fairly constant decline in skill over the best 11 models (*ingv* to *inm_cm3.0*) with no one field standing out as particularly poor. However, beyond that, the individual fields are more variable (e.g. *cccma_cgcm3_t63* has a particularly poor pattern correlation for cyclone density).

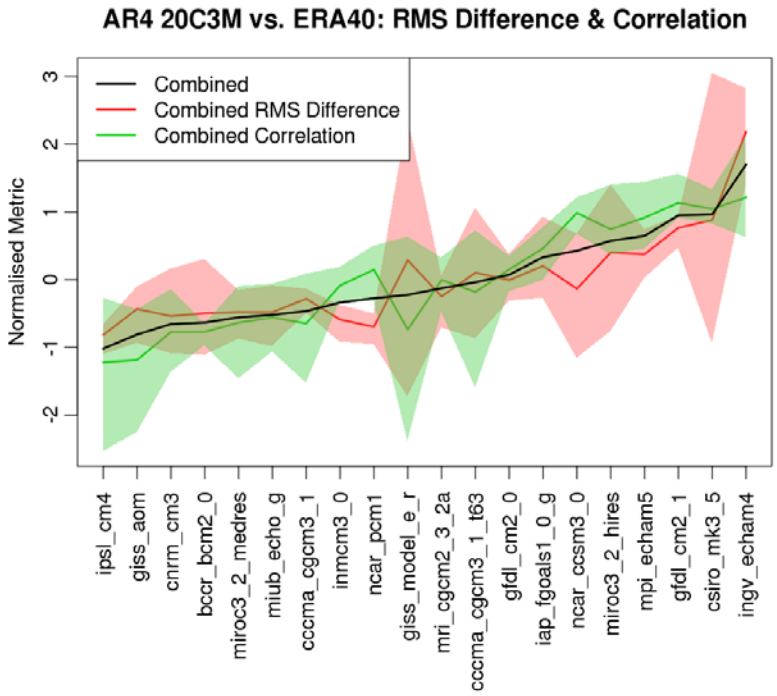

Figure 16: Spatial correlation (green) and RMS difference (red) between ERA40 and each CMIP3 ensemble member plotted as a normalised metric for cyclone density, radius and central pressure combined. Higher values represent better model performance. The mean of the two metrics is shown by the black line.

When including RMS difference in the comparisons, there is little change to the 'best' models; the best 8 models (*ingv* to *gfdl_cm2.0*) being the same in both figures. Two models, *giss_er* and *cccma_cgcm_t63*, score poorly with just correlation, but rank higher in this second figure. However, they both have very large spreads for both correlation and RMS difference, and if they are removed, the top 11 models are the same in both figures. The eleventh model (*inm_cm3.0*) scores poorly in RMS difference and as can be observed in Figure 13, no cyclones were identified north of latitude 25°S. This model has therefore been removed from the top 11.

The remainder of this cyclone analysis uses only the "top 10" models as identified by this validation exercise (Table 7). Unfortunately only five of the "top 10" models have data available for all three future scenarios (A1B, A2, B1), so in some cases, just these 5 models have been used.

Table 7: CMIP3 models that validate best against ERA40 cyclone characteristics in the New Zealand region: "top 10" (left column); five models with daily MSLP data for all three future SRES scenarios (right column).

Top 10 models from 20th century	Models with data for B1, A1B and A2 scenarios
ingv_echam5	
csiro_mk3.5	csiro_mk3.5
gfdl_cm2.1	gfdl_cm2.1
mpi_echam5	mpi_echam5
miroc3_hires	
ncar_ccsm3.0	
iap_fgoals1.0	
gfdl_cm2.0	gfdl_cm2.0
mri_cgcm_232	mri_cgcm_232
ncar_pcm1	

4.3 Future Changes in Cyclone Density

Figures 17 and 18 the show mean annual cyclone density (as in Figure 13, but with an expanded contour scale), where only the better validating models listed in Table 7 have been retained. The top left panel in each of these figures reproduces the ERA40 observations of cyclone density. Model ensemble averages are shown rather than each model individually: Figure 17 gives the 5-model average, and Figure 18 the 10-model average (Table 7).

The mean of the CMIP3 control simulations (for both 5-models and 10-models) follows the same general pattern as observed in the ERA40 data. However, the density is in general underestimated, particularly in the Tasman Sea.

The future scenarios are presented for two time periods, 2046–2065 and 2018–2100, and for three SRES emission scenarios B1 (low emissions), A1B and A2 (medium to high emissions). All of the scenarios show an overall decrease in cyclone density over New Zealand and the Tasman Sea, but an increase over Australia.

The differences between Figures 17 (5-model average) and 18 (10-model average) are small, although the increase over Australia is not so pronounced in the 10-model average. Examination of Figure 13 suggests that this increase over Australia is due

primarily to the *csiro_mk3.5* model, which has less dominance in the 10-model average. There is a tendency to have larger changes in cyclone density for stronger greenhouse gas forcing (ie, A2 scenario) and further ahead in time (ie, 2081–2100). In order to make the trends with time and scenario more apparent, subsequent figures in this section will look at *differences*, where the future pattern (either 2046–2065 or 2081–2100) has had the 20th century pattern subtracted from it.

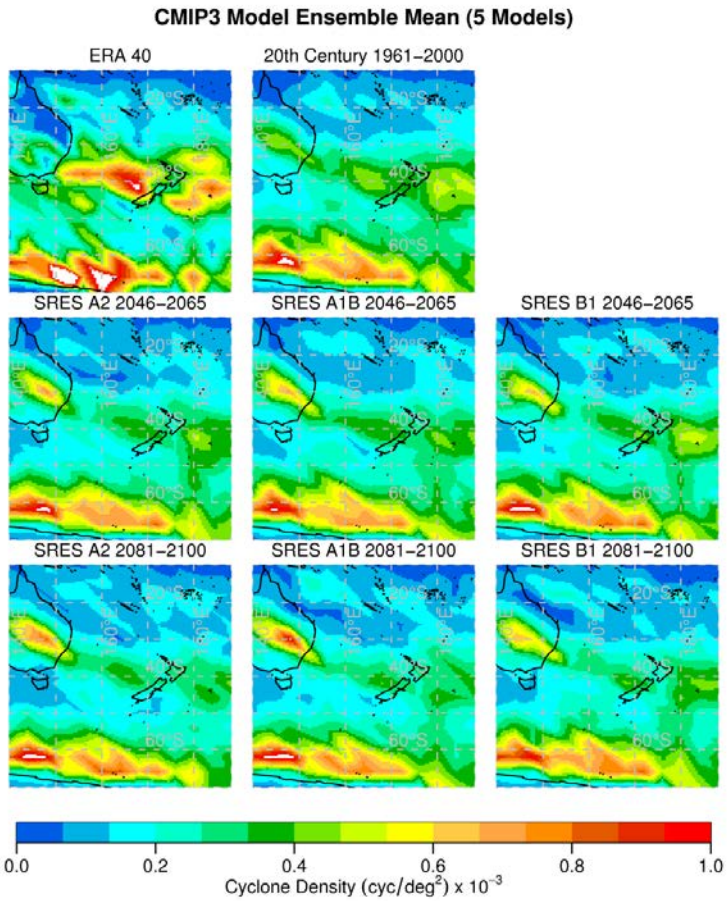

Figure 17: Cyclone density in the NZ region. The top-left plot contains the ERA40 reanalysis data and the remaining plots contain the CMIP3 ensemble mean of the 5 representative models from Table 7. The centre-top image shows the 1961-2000 control, while the second and third rows contain future scenarios at 2046-2065 and 2081-2100 respectively. The three images in each row show the different scenarios (A2, A1B and B1, as labelled).

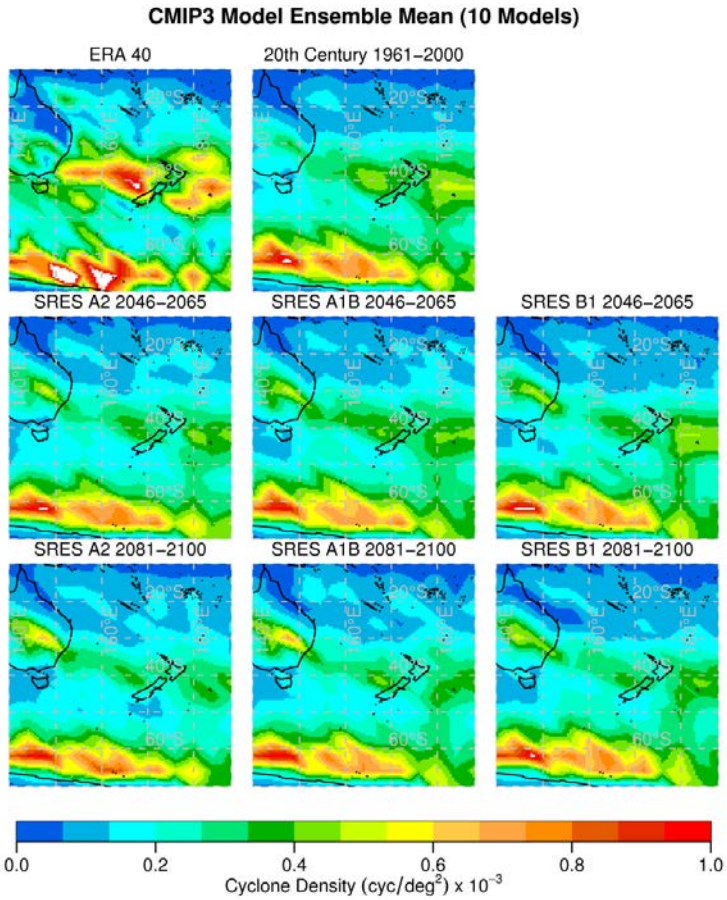

Figure 18: As in Figure 17, but for all 10 models in Table 7. In this figure, some future scenarios have more ensemble members included in the average than others.

Figures 19 through 22 show the *change* from the control to the 2050 and 2090 time periods, split into the winter and summer seasons for both the 5 and 10 model ensembles. For winter (Figure 19) there is a marked decrease in cyclone density over the North Island and to the east of New Zealand for all scenarios. There is a general increase in density south of 50°S and for primarily the 2046–2065 period this increase extends to the South Island. The most significant changes are observed in the 2081–2100 period in the A2 scenario (and to a lesser extent the A1B scenario) where there is reduced number of cyclones in the ocean surrounding the North Island. With the additional 5 models added (Figure 21) there is a general reduction in the magnitude of the differences observed, but the spatial pattern remains similar.

For summer (Figure 20), the picture is quite different, as there is in most of the scenarios a slight increase in cyclone density over New Zealand. There is also a suggestion of more storms in the Tasman Sea. The most notable feature in summer is

the strong increase in density over Australia. This is observed, although slightly reduced, when the *csiro_mk3.5* model is removed from the ensemble (not shown), so is not solely an artifact of the anomalous maximum observed in the model in Figure 13. Again the pattern is generally the same, but with reduced magnitude, when all 10 models are included (Figure 22).

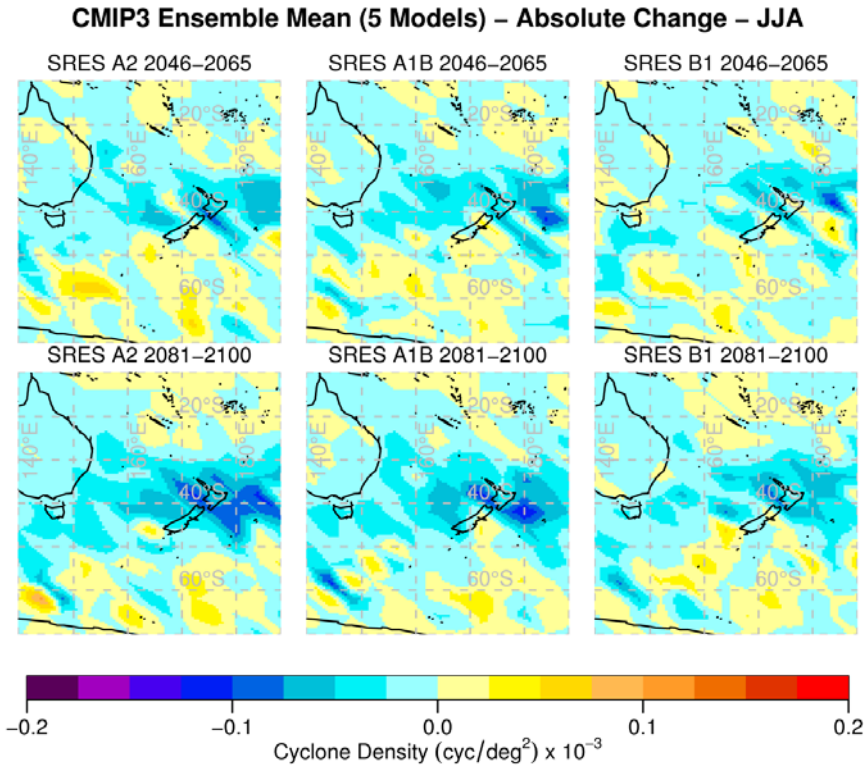

Figure 19: Ensemble mean (Table 7 models) of the change in cyclone density from the 20th century to the mid (top row) and late (bottom row) 21st century in winter (Jun–Aug). Three SRES scenarios are shown.

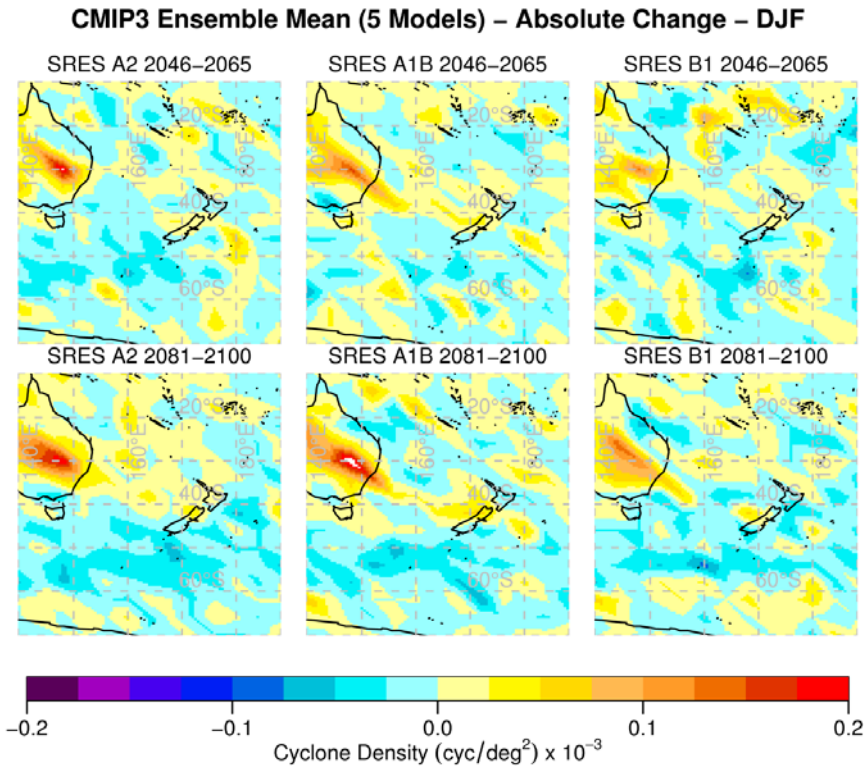

Figure 20: As in Figure 19 but for summer (Dec–Jan).

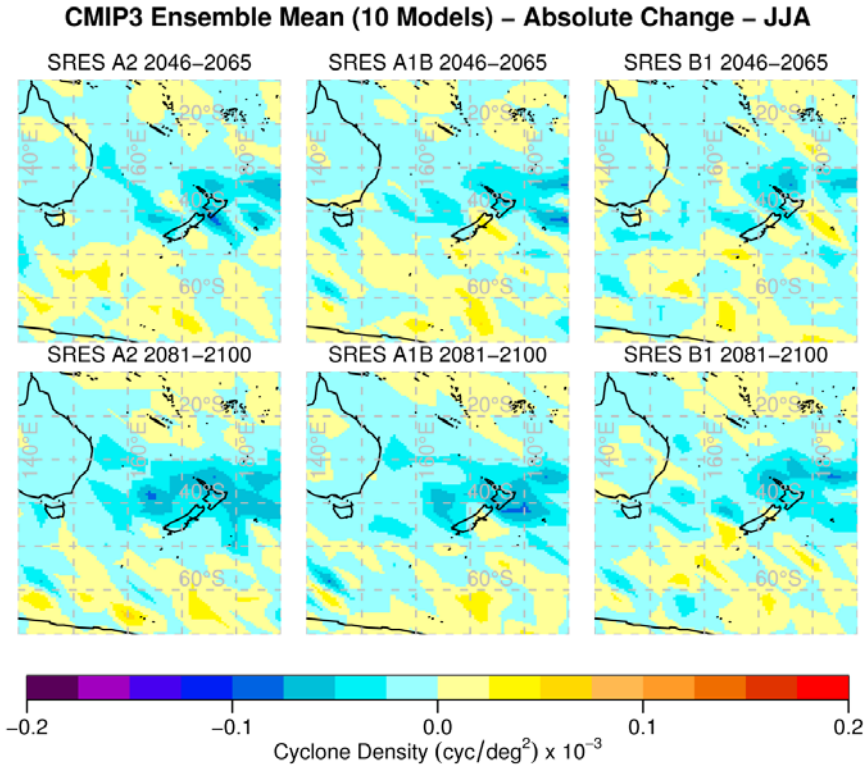

Figure 21: As in Figure 19 but using the 10-model ensemble from Table 7.

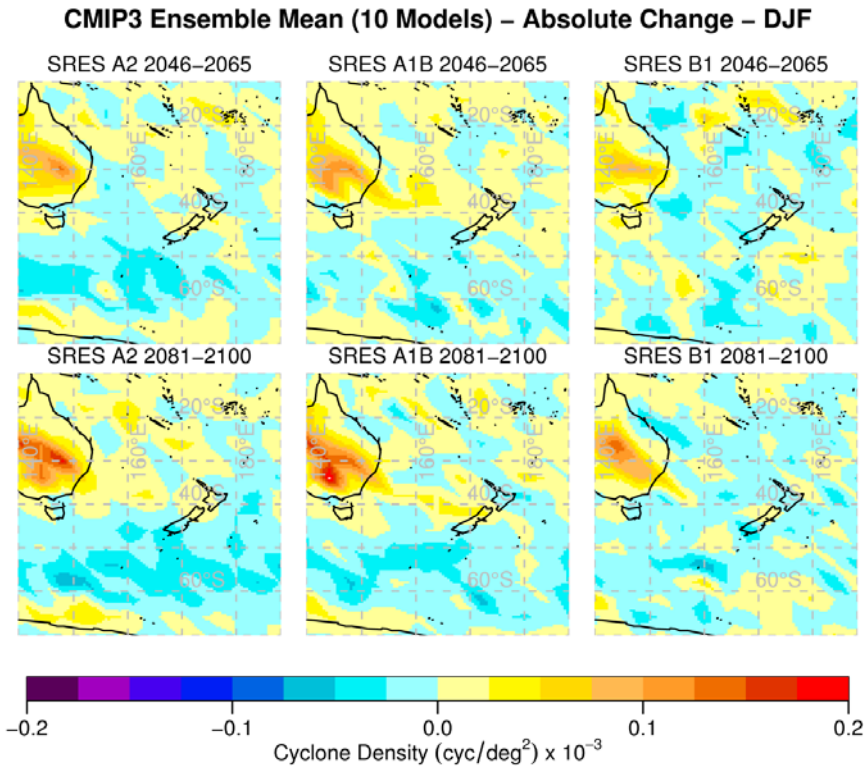

Figure 22: As in Figure 19 but for summer and using the 10-model ensemble from Table 7.

4.4 Future Changes in Cyclone Central Pressure

Figure 23 shows the mean cyclone central pressure for ERA40 and the 5-model CMIP3 ensemble mean. The 20th century CMIP3 ensemble mean shows a similar pattern to the ERA40 reanalysis, although the mean cyclone central pressure is typically lower in the CMIP3 models than in the observations. This is particularly true south of about 40°S. The mean annual central pressure from the 10-model average (Table 7) is almost identical to that in Figure 23 so is not shown.

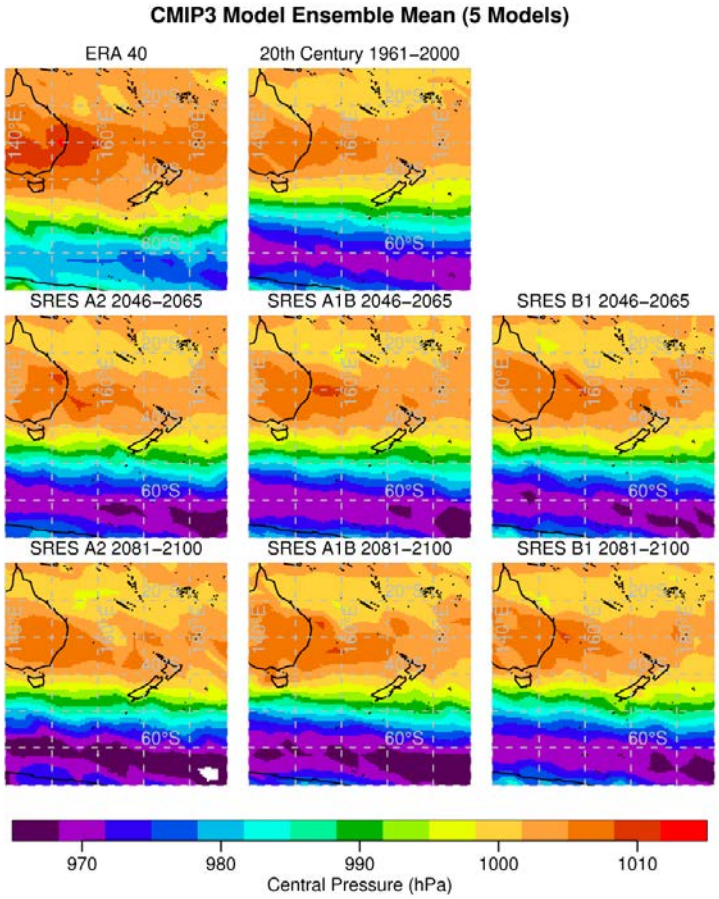

Figure 23: As in Figure 17, but for mean annual cyclone central pressure.

From Figure 23 and Figures 24 and 25 (the latter showing the seasonal *change* between the current and future climates), it is clear that cyclone central pressure increases over most of New Zealand in the future climate projections. This suggests that the cyclones will on average be weaker. In winter (particularly for the A2 and A1B scenarios) there is a significant deepening of the cyclones south of 45°S. This would result in a strengthening of westerly and southerly winds over the South Island when low centres pass to the south of the country during winter.

The 10-model average shown in Figures 26 and 27 paints a similar picture, although the magnitude of the changes is reduced in comparison with the 5-model average.

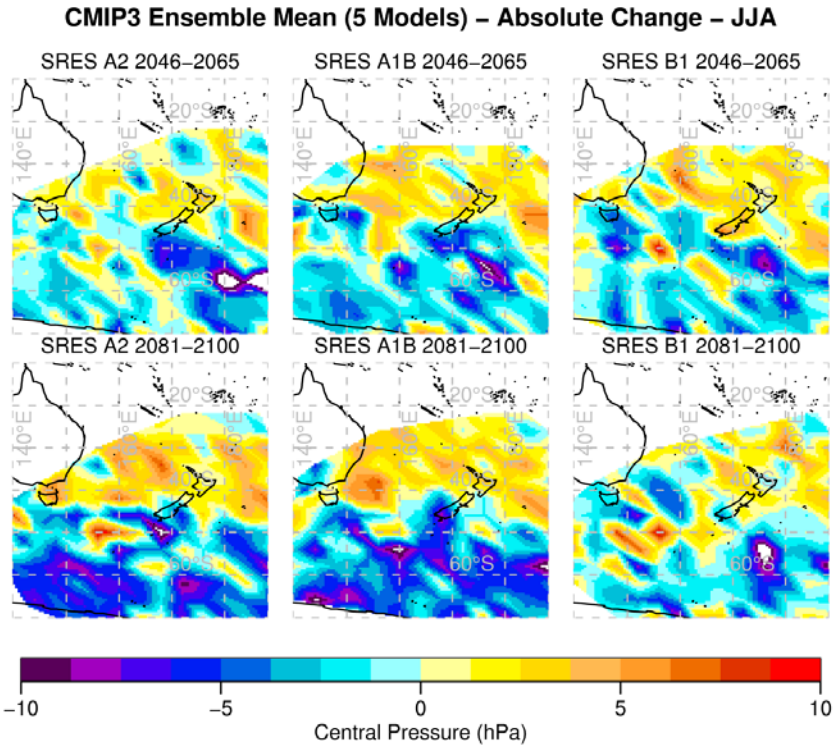

Figure 24: As in Figure 19, but for mean winter cyclone central pressure. White regions indicate no data (ie, the cyclone density is zero).

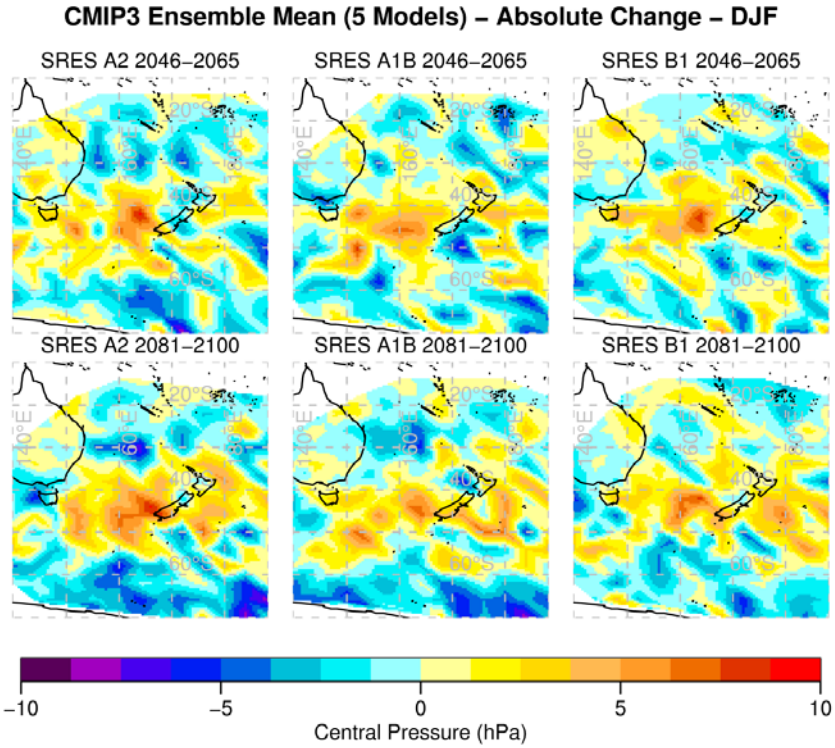

Figure 25: As in Figure 24, but for summer (Dec–Jan).

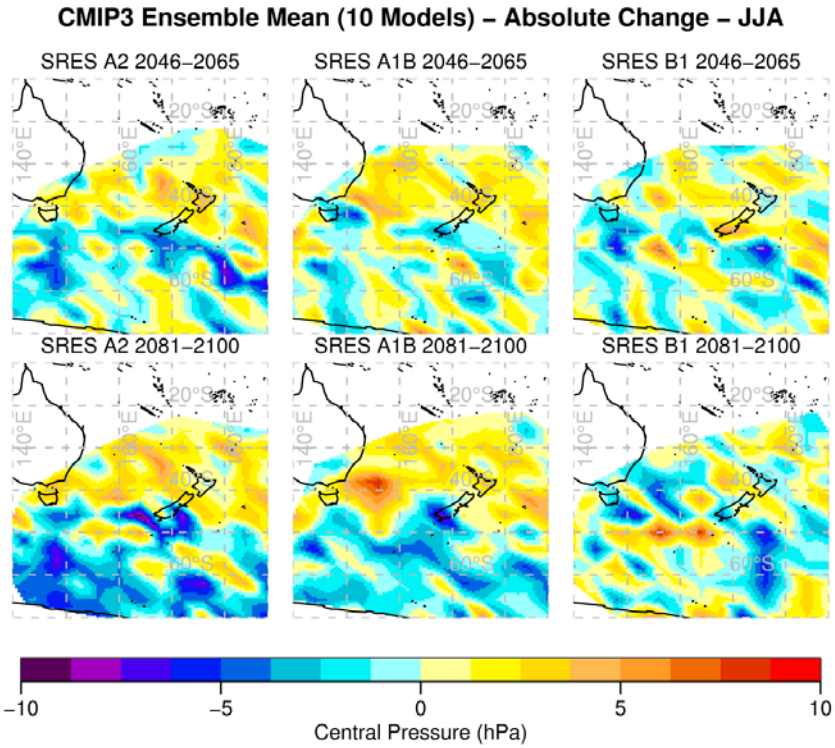

Figure 26: As in Figure 24, but using the 10 model ensemble from Table 7.

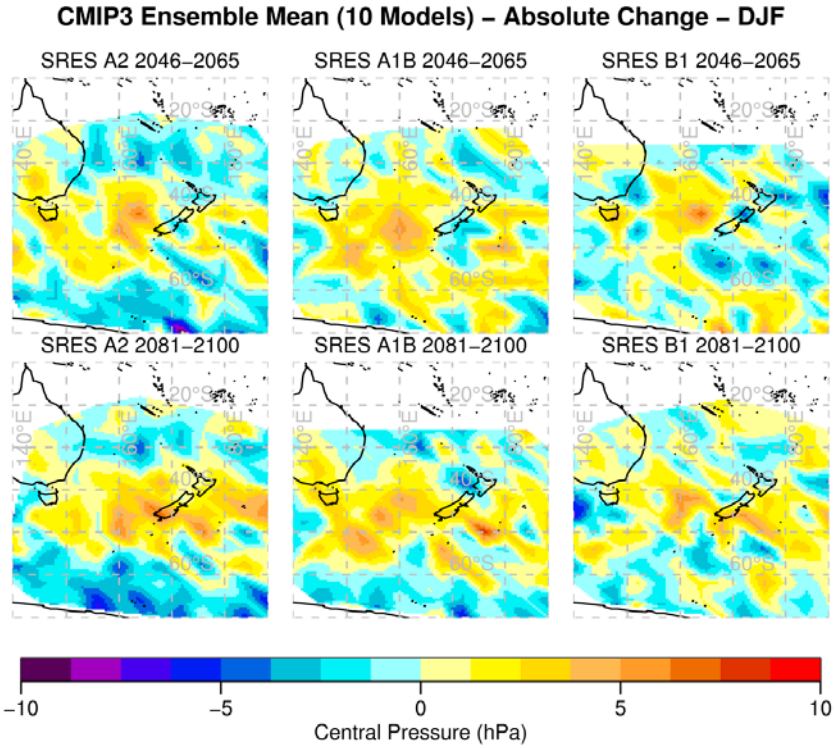

Figure 27: As in Figure 26, but for summer.

4.5 Discussion

This analysis is consistent with results from previous studies showing that there is likely to be a poleward shift in the cyclone track in a future, warmer climate (Bengtsson *et al.*, 2006; Lambert and Fyfe, 2006). In the New Zealand context, this equates to a reduction in the number of cyclones over the North Island and to the east of the country in winter, with the chance of slightly increased cyclone frequency to the south of the country. In summer, however, it is likely that there will be increased cyclone activity over the Tasman Sea and a decrease in activity south of New Zealand.

These seasonal changes in cyclone density are consistent with the Chapter 3 findings of the likely changes in the Kidson circulation types. Only three Kidson types have low pressure centres near New Zealand and north of 45°S: types TSW, NE and R. Chapter 3 concluded that the frequency of all three types is projected to decrease in winter and increase in summer.

The analysis in this chapter also shows that cyclone intensity is likely to decrease over New Zealand in both summer and winter. However, a significant intensification is possible south of the country during winter. This could produce a stronger pressure gradient over the South Island, and a possible increase in extreme winds in that part of New Zealand, depending of course on how far south of the country the low centres are.

5. Extreme Wind Pattern Analysis

This chapter focuses explicitly on trends in the most extreme winds, defined here as the top 1-percentile, in observed data and in climate model simulations. A new technique known as "trend empirical orthogonal function" (TEOF) analysis (Hannachi, 2007) is applied to these daily gridded data sets. The TEOF technique is designed to detect dominant trends in noisy data, and is applied to the top 1-percentile WS10 (wind speed at 10m) data and related mean sea level pressure (MSLP) data for the New Zealand region.

The daily data available from IPCC Fourth Assessment model simulations cover the period 1961-2000 of the 20th century, and two future periods: 2046-2065 and 2081-2100. We first describe observed trends in extreme winds from gridded ERA40 reanalysis data, and then ask whether the climate models also identify similar trend patterns for the 20th century period. Trends out to 2100 are then analysed for 14 GCMs under the AR4 SRES A1B emission scenario (a medium emission scenario), and agreement between models is quantified.

The main questions addressed in this section are:

- Are there detectable trends in extreme winds in the past climate and future climate scenarios over NZ?
- If yes, are they significant; what is their magnitude and how large are the uncertainties associated with estimated trends? Can they be characterized regionally, locally, seasonally, etc.?
- Are the trends consistent with changes in cyclone density (Chapter 4) and weather patterns (Chapter 3), e.g. as described by Kidson types?

5.1 Trend EOF Methodology

The conventional EOF (empirical orthogonal function) analysis method looks for dominant patterns of variability in data, either spatial or temporal (Richman, 1986). The time series associated with these patterns may, or may not, show a trend in time. Any trend if present may be distributed over a number of EOF modes. The purpose of a trend EOF (TEOF) analysis is to isolate patterns that have a dominant monotonic trend. Barbosa and Andersen (2009) applied TEOF analysis to global sea surface temperatures, and demonstrated that the method was much superior to conventional EOF analysis in isolating the low-frequency El Niño-Southern Oscillation signal from the long-term trend of global sea surface temperature.

To compute the dominant trend in a spatio-temporal field, a measure of 'monotonicity' is incorporated in the EOF analysis. A new transformation is applied to the data prior to the analysis, based on inverse ranks to quantify monotonous change, i.e. an increase or decrease, in all time series at each spatial grid point simultaneously.

More explicitly, let $\boldsymbol{X} = \boldsymbol{x}_k$ be a time series of length n, $(k = \{1, 2, ..., n\})$ and $\boldsymbol{p}_k$ be the time series of the corresponding ranks. The original time series $\boldsymbol{x}_k$ is strongly correlated to $\boldsymbol{p}_k$. The data in each time series $\boldsymbol{x}_k$ is sorted in decreasing (or increasing) order and mapped onto the location in the original time series to produce a new time series $\boldsymbol{q}_k$ which is simply a permutation of the indices of location (inverse rank mapping), $\{1, 2, ..., n\}$. The correlation of $\boldsymbol{q}_k$ to $\{1, 2, ..., n\}$ is a robust measure of monotonicity of all (at each spatial location) time series.

In the presence of a detectable trend, the leading modes of correlations between the $\boldsymbol{q}_k$ for all k, i.e., the TEOF, will have a pattern which follows the trend even if it is weak or nonlinear. If the time series are random, there will be no coherent pattern. The covariance between the linear combinations of time series $\boldsymbol{q}_k$ is a measure of monotonicity. Maximizing this measure produces the strongest trend. This pattern is then projecting onto the physical space $\boldsymbol{X}$ to compute the corresponding trend pattern (TP) and the time series of the trend pattern (TSTP) of the original data. Note that the trend picked up is not necessarily linear. See Hannachi (2007) and Suselj and Sood (2010) for further technical information.

5.1.1 Data selection and description

First, the top 1-percentile (extreme) WS10 data, defined to cross the 99-percentile threshold of the spatial mean wind speed time series over the "New Zealand domain" (34–47°S, 167–178°E), and the related mean sea-level pressure (MSLP) data, are extracted from the daily 2.5 degree ECMWF ERA40 data set for the analysis domain (20–70°S, 130°E–150°W). These data are the "observational" data used in this analysis. The definition of the NZ domain is reasonable considering the low spatial resolution of the AR4 models, however a number of sea points are included which may contaminate the trend signal of the New Zealand land points. The ERA40 data spatial and temporal resolution is selected to be compatible with the CMIP3 GCM resolutions.

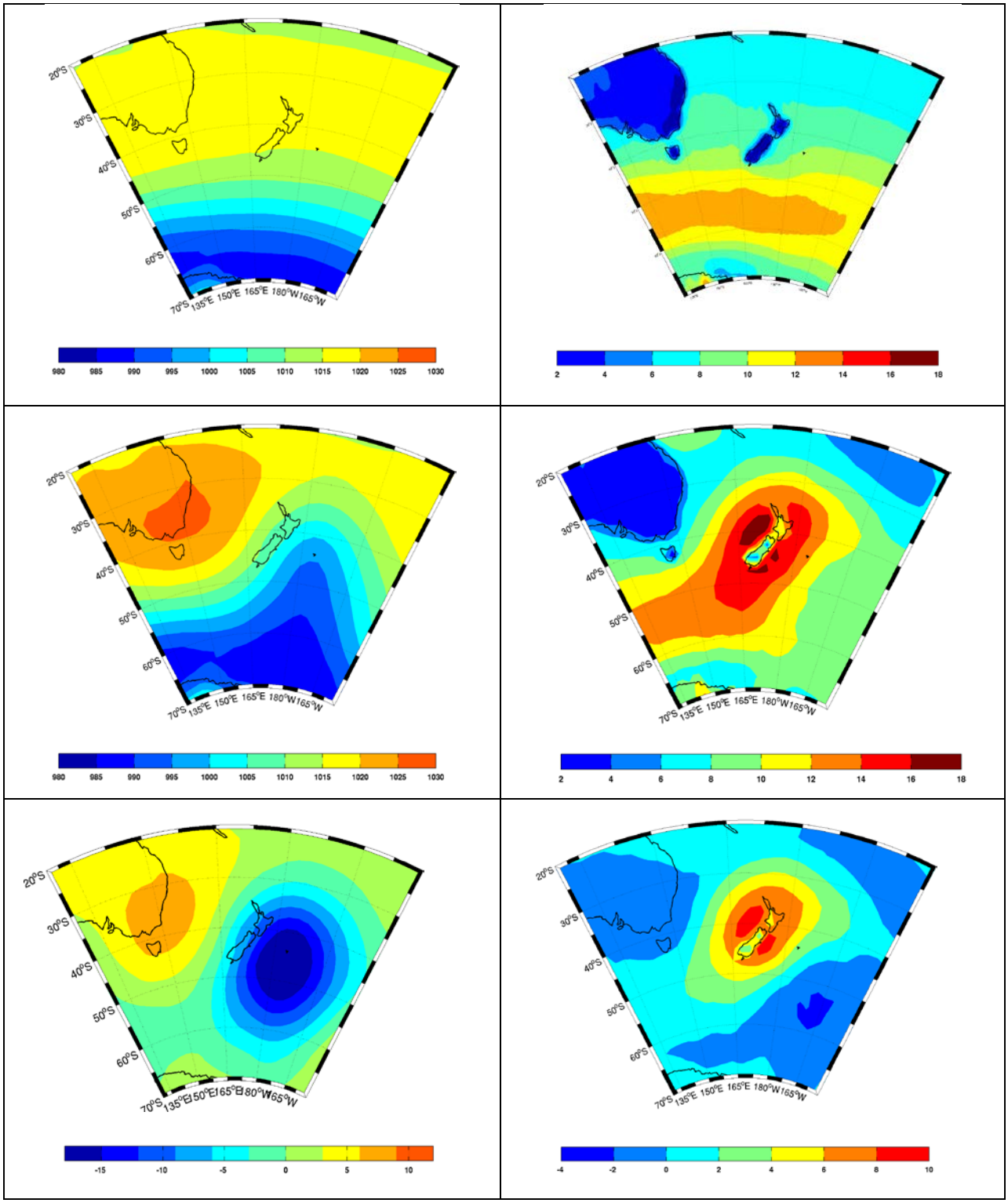

Figure 28: MSLP (hPa, left column) and WS10 speed (m/s, right column): (first row) the average from the complete daily series; (second row) average based on the top 1-percentile WS10 time series over "NZ domain" (34-47°S, 167-178°E); (third row) their difference.

Note that the maps in this chapter show patterns over the larger "analysis" domain that includes part of southeastern Australia, even though the selection criterion for the top 1% extreme wind is focused over the New Zealand domain. The wind and mean sea level pressure data are normalised by removing the mean before trend EOF analysis.

In Figure 28, the MSLP (left column) and WS10 (right column) are shown for the complete data set (top row), extreme winds (second row) and their difference. The MSLP average anomaly pattern related to extreme winds (left column, bottom row) corresponds closely to the SW Kidson weather type and is consistent with VCS results (see Figure 3, Chapter 2).

Table 8 shows WS10 wind speed characteristics (99-percentile threshold, mean speed, and maximum of daily data) over the "New Zealand domain", for the ERA40 reanalysis "observed" data and for the 14 GCMs for the "Past period" (1961–2000), and for the 14 GCMs only for the "Past & future period" (a concatenation of the three periods 1961–2000, 2046–2065 and 2081–2100).

Table 8: The mean, maximum and extreme (99-percentile) wind speed thresholds over the New Zealand domain [34–47°S], [167–178°E] for ERA40 reanalysis data and selected IPCC Fourth Assessment GCMs (Table 1).

Model Name	Label	Past period (1961–2000)			Past & future period (1961–2100)		
		99%ile	mean	max	99%ile	mean	max
bccr_bcm20	1	10.96	6.36	15.49	10.96	6.27	15.78
cccma_cgcm31_t47	2	15.05	8.86	19.71	14.94	8.66	19.71
cccma_cgcm31_t63	3	14.57	8.29	17.18	14.51	8.09	19.35
cnrm_cm3	4	10.72	6.27	14.83	10.83	6.31	14.83
csiro_mk30	5	13.19	7.27	16.33	13.26	7.22	16.63
csiro_mk35	6	13.46	7.15	17.12	13.47	7.12	17.91
gfdl_cm20	7	10.49	6.41	13.71	10.64	6.41	13.71
gfdl_cm21	8	10.17	5.84	12.61	10.21	5.76	13.07
iap_fgoals_10g	9	13.21	7.59	18.21	13.36	7.56	18.61
ingv_echam4	10	11.62	6.14	15.61	11.61	6.08	15.61
miroc32_hires	11	12.16	7.04	16.07	12.19	6.99	16.07
miroc32_medres	12	10.76	6.24	13.92	10.89	6.22	14.37
mpi_echam5	13	12.85	7.24	16.86	13.21	7.28	16.86
mri_cgcm232a	14	9.78	5.41	11.96	9.87	5.41	12.38
ERA-40	-	12.74	6.63	16.62			

The mean, 99-percentile and maximum wind speeds simulated by the climate models for the "Past period" presented in Table 8 compare reasonably well with the ERA40 analysis. The Japanese *mri* model has the lowest speeds, and the lower resolution Canadian model (*cccma_t47*) has the highest speeds. Comparing the "Past period"

with the "Past & future period" in Table 8, the 99-percentile threshold is considered here as an indicator of a shift in the extreme wind distribution; where an increase in the 99-percentile threshold indicates more frequent extreme events. Ten of the 14 models show an increase in the 99-percentile threshold, but the increases are small and since these values are based on one realization of each model only, there is large uncertainty in the data.

5.2 Past trends and model validation

In this section, the daily extreme wind (WS10) trend pattern from the AR4 models is compared annually and seasonally (winter and summer half years) with the ERA40 reanalysis data for the "Past period" (1961–2000), using the TEOF method.

Figure 29 shows the first 12 extreme (top 1%) wind TEOF patterns derived using low resolution daily ERA-40 anomalies (covariance method). Importantly, the leading eigenvalues (amounts of variance accounted for by each pattern) from the TEOF analysis are not well-separated (the first 12 eigenvalues each explain between 2.3 and 1.7 percent), implying that there is no single dominant pattern, and that different combinations of the patterns in Figure 29 would describe the original data equally well. The first trend pattern shown as the top left map of Figure 29 has the strongest trend. Of the 12 trend patterns in Figure 29, patterns 1, 2, 4, 6, 7, 8 (counting from top left across the rows) all have associated time series with a significant (at 5% level) positive trend. Qualitatively, all trend patterns (with the exception of #5) over the New Zealand domain suggest a north-south and west-east gradient with a weak increase in extreme wind over the southern and western South Island and no change or weak decrease over the northern North Island.

This observation is consistent with an analysis based on daily sea level station data observations since 1960s which indicates a slight increase in extreme westerly and decrease in extreme easterly activity over New Zealand and to the south of New Zealand (Salinger *et al*., 2005).

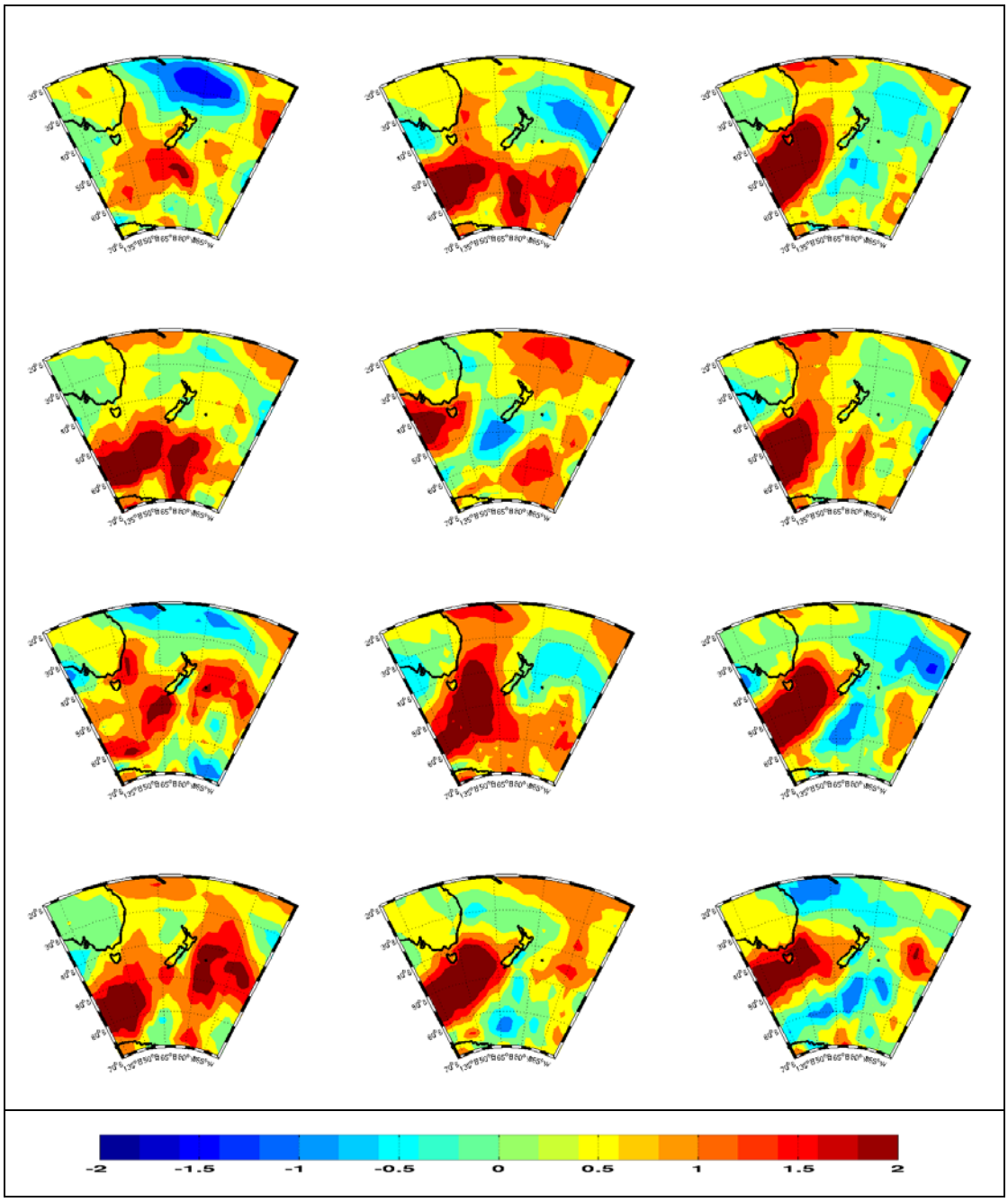

Figure 29: First 12 extreme wind trend pattern in units [m/s] of annual ERA40 reanalysis data numbered from top left, 1, to bottom right, 12. Note that the first extreme wind trend pattern (top left) is the same as in top row of Figure 30.

Table 9 shows the ranking of models based on the spatial pattern correlation of the first trend EOF pattern of each GCM against the first trend EOF pattern derived from the ERA40 data for the "Past period". The individual model correlations are weak or even negative and highly variable and the GCM ensemble average is very weakly correlated. The top six ranked models are *mpi_echam5, miroc32_hires, cccma_cgcm31_t47, gfdl_cm21, csiro_mk35* and *csiro_mk30.*

Table 9: Model ranks based on correlation of first trend pattern of AR4 models with ERA40 reanalysis data for the "Past period".

Model Name	Model Label	Past period	
		Rank	corr
bccr_bcm20	1	8	0.08
cccma_cgcm31_t47	2	3	0.36
cccma_cgcm31_t63	3	13	-0.33
cnrm_cm3	4	10	-0.00
csiro_mk30	5	6	0.20
csiro_mk35	6	5	0.25
gfdl_cm20	7	14	-0.48
gfdl_cm21	8	4	0.33
iap_fgoals_10g	9	12	-0.18
ingv_echam4	10	7	0.16
miroc32_hires	11	2	0.44
miroc32_medres	12	11	-0.09
mpi_echam5	13	1	0.45
mri_cgcm232a	14	9	0.06
ensemble average			0.04

The first extreme wind trend EOF pattern, representing the most dominant trend in ERA40 extreme winds, and its related sea level pressure anomaly pattern are presented in Figure 30 for all times of year and by season. For the annual pattern (top row), the related sea level pressure anomaly pattern has a north-south gradient with a high situated north-east of North Island and a low south-east of South Island. The MSLP pattern has an additional weak low along the east coast of Australia and a high south of the south-east coast of Australia. The strongest wind pattern trends are located at the boundaries upstream of the strongest pressure gradients.

The summer (middle row, Figure 30) and winter (bottom row, Figure 30) seasonal patterns are quite distinct. The east-west gradient in the summer half year is reversed in the winter half year and north-south gradient is strengthened. The related sea level pressure patterns are consistent with the extreme wind trend pattern with the signal strengthening at locations with strongest pressure gradient. The dramatically different large scale seasonal patterns partially dampen the annual signal. The trend is stronger but not significant in the winter half year. In summer, the trend EOFs show a coherent structure and separated eigenvalues, indicating stronger significance though the magnitude over New Zealand is weaker.

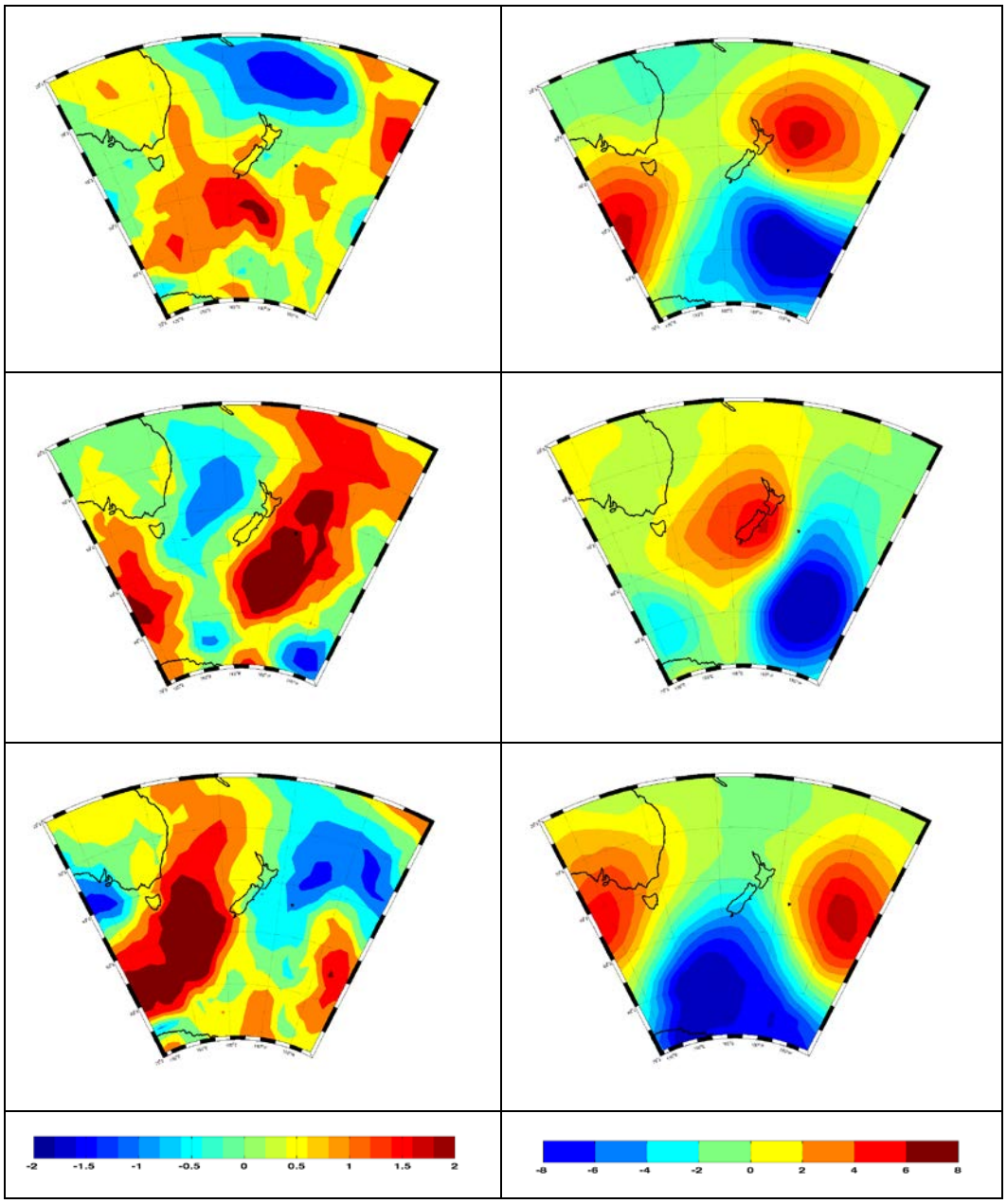

Figure 30: First WS10 (left) and related MSLP (right) trend pattern for annual (top row), summer/autumn (DJFMAM, middle row) and winter/spring (JJASON, bottom row) ERA-0 99-percentile WS10 speed. The first eigenvalue is slightly separated from the other eigenvalues only in the summer half-year suggesting no significant trends in the data.

In Table 10, the seasonal variability of the trend in the "Past" climate of 14 GCMs is examined further. A trend signal is detected in some individual models in the summer and winter half years, but as the ranking based on the model ensemble average and the ERA40 data is not consistent, there is little confidence in the significance of the trend signal based on a multi-model approach. Neither of the two models (*miroc32_hires*

and *cnrm_cm3*) that rank highly (1 and 2, highlighted in green) when compared with ERA40 in both seasons have detectable trends, while three low ranked (between 9 and 13) models (*bccr_bcm20*, *cccma_cgcm31_t47* and *miroc32_medres)* show trends in both half years. This suggests low confidence in the seasonal trends.

Table 10: Model ranks based on winter/spring (JJASON) and summer/autumn (DJFMAM) first trend pattern correlation of AR4 SRES A1B models with ERA40 reanalysis data and the multi-model ensemble average. The weak (x) and strong (X) trend signal, if separable from the noise, is indicated.

Model Name	Model Label	Winter/Spring			Summer/Autumn		
		Signal	Rank ens	Rank obs	Signal	Rank ens	Rank obs
bccr_bcm20	1	x	14	12	X	5	9
cccma_cgcm31_t47	2	x	12	11	x	9	13
cccma_cgcm31_t63	3		1	10	x	2	8
cnrm_cm3	4		4	2		4	2
csiro_mk30	5		9	7		3	10
csiro_mk35	6	X	7	6		10	5
gfdl_cm20	7	X	3	14		14	3
gfdl_cm21	8	x	2	8		7	4
iap_fgoals_10g	9		6	3		12	11
ingv_echam4	10	x	13	5		13	7
miroc32_hires	11		11	1		8	1
miroc32_medres)	12	X	8	13	x	1	12
mpi_echam5	13	x	10	4		6	14
mri_cgcm232a	14		5	9		11	6
ERA_40					x		

The "Past period" extreme wind trend pattern for the 14 CMIP3 models and their ensemble average are presented in Figure 31. There are substantial differences between the 14 individual ensemble members, as was indicated by the large variability in the pattern correlations shown in Table 9. The ensemble average (bottom-right), though less intense, has a similar but much smoothed pattern compared with the ERA reanalysis data for the same period. The highest ranking models (*miroc32_hires* and *cnrm_cm3*) have different trend patterns but they both exhibit similar north-south and east-west gradients. The next ranking models perform well only in one season; therefore they are not likely to show correct features in the annual pattern.

A number of the AR4 models show a tendency for a too strong Southern Annular Mode (SAM, e.g. Thompson and Solomon 2002) pattern, and for the pattern to be too zonal, which may deteriorate the signal in the tail of the wind distribution.

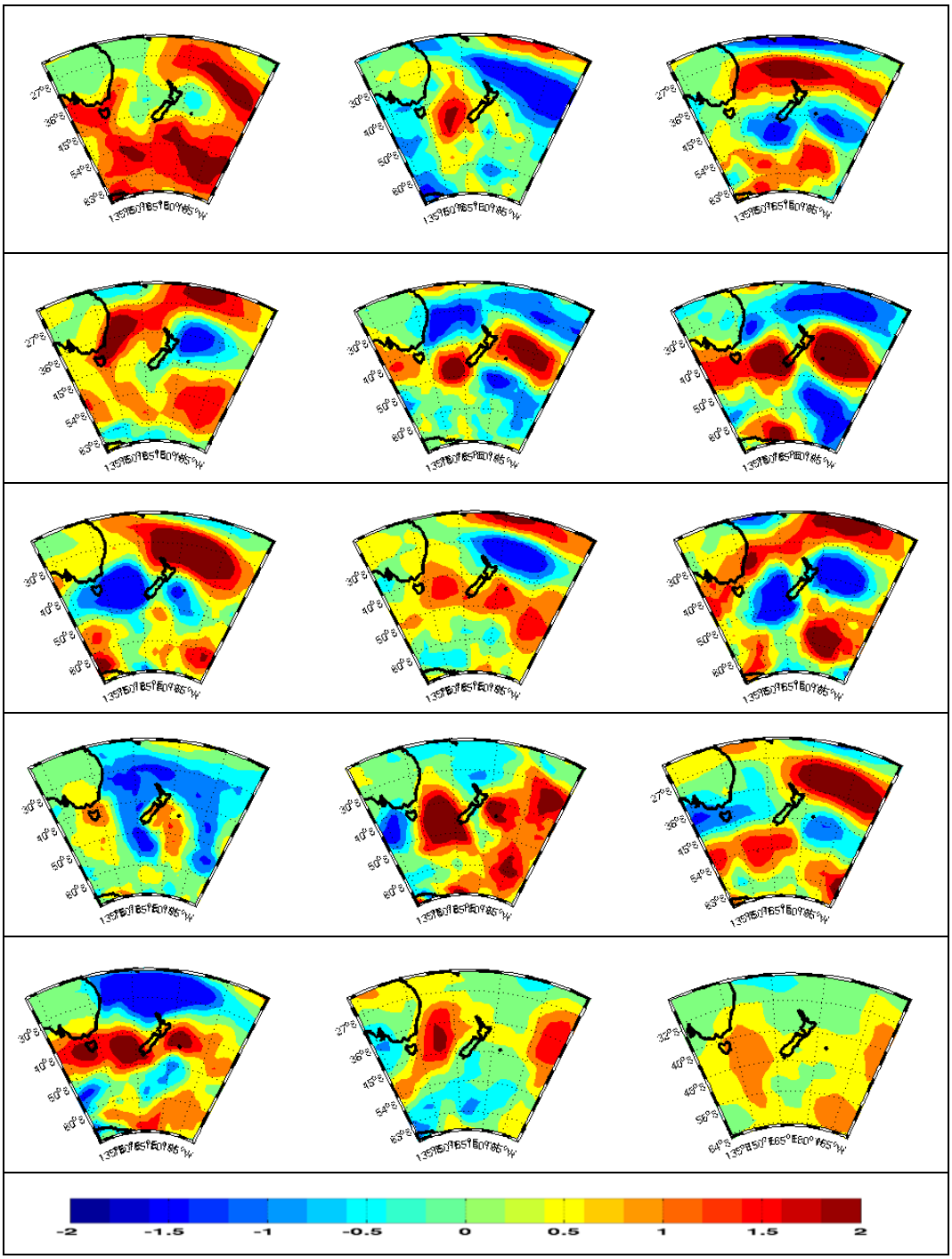

Figure 31: The first annual trend pattern of extreme (top 1%) wind over the past period (1961-2000) for the 14 CMIP models. The models are ordered 1 through 14 (as in Table 8). For example, the model at the start of the second row is model number 4 (*cnrm_cm3*). The bottom right-hand map is the 14-model average. The colour bar shows the contour intervals, except for the ensemble average which is half-scale (ie, colour bar range is from -1 to +1 SD units).

5.3 Future trends in extreme winds

Table 11 quantifies how each model compares to the 14-model ensemble average. For the historical period (1961–2000), the Japanese high resolution model (*miroc32_hires*) and the German model (*mpi_echam5*) are closest to the ensemble average in terms of the wind trend pattern. The GFDL model *gfdl_cm21* and *mpi_echam5* are closest in terms of the MSLP pattern associated with the wind trend. The ranks change for the "Past & future" period[6] where the Chinese low resolution model (*iap_goals_10g*) is the closest to the model ensemble average pattern for the extreme wind trend pattern and the related sea level pressure.

Table 11: Model ranks based on the spatial pattern correlation of the first WS10 trend EOF pattern and its related MSLP of AR4 models with the multi-model ensemble average for the "Past period" (1961–2000) and the "Past & future" period (1961–2100).

Model Name	Label	Past Period (1961–2000)				Past & future period (1961–2100)			
		Rank	Wind	Rank	MSLP	Rank	Wind	Rank	MSLP
bccr_bcm20	1	4	0.43	6	0.54	14	0.02	13	0.43
cccma_cgcm31_t47	2	6	0.27	3	0.81	5	0.67	6	0.80
cccma_cgcm31_t63	3	13	-0.10	13	-0.57	13	0.11	14	-0.33
cnrm_cm3	4	9	0.20	7	0.48	2	0.74	2	0.81
csiro_mk30	5	8	0.23	10	0.23	12	0.21	11	0.37
csiro_mk35	6	10	0.20	8	0.39	11	0.35	12	0.35
gfdl_cm20	7	14	-0.41	14	-0.88	10	0.43	9	0.72
gfdl_cm21	8	3	0.45	1	0.93	8	0.53	5	0.81
iap_fgoals_10g	9	12	-0.05	11	0.11	1	0.92	1	0.92
ingv_echam4	10	7	0.26	9	0.31	9	0.53	8	0.72
miroc32_hires	11	1	0.67	4	0.75	4	0.68	7	0.75
miroc32_medres	12	11	0.00	12	-0.53	7	0.53	10	0.65
mpi_echam5	13	2	0.65	2	0.85	6	0.61	4	0.81
mri_cgcm232a	14	5	0.28	5	0.67	3	0.73	3	0.83

Considering the two best-performing models in the previous section, the trend pattern in models *miroc32_hires* (2nd row, left) and *cnrm_cm3* (4th row, middle) in Figure 32, are intensified in the "Past & future period" compared with the "Past period" with a stronger north-south gradient consistent with the poleward movement of the storm tracks and more positive SAM. The related MSLP pattern shows high pressures north and west of New Zealand consistent with the zonal Kidson types indicating stronger westerlies.

[6] In "Past and future", trend patterns are diagnosed from extreme daily winds over periods 1961-2000, 2046-2065 and 2081-2100, where data for the latter two periods are taken from GCM output under the SRES A1B emission scenario.

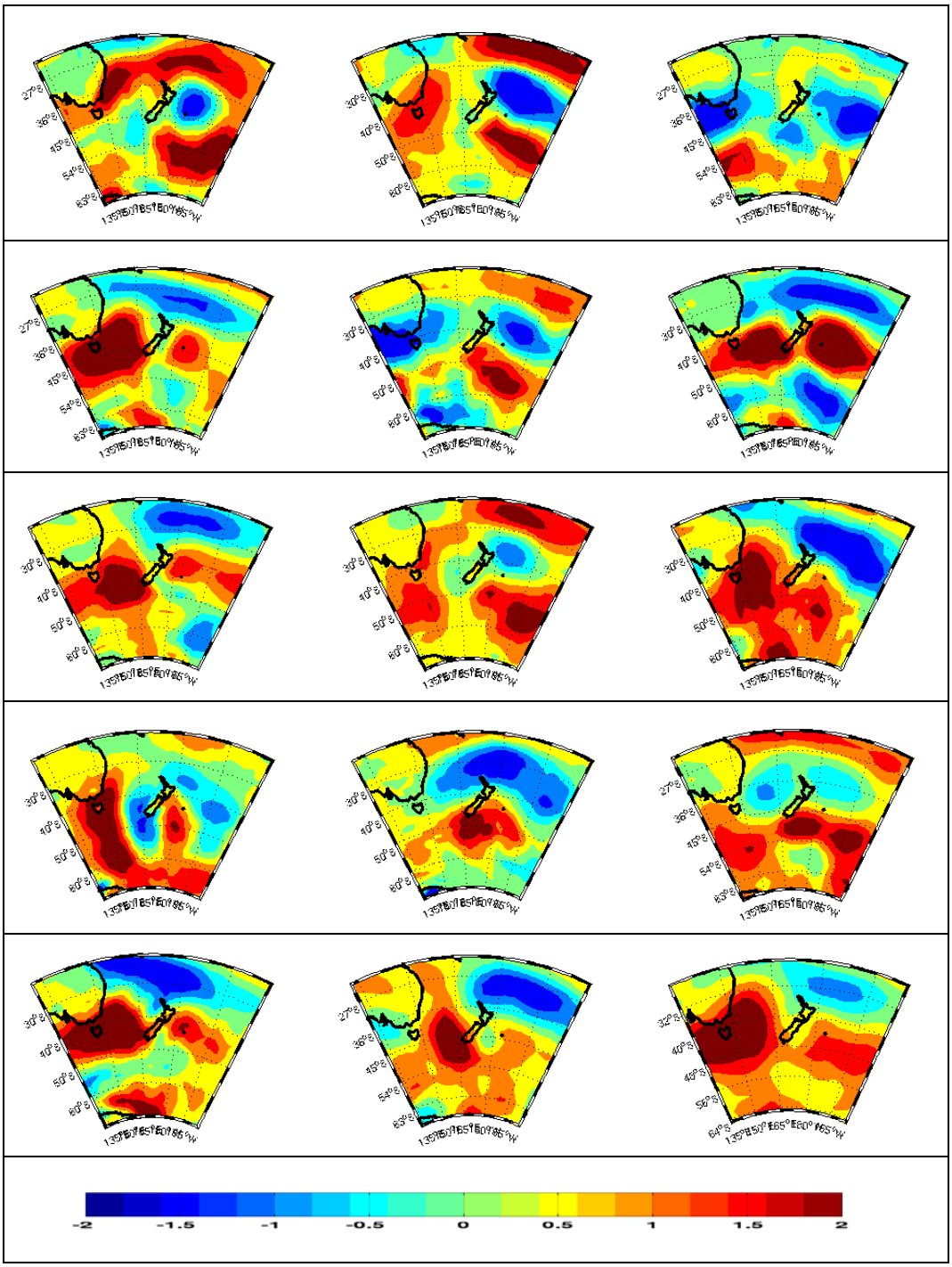

Figure 32: As Figure 31, but for first trend EOF pattern of the "Past & future period". The bottom right panel is again the 14-model ensemble average, with contour intervals at half-scale from -1 to +1). Units are m s^{-1}.

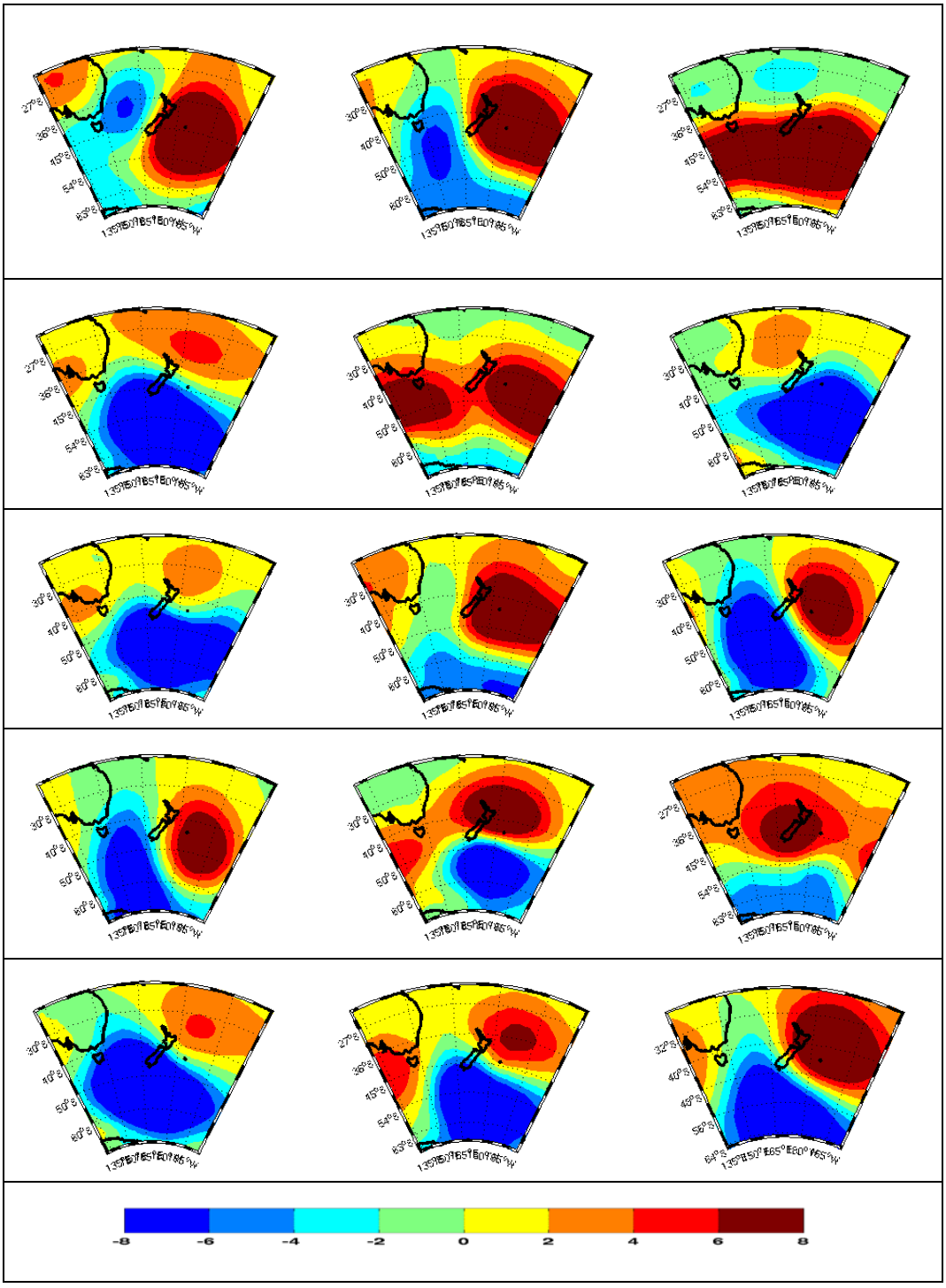

Figure 33: The MSLP patterns associated with the first extreme wind EOF trend patterns of Figure 32. Units are hPa, with a 2 hPa contour interval.

However, we need to consider not just the pattern of extreme winds (as in Figure 32), but also the trend in the associated time series (Table 12). All but 2 of the 14 GCMs have trends in the first EOF that are highly significant from a statistical point of view. To obtain the change in wind speed over New Zealand by 2100 associated with the trend pattern, one must multiply the trend (Table 12) by the pattern value (Figure 32). Over New Zealand, these pattern values generally are no larger than 0.5; thus the actual increase in the extreme wind speeds is no more than about 0.2 m/s. Even these patterns with significant trends are not frequent (i.e., a low value of explained variance).

Most of the EOFs are not well separated (last column of Table 12), and thus more than one pattern may be relevant. There are four models where the first wind EOF is separated (in terms of its eigenvalue) from subsequent patterns (*cnrm_cm3*, *csiro_mk35*, *gfdl_cm21*, *mpi_echam5*), and these models show the largest trends in the extreme wind patterns, all the trends being significant at the 1% level.

Table 12: Results for the first WS10 trend EOF pattern, from the AR4 multi-model ensemble, for the combined "Past & future" period (1961–2100): the 'Trend' refers to the linear trend (change from 1961 to 2100, non-dimensional) in the time series associated with the first wind EOF patterns shown in Figure 32; the next column indicates the statistical significance of this trend in terms of its p-value; the final column shows those models (marked by 'x') where the first EOF is well separated from the subsequent EOFs for that model.

Model Name	Label	Past & Future Period (1961–2100)		
		Trend	Significance	Separated
bccr_bcm20	1	0.26	p<0.01	
cccma_cgcm31_t47	2	0.30	p<0.01	
cccma_cgcm31_t63	3	0.24	p<0.01	
cnrm_cm3	4	0.41	p<0.01	x
csiro_mk30	5	0.04	p>0.05	
csiro_mk35	6	0.38	p<0.01	x
gfdl_cm20	7	0.25	p<0.01	
gfdl_cm21	8	0.41	p<0.01	x
iap_fgoals_10g	9	0.25	p<0.01	
ingv_echam4	10	0.25	p<0.01	
miroc32_hires	11	0.09	p>0.05	
miroc32_medres	12	0.30	p<0.01	
mpi_echam5	13	0.34	p<0.01	x
mri_cgcm232a	14	0.29	p<0.01	

5.4 Discussion

The trends in extreme winds from 14 GCMs for the "Past" and "Past & future" periods are investigated and compared with trends in the ERA40 reanalysis data for the "Past" period. The Trend EOF method is used to extract the trend signal from noisy extreme wind (WS10) data. There is strong inter-model variability for both periods. Two models (*miroc32_hires* and *cnrm_cm3*) performed well in the past period compared with the ERA40 reanalysis data.

No significant seasonal or annual trend was observed over the historical period 1961-2000 with the two best-performing models, though seasonal trends were captured in some other models (*bccr_bcm20*, *cccma_cgcm31_t47* and *miroc32_medres)* which however did not validate as well with the reanalysis data (see Table 10). The annual trend pattern features (Figure 32) in the two highest ranking models are consistent with results from other chapters in this report depicting strengthening of the north-south and east-west gradient. The trend in the north-south gradient is associated with weakening extremes over the northern part of the North Island and strengthening extremes over the lower South Island. The trend in the east-west gradient is associated with a larger increase in extremes in the Tasman Sea relative to the east of New Zealand. However, the large variability in wind speed and weak trend patterns mean that these patterns often cannot be separated from the background noise.

The trend patterns increase in intensity for the 14 models and the ensemble mean over the "Past & future period" (1961–2100). Most of the trend patterns show increases in extreme winds in the Tasman Sea, and over and south of the South Island. The related change in MSLP pattern is consistent with a more frequent zonal Kidson regime. However, the magnitude of the wind change is small, at most a few per cent of the 99 percentile wind speed in the current climate. Four GCMs (*cnrm_cm3, csiro_mk35, gfdl_cm21, mpi_echam5*) have trend patterns that are well separated from the background noise, and these four have the strongest linear trends that are significant at the 1% level.

6. Severe Weather Indices from the NZ Regional Model

In situations where it is not possible to estimate the frequency and magnitude of extreme wind events directly, it can be useful to examine a selection of indices describing the likelihood of extreme events occurring. The AR4 CMIP3 global models do not have suitable meteorological variables in their archived data set, nor adequate resolution over New Zealand, to make these calculations. This section, therefore, examines a selection of severe weather indices calculated from current and future regional climate model (RCM) simulations over New Zealand.

6.1 Modified K Stability Index

Stability indices represent an air parcel's virtual temperature excess, and thus relate to the likelihood for vertical convection to occur. An index which has been found most useful for forecasting thunderstorms in the absence of strong, larger-scale forcing is known as the "*K*-index", and is defined as

$$K = T^{850\text{mb}} - T^{500\text{mb}} + T_d^{850\text{mb}} - (T^{700\text{mb}} - T_d^{700\text{mb}})$$

where T and T_d are the temperature and dewpoint temperature at the specified level. This index provides a combined indication of the potential instability in the lower half of the atmosphere (1st two terms), the availability of moisture in the boundary layer (middle term), and the reduction of buoyancy through entrainment of dry air (near 700 hPa, last two terms) (Bluestein, 1993). In general, the higher the ambient or inflow *K*-index value, the greater the potential for heavy rain and high winds; with values above 30 implying strong potential for thunderstorm activity.

RCM output has been used to calculate a "modified *K*-index", which is similar to the *K*-index except that in place of the T and T_d at 850 hPa, the average temperature and dew point between 850 hPa and the surface are used. Calculations are based on instantaneous data every 12 hours, as output by the regional climate model.

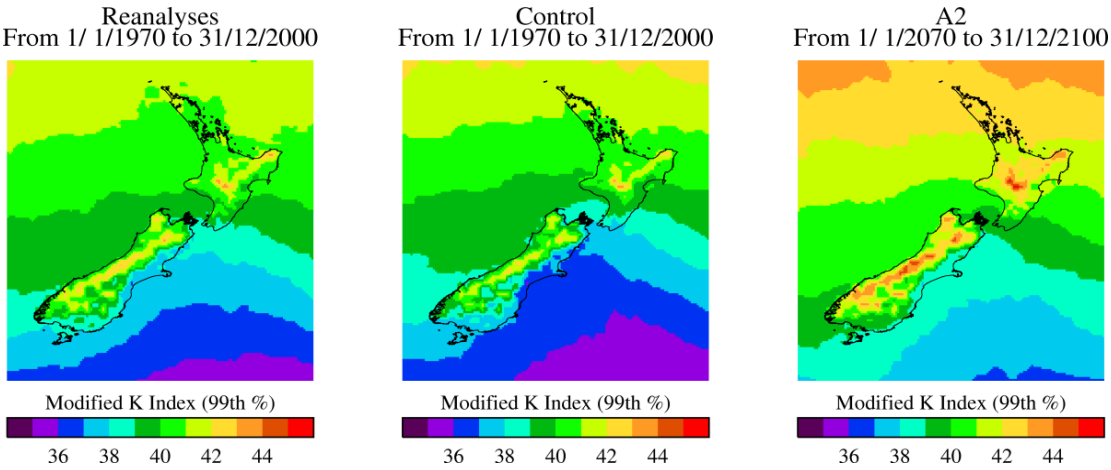

Figure 34: The 99th percentile of the modified K-index over 30 years for the RCM driven by ERA40 reanalyses (left), the RCM 20th century control (centre) and the RCM driven by the A2 emissions scenario (right).

The 99th percentile of the modified K index is shown in Figure 34 for three different RCM simulations; two for the current climate and one for a realization of the future climate under the SRES A2 (medium-high) emissions scenario. The left panel of Figure 34, labelled "Reanalyses", is a simulation where the regional model is forced by National Centers for Environmental Prediction (NCEP) reanalysis boundary conditions around the edge of the domain (only slightly larger than that shown in the figure): thus, the actual weather systems as observed in the NCEP reanalysis are provided to the RCM. The "Control" simulation (centre panel, Figure 34) takes boundary conditions from a free-running global model not constrained by observations: thus, weather sequences, El Nino events, etc, will not line up in time with the real weather observations. The fact that this makes no difference to the extreme K index is further evidence that the global model (a version of the UKMO HadCM3 model, see Table 1) provides a realistic background climatology in the New Zealand region. The right panel of Figure 34 shows a stronger K index, and increased likelihood of severe convection, over much of the domain in a future climate that is approximately 2°C warmer than the Control.

Figure 35 shows the percentage difference between the 99th percentile modified K index for the RCM simulations. The difference between the control and reanalyses (left) is significantly less than the difference between the control and the A2 simulation (right). The increase in the K index under the A2 emissions scenario is between 3 and 6% over most of New Zealand.

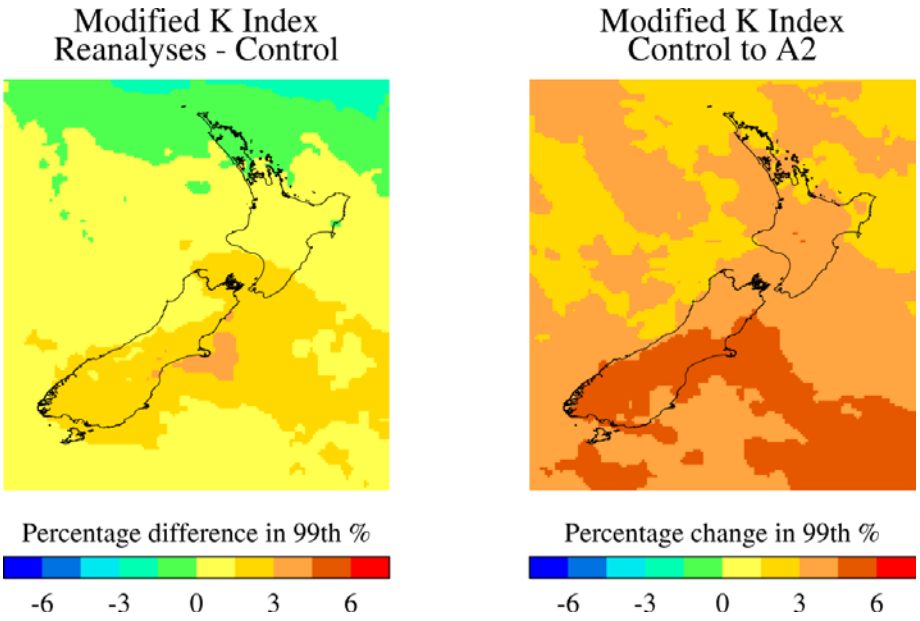

Figure 35: The percentage difference between the two 20th century RCM simulations (left) and the control and future simulations (right) for the 99th percentile of the modified K index.

6.2 Convective Available Potential Energy

Convective available potential energy (CAPE) represents the amount of buoyant energy available to accelerate a parcel of air vertically. The greater the temperature difference between the warmer parcel and the cooler environment, the greater the CAPE and updraft acceleration to produce strong convection (Bluestein, 1993). CAPE is calculated from vertical profiles of temperature and mixing ratio.

Typical values of CAPE for days when moderate to strong convection occurs range from 1000–3000 J/kg. Maximum observed values of CAPE are around 5000–7000 J/kg. The maximum vertical velocity can be calculated from CAPE using:

$$w_{\max} = \sqrt{2\,\mathrm{CAPE}}$$

Figure 36 illustrates the extreme CAPE values (defined as the 99th percentile) for the two current and one future RCM simulation. From these plots it is clear that CAPE is higher in the northern part of the domain and in mountainous regions. It is also apparent from Figure 36 that the difference between the RCM control and reanalyses simulations is again much smaller than the difference between the control and future simulations.

Figure 37 shows the difference in extreme CAPE from the control to the future RCM simulations. The first point to note is that for all four seasons and all points on the domain, the frequency of extreme CAPE events has increased in the future simulation. Secondly the spatial pattern of the change is different in the different seasons. For summer (top left), the largest increase occurs in the Tasman Sea and over the South Island and central North Island. For autumn (top right), the increase is fairly uniform over the domain, with the smallest increases over the land. For spring (bottom right), the pattern is also quite uniform (although smaller in magnitude than for autumn), but the smallest increases are now over the ocean. For winter (bottom left), the largest increases are in the south of the domain, but as this is the region with the lowest CAPE values (see Figure 36), this increase is not so important for possible extreme wind events.

These seasonal changes match reasonably well with the cyclone analysis of Chapter 4, where the future projections are different for summer (December–February) *versus* winter (June–August). In summer, there is an increased frequency of low pressure centres (and presumably also the associated convective activity) in the Tasman Sea (see Figures 20 and 22). By contrast, in the winter season, cyclone activity increases at the southern boundary of New Zealand (Figures 19 and 21). Note that the UKMO model (the driving GCM here) was not included in the Chapter 3 analysis, because it did not have the appropriate archived fields. However, other NIWA analyses have shown that this model increases both the frequency and intensity of cyclones in the Tasman Sea in summer in future scenarios (Dean, pers. comm.).

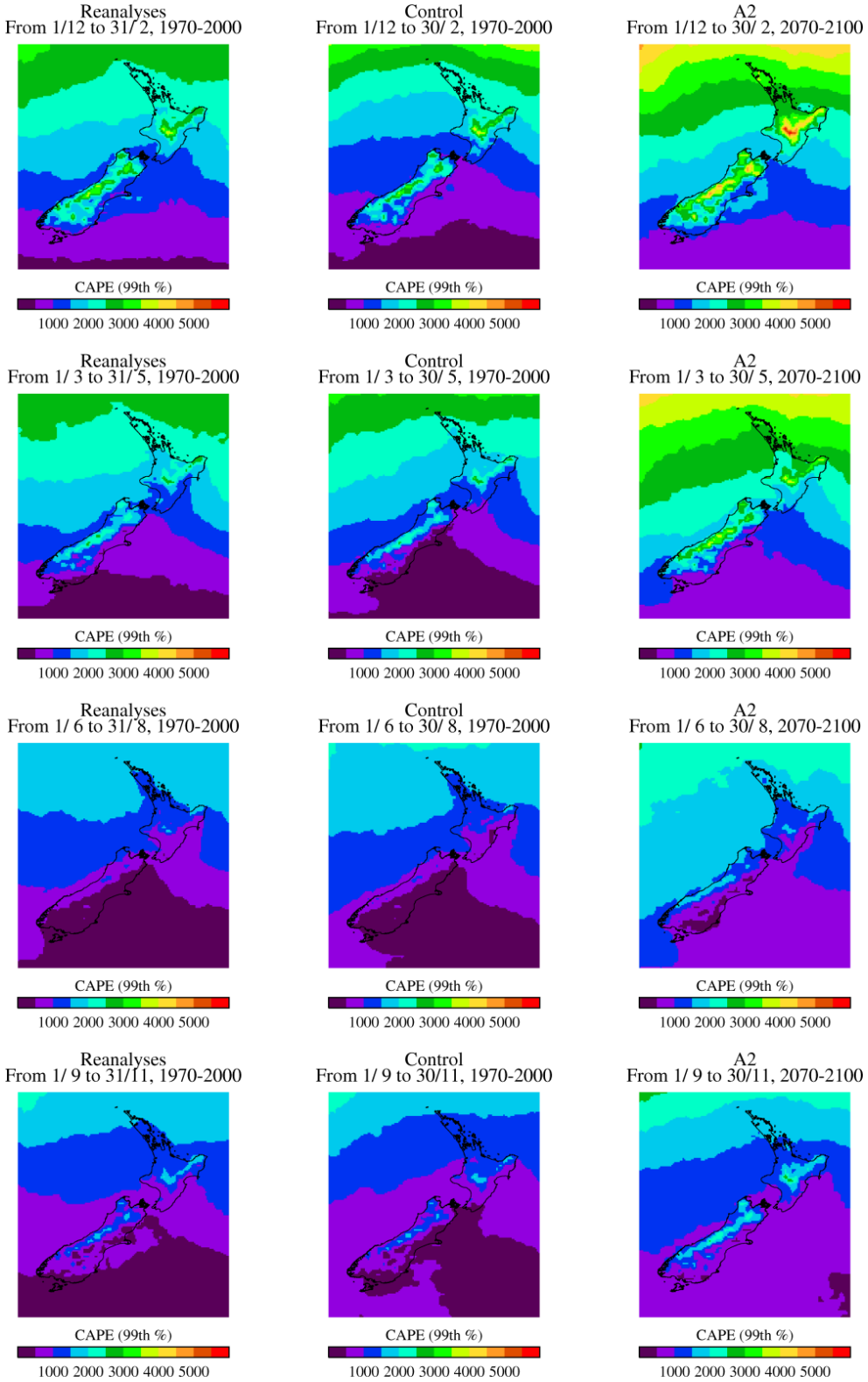

Figure 36: The seasonal 99th percentile CAPE field over 30 years for the RCM reanalyses (left column), control (centre column) and A2 (right column) simulations. The rows contain the seasons (summer, autumn, spring, winter).

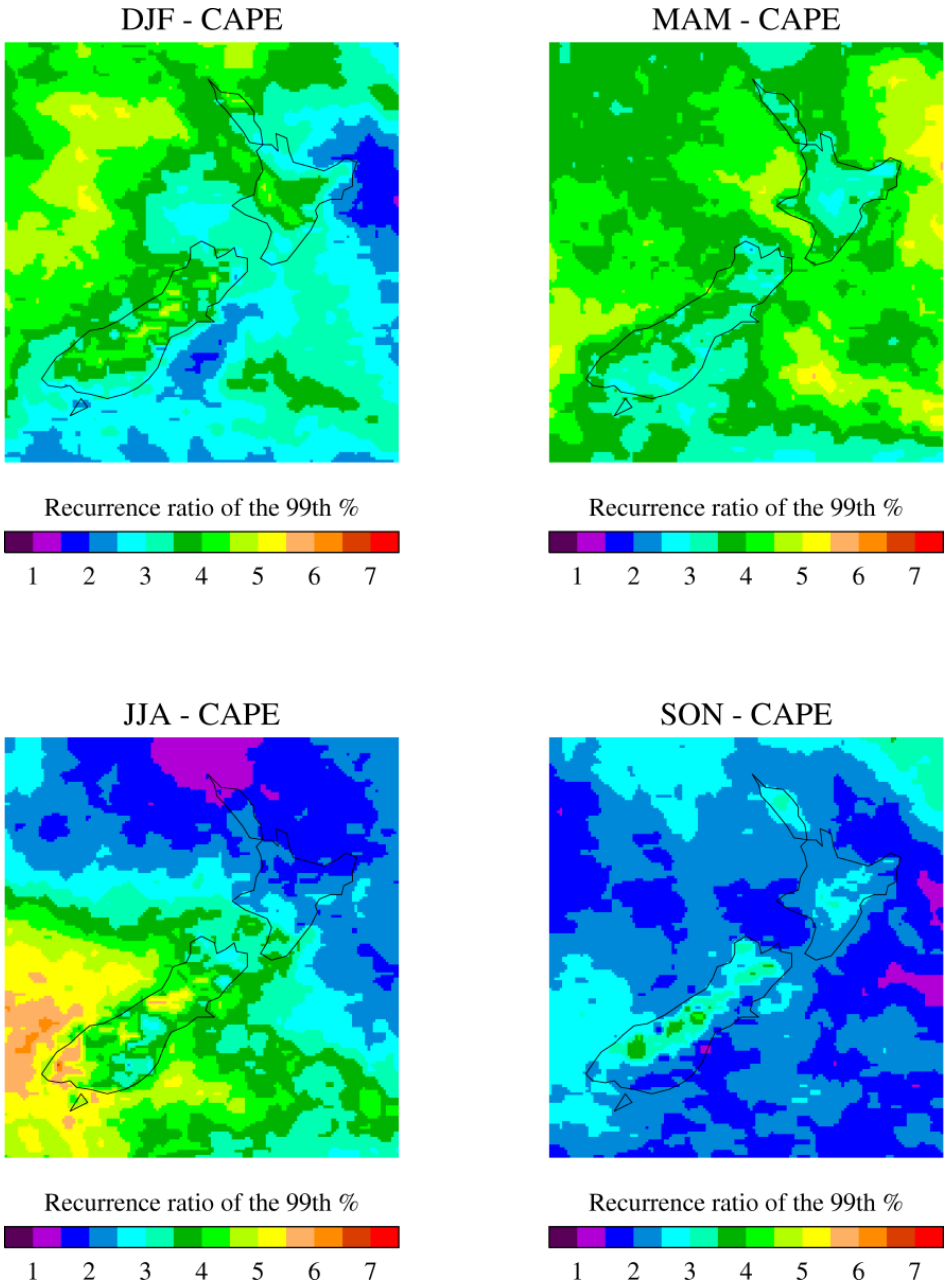

Figure 37: Seasonal plots showing the increase in occurrence of a (current climate) 99th percentile event in a future climate. That is the number of times an "extreme" CAPE event occurs in a future scenario relative to the current climate. For example, in summer an extreme CAPE event (99th percentile in the RCM control) in the Tasman Sea would occur 4 to 5 times more frequently between 2070 and 2100 under the A2 emissions scenario, in this simulation.

6.3 Vertical Wind Shear

The vertical shear (increase in wind speed with height) of the horizontal wind vector is an important factor in storm development, evolution, and organization. An environment where CAPE is high and vertical shear is strong can produce a steady, persistent rotating updraft resulting in the formation of a supercell thunderstorm (Bluestein, 1993).

The 99th percentile of "surface layer wind shear" (a diagnostic output from the RCM every 6 hours) is shown in Figure 38 for the two current and one future RCM simulation. The seasonal breakdown has not been shown as there is very little difference in spatial structure between the seasons. As can be observed in Figure 38, there are also only minor differences between the three simulations.

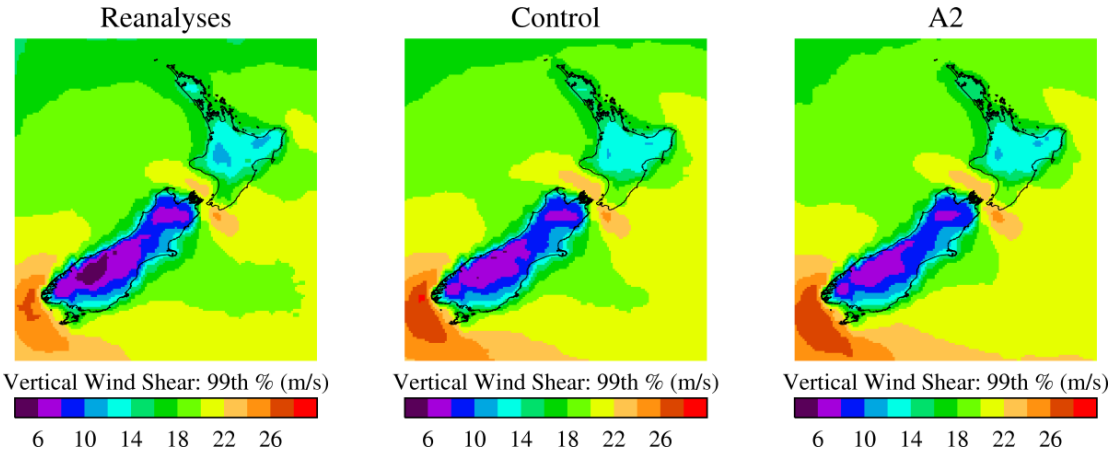

Figure 38: The 99th percentile wind shear field over 30 years for the RCM reanalyses (left), control (centre) and A2 (right) simulations.

This similarity is borne out in Figure 39 which shows the percentage difference between the 99th percentile wind shear for the RCM simulations. In this case, the difference between the control and reanalyses (left) is of the same magnitude as the difference between the control and the A2 simulation (right). The percentage differences are mostly less than 10% for both plots in Figure 39.

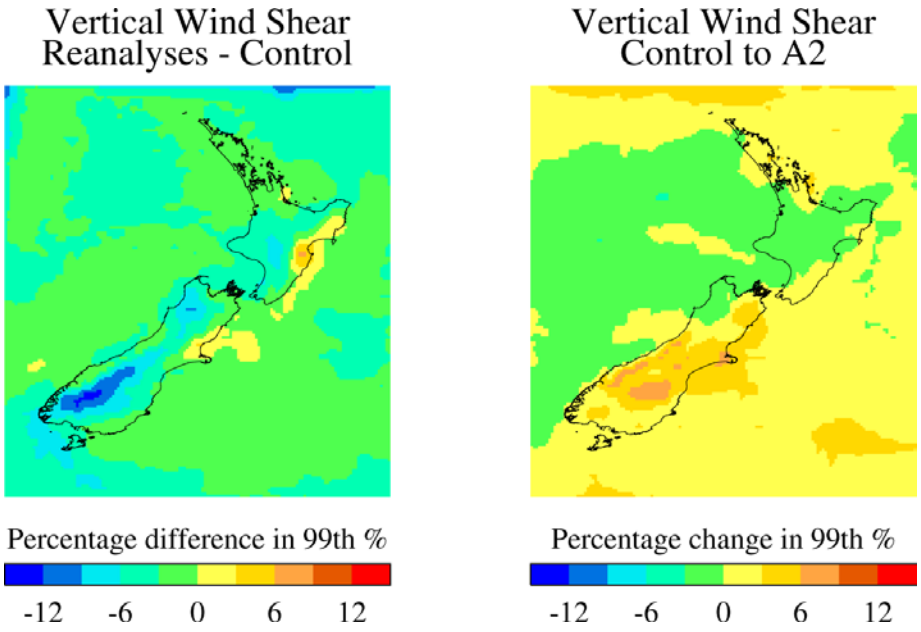

Figure 39: The percentage difference between the two 20th century RCM simulations (left) and the control and future simulations (right) for extreme wind shear.

6.4 Discussion

An analysis of three indices of severe weather – the K index, Convective available potential energy (CAPE), and vertical wind shear using past (forced by both NCEP reanalysis data and a free running GCM) and future (for a realization of the future climate under the SRES A2 emissions scenario) runs of the NIWA RCM has been performed.

Both the K index and the CAPE show increases in the frequency of severe weather events over much of the New Zealand domain in a future climate that is approximately 2°C warmer than present. The comparison of vertical shear shows only minor differences between the two past climate and one future climate simulations.

Thus, we would expect vigorous small-scale convective events to be more common and more intense in a future warmer climate. However, further work would be required to relate these severe weather indices to quantitative changes in extreme surface winds.

7. Conclusions

Several parallel and complementary approaches are taken in this report, involving low-resolution global model pressure and wind fields, and high resolution three-dimensional dynamical output from the NIWA regional climate model (RCM). This allows us to build up a picture of projected changes in: prevailing winds and weather patterns, storm frequency and intensity, extreme winds, and severe convective weather.

The principal findings of this study are that, based on multiple lines of investigation, the frequency of extreme winds over this century is likely to increase in almost all regions in winter and decrease in summer, especially for the Wellington region and the South Island. In addition, it is likely that there will also be an increase in cyclone activity over the Tasman Sea in summer and a decrease in activity south of New Zealand.

The Kidson weather typing scheme was applied to daily mean sea level pressure data from 23 AR4 GCMs for 40 years of their 20th century runs. Trough types over the winter season are projected to become more frequent (less frequent in summer). This may lead to an increase in the frequency of extreme winds (related to trough types) in almost all regions in winter (decreased frequency in summer), but especially for Wellington and the South Island regions.

All three zonal types are projected to decrease in frequency in summer but increase in frequency in winter. These weather types have their biggest influence on the occurrence of extreme winds in Canterbury, Otago and Southland. Thus, the projections suggest fewer extreme winds, associated with zonal weather types, in summer but more extremes in winter for the south and east of the South Island.

Further, an increase in the frequency of summer extreme winds, associated with increased blocking weather types, could occur in Northland, Coromandel, Bay of Plenty, Gisborne and Taranaki. In winter, the reverse case is projected.

An analysis of cyclone frequency has confirmed results from previous studies showing that there is likely to be a poleward shift in the cyclone track in a future, warmer climate. In the New Zealand context, this equates to a reduction in the number of cyclones over the North Island and to the east of the country in winter, with the chance of slightly increased cyclone frequency to the south of the country. In summer, however, it is likely that there will be increased cyclone activity over the Tasman Sea and a decrease in activity south of New Zealand.

Cyclone intensity is likely to decrease over New Zealand in both summer and winter. However, a significant intensification is possible south of the country during winter. This could produce a stronger pressure gradient over the South Island, and a possible increase in extreme winds in that part of New Zealand.

No significant trends in extreme wind were identified in the ERA40 or climate model data for the 1961-2000 period. Qualitatively however, 20th century extreme wind trend patterns over New Zealand suggest a north-south and west-east gradient with a weak increase in extreme wind over the southern and western South Island and no change or weak decrease over the northern North Island.

The trend patterns over the 140 year period 1961–2100 for the *miroc32_hires* and *cnrm_cm3* models (the two highest ranked models when compared with ERA40 wind speeds) show intensification of the north-south gradient and the related MSLP pattern is consistent with the zonal Kidson regime. However, no significant trends in extreme winds can be detected, suggesting that these future changes cannot be separated from the background noise.

The percentage difference between the 99th percentile modified K index (a severe weather index) between the control and reanalyses (historic runs) is significantly less than the difference between the control and the A2 (future) simulation. The increase in the K index under the A2 emissions scenario is between 3 and 6% over most of New Zealand.

The frequency of extreme CAPE events (another severe weather index) also increases in the future A2 simulation. For summer, the largest increase occurs in the Tasman Sea and over the South Island and central North Island. For autumn, the increase is fairly uniform over the domain, with the smallest increases over the land. For spring, the pattern is also quite uniform (although smaller in magnitude than for autumn), but the smallest increases are now over the ocean. For winter, the largest increases are in the south of the domain, but as this is the region with the lowest CAPE values, this increase is not so important for possible extreme wind events.

8. References

Baldi, M.; Salinger, J.; Mullan, B.; Thompson, C. (2008). Climate Trends, Hazards and Extremes – Taranaki. Synthesis Report. NIWA Client Report AKL 2008-080.

Barbosa, S.M., Andersen, O.B. (2009). Trend patterns in global sea surface temperature. *International Journal Climatology, 29:* 2049–2055.

Bengtsson, L.; Hodges, K.I.; Roeckner, E. (2006). Storm tracks and climate change. *Journal of Climate, 19:* 3518–3543.

Beniston, M.; Stephenson, D.B.; Christensen, O.B.; Ferro, C.A.T.; Frei, C.; Goyete, S.; Halsnaes, K.; Holt, T.; Jylha, K.; Koffi, B.; Palutikof, J.; Scholl, R.; Semmler, T.; Woth, K. (2007). Future extreme events in European climate: an exploration of regional climate model projections. *Climatic Change, 81:* 71–95.

Bhaskaran, B.; Mullan, A.B.; George, S.E. (1999). Modelling of atmospheric climate variations at NIWA. *Weather and Climate, 19:* 23–36.

Bhaskaran, B.; Renwick, J.; Mullan, A.B. (2002). On the application of the Unified Model to produce finer scale climate information for New Zealand. *Weather and Climate, 22:* 19–27.

Bluestein, H.B. (1993). *Synoptic-Dynamic Meteorology in Midlatitudes. Volume II: Observations and Theory of Weather Systems*. Oxford University Press.

Brooks, H.E.; Lee, J.W.; Craven, J.P. (2003). The spatial distribution of severe thunderstorm and tornado environments from global reanalysis data. *Atmospheric Environment, 67:* 73–94.

Burgess, S. (2004). Major weather events to 30 June 2004. Internal NIWA document.

Burgess, S.; Salinger, M.J.; Gray, W.; Mullan, A.B. (2006). Climate Hazards and Extremes – New Plymouth District; Cyclones of tropical origin. NIWA Client Report WLG2006-27.

Burgess S.; Salinger, M.J.; Turner, R.; Reid, S. (2007): Climate hazards and extremes – Taranaki Region: High winds and tornadoes. NIWA Client Report WLG2007-48 for New Plymouth District Council, June 2007.

Dean, S.; Mullan, B.; Renwick, J. (2006). More shorts and gumboots? New Zealand climate at the end of this century as simulated by a regional climate model. Paper presented at: Resource Management under Stormy Skies Conference (Meteorological Society of NZ +others), 20-23 November 2006, Christchurch.

Fyfe, J.C. (2003). Extratropical southern hemisphere cyclones: Harbingers of climate change? *Journal of Climate*, *16:* 2802–2805.

Griffiths, G.; Burgess, S.; Reid, S. (2004). Meteorological report on extreme weather events since 1 April 2003 impacting on the Vector network. NIWA Client Report AKL2004-055.

Hannachi, A. (2007). Pattern hunting in climate: a new method for finding trends in gridded climate data. *International Journal Climatology*, *27:* 1–15.

Hill, H. (1979). Severe damage to forests in Canterbury, New Zealand, resulting from orographically reinforced winds. *New Zealand Meteorological Service: Technical Information Circular*, 169.

IPCC. (2007). Summary for Policymakers. In: Climate Change 2007: The Physical Science Basis. Contribution of Working Group I to the Fourth Assessment Report of the Intergovernmental Panel on Climate Change. Solomon, S., Qin, D., Manning, M., Chen, Z. Marquis, M., Averyt, K.B., Tignor, M. and Miller, H.L. (Eds.), Cambridge University Press, Cambridge, UK and New York, NY, USA. Available at http://ipcc-wg1.ucar.edu/wg1/Report/AR4WG1_Pub_SPM-v2.pdf

Kalnay, E.; Kanamitsu, M.; Kistler, R.; Collins, W.; Deaven, D.; Gandin, L.; Iredell, M.; Saha, S.; White, G.; Woollen, J.; Zhu, Y.; Chelliah, M.; Ebisuzaki, W.; Higgins, W.; Janowiak, J.; Mo, K.C.; Ropeleski, C.; Wang, J.; Letmaa, A.; Reynolds, R.; Jenne, R.; Joseph, D. (1996). The NCEP/NCAR 40-year reanalysis project. *Bulletin American Meteorological Society*, *77:* 437–471.

Kidson, J.W. (2000). An analysis of New Zealand synoptic types and their use in defining weather regimes. *International Journal of Climatology*, *20:* 299–316.

Lambert, S.J.; Fyfe, J.C. (2006). Changes in winter cyclone frequencies and strengths simulated in enhanced greenhouse warming experiments: results from the models participating in the IPCC diagnostic exercise. *Climate Dynamics*, 26: 713–728, doi:10.1007/s00382-006-0110-3.

Leckebusch, G.C.; Koffi, B.; Ulbrich, U.; Pinto, J.G.; Spangehl, T.; Zacharias, S. (2006). European winter storms and their modification under climate change from a multi-model perspective. *Geophysical Research Abstracts, 8:* 01945.

Lim, E.P.; Simmonds, I. (2002). Explosive cyclone development in the Southern Hemisphere and a comparison with Northern Hemisphere events. *Monthly Weather Review, 130*: 2188–2209.

Lim, E.P.; Simmonds, I. (2009). Effect of tropospheric temperature change on the zonal mean circulation and SH winter extratropical cyclones. *Climate Dynamics, 33:* 19–32, doi:10.1007/s00382-008-0444-0.

McInnes, K.L.; Abbs, D.J.; Bathols, J.A. (2005). Climate Change in Eastern Victoria: The effect of climate change on coastal wind and weather patterns. CSIRO Client Report for Gippsland Coastal Board, 26p.

Meehl, G.A.; Covey, C.; Delworth, T.; Latif, M.; McAvaney, B.; Mitchell, J.F.B.; Stouffer, R.J.; Taylor, K.E. (2007). The WCRP CMIP3 multimodel dataset: A new era in climate change research. *Bulletin American Meteorological Society, 88:* 1383–1394.

Ministry for the Environment. (2008). *Climate change effects and impacts assessment: A guidance manual for local government in New Zealand*, 2nd Edition. Prepared by Mullan, B.; Wratt, D.; Dean, S.; Hollis, M. (NIWA); Allan, S.; Williams, T (MWH New Zealand Ltd), and Kenny, G. (Earthwise Consulting), in consultation with Ministry for the Environment. NIWA Client Report WLG2007/62, February 2008, 156p.

Pryor, S.C.; Schoof. J.T.; Batthelmie, R.J. (2006). Winds of change?: Projections of near-surface winds under climate change scenarios. *Geophysical Research Letters, 33:* L11702, doi:10.1029/2006GL026000.

Ray, D. (2008). Impacts of climate change on forestry in Scotland – a synopsis of spatial modelling research. Scotland Forestry Commission Research Note 101, 8p.

Richman, M.B. (1986). Rotation of principal components. *J. Climatology, 6:* 293–335.

Rockel, B.; Woth, K. (2007). Extremes of near-surface wind speed over Europe and their future changes as estimated from an ensemble of RCM simulations. *Climatic Change, 81:* 267–280.

Salinger M.J.; Griffiths, G.M.; Gosai, A. (2005). Extreme pressure differences at 0900 NZST and winds across New Zealand. *International Journal of Climatology, 25:* 1202–1222.

Semmler, T.; Varghese, S.; McGrath, R.; Nolan, P.; Wang, S.; Lynch, P.; O'Dowd, C. (2008). Regional climate model simulations of North Atlantic cyclones: frequency and intensity changes. *Climate Research, 36:* 1–16.

Showalter, A.K. (1953). A stability index for thunderstorm forecasting. *Bull. Am. Meteorol. Soc., 34:* 250–252.

Simmonds, I.; Keay, K. (2000a). Variability of Southern Hemisphere extratropical cyclone behaviour, 1958-97. *Journal of Climate, 13:* 550–561.

Simmonds, I.; Keay, K. (2000b). Mean Southern Hemisphere extratropical cyclone behavior in the 40-year NCEP-NCAR reanalysis. *Journal of Climate, 13:* 873–885.

Simmonds, I.; Murray, R.J.; Leighton, R.M. (1999). A refinement of cyclone tracking methods with data from FROST. *Australian Meteorological Magazine, 28:* 617–624.

Somerville, A.R., Wakelin, S.J., Whitehouse, L. (Eds.), (1989). Workshop on wind damage in New Zealand exotic forests. FRI Bulletin 146. Ministry of Forestry, Rotorua, New Zealand, 76 pp.

Steiner, J.T. (1989). New Zealand hailstorms. *New Zealand Journal of Geology and Geophysics, 32:* 279-291.

Sturman, A.P.; Tapper, N.J. (1996). *The Weather and Climate of Australia and New Zealand*. Oxford University Press, Melbourne.

Suselj, K.; Sood, A. (submitted). The near surface wind speed over Europe and the North Atlantic in future climate. *Tellus A* (submitted).

Tait, A.; Henderson, R.; Turner, R.; Zheng, X. (2006). Thin plate smoothing spline interpolation of daily rainfall Zealand using a climatological rainfall surface. *International J. Climatology, 26:* 2097–2115.

Thompson, D.W.J.; Solomon, S. (2002). Interpretation of recent Southern Hemisphere climate change. *Science, 296:* 895–899.

Trapp, R.J.; Diffenbaugh, N.S.; Brooks, H.E; Baldwin, M.E.; Robinson, E.D.; Pal, J.S. (2007). Changes in sever thunderstorm environment frequency during the 21st century caused by anthropogenically enhanced global radiative forcing. *Proceedings National Academy of Sciences, 104:* 19717–19723.

Turner, R.; Burgess, S.; Reid, S. (2006). Meteorological report on extreme weather events since 1 April 2005 impacting on the Vector network. NIWA Client Report WLG2006-024.

Turner, R.; Burgess, S.; Reid, S. (2007). Meteorological report on extreme weather events between 1 April 2006 and 31 March 2007 impacting on the Vector network. NIWA Client Report WLG2007-033.

Ulbrich, U.; Leckebusch, G.C.; Pinto, J.G. (2009). Extra-tropical cyclones in the present and future climate: a review. *Theoretical and Applied Climatology, 96:* 117-131, doi:10.1007/s00704-008-0083-8.

Uppala, S.M.; Kållberg, P.W.; Simmons, A.J.; Andrae, U.; da Costa Bechtold, V.; Fiorino, M.; Gibson, J.K.; Haseler, J.; Hernandez, A.; Kelly, G.A.; Li, X.; Onogi, K.; Saarinen, S.; Sokka, N.; Allan, R.P.; Andersson, E.; Arpe, K.; Balmaseda, M.A.; Beljaars, A.C.M.; van de Berg, L.; Bidlot, J.; Bormann, N., Caires, S.; Chevallier, F.; Dethof, A.; Dragosavac, M.; Fisher, M.; Fuentes, M.; Hagemann, S.; Hólm, E.; Hoskins, B.J.; Isaksen, L.; Janssen, P.A.E.M.; Jenne, R.; McNally, A.P.; Mahfouf, J.-F.; Morcrette, J.-J.; Rayner, N.A.; Saunders, R.W.; Simon, P.; Sterl, A.; Trenberth, K.E.; Untch, A.; Vasiljevic, D.; Viterbo, P.; and Woollen, J. (2005). The ERA-40 re-analysis. *Quart. J. R. Meteorol. Soc., 131:* 2961–3012, doi:10.1256/qj.04.176.

Webster, S.; Uddstrom, M.; Oliver, H.; Vosper, S. (2008). A high resolution modeling case study of a severe weather event over New Zealand. *Atmospheric Science Letters, 9:* 119 – 128.

Wendelken, W.J. (1966). Eyrewell Forest: A search for stable management. *New Zealand Journal of Forestry, 11:* 43–65.